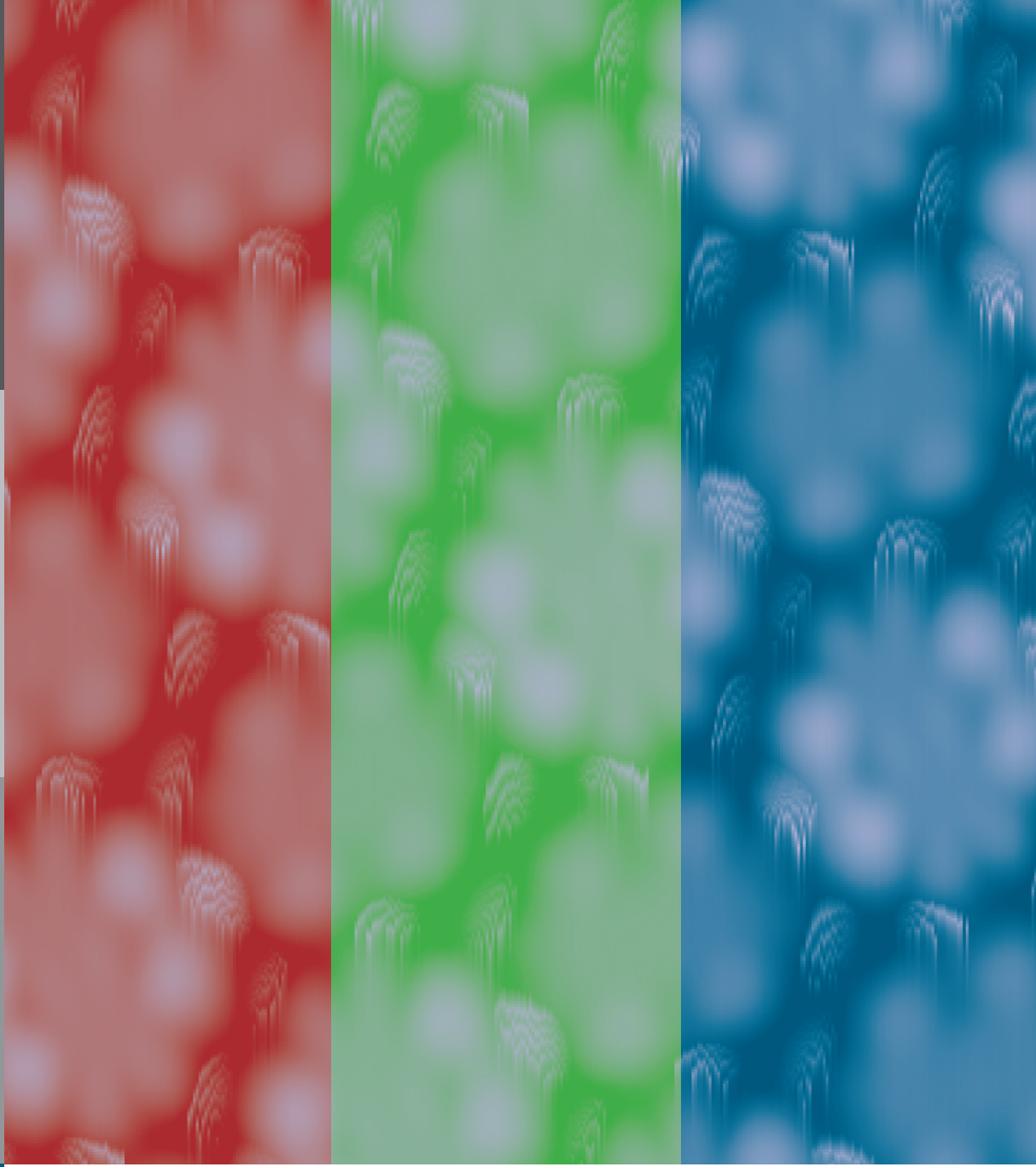

Investigation of a metal-organic interface – realization and understanding of a molecular switch

Olga Neucheva

Mitglied der Helmholtz-Gemeinschaft

JÜLICH
FORSCHUNGSZENTRUM

Schriften des Forschungszentrums Jülich
Reihe Schlüsseltechnologien / Key Technologies Band / Volume 17

Forschungszentrum Jülich GmbH
Institute of Bio- and Nanosystems (IBN)
Functional Nanostructures at Surfaces (IBN-3)

Investigation of a metal-organic interface – realization and understanding of a molecular switch

Olga Neucheva

Schriften des Forschungszentrums Jülich
Reihe Schlüsseltechnologien / Key Technologies Band / Volume 17

ISSN 1866-1807 ISBN 978-3-89336-650-7

Bibliographic information published by the Deutsche Nationalbibliothek.
The Deutsche Nationalbibliothek lists this publication in the Deutsche Nationalbibliografie; detailed bibliographic data are available in the Internet at http://dnb.d-nb.de.

Publisher and Distributor:	Forschungszentrum Jülich GmbH Zentralbibliothek 52425 Jülich Phone +49 (0) 24 61 61-53 68 · Fax +49 (0) 24 61 61-61 03 e-mail: zb-publikation@fz-juelich.de Internet: http://www.fz-juelich.de/zb
Cover Design:	Grafische Medien, Forschungszentrum Jülich GmbH
Printer:	Grafische Medien, Forschungszentrum Jülich GmbH
Copyright:	Forschungszentrum Jülich 2010

Schriften des Forschungszentrums Jülich
Reihe Schlüsseltechnologien / Key Technologies Band / Volume 17

D 82 (Diss. RWTH Aachen University, 2010)

ISSN 1866-1807
ISBN 978-3-89336-650-7

The complete volume ist freely available on the Internet on the Jülicher Open Access Server (JUWEL) at http://www.fz-juelich.de/zb/juwel

Dedication

This work is dedicated to my parents whose love and encouragement have always been infinite.

Acknowledgement

Although there is only one name in the author line of this thesis, its appearance would not be possible without the greatly appreciated assistance of many people. First, and foremost, I would like to thank my PhD mentor Professor Stefan Tautz for giving me the opportunity to work at his research group and providing all of the indispensable conditions required for my PhD studies.

I am very grateful to my colleagues from School of Engineering and Science at Jacobs University Bremen and from the Institute for Bio-and Nanosystems -3, especially to Dr. Sergey Subach for the support during my whole time in Germany, Dr. Vasily Cherepanov for the tolerance to my naive questions and for sharing an office with me, to Dr. Ruslan Temirov for the scientific support, to Prof. Bert Voigtländer for the very fruitful Friday seminars, to Christian Weiss for helping me in many small but meaningful things, to Adam Lassise for improving my English and just being a good friend.

I would also like to thank the collaborators from Dresden Technical University for their everyday availability to explain me the depths of the theoretical wisdom and of course, for performing the theoretical calculations: Dr. Cormac Toher, Dr. Rafael Gutierrez, Thomas Brumme, and to Prof. Gianaurelio Cuniberti for his refined sense of beauty. I am very grateful to Prof. Michael Rohlfing and his group for providing the results of calculations.

And finally, this work would have been much more difficult without the support of my friends Pavel, Sergey, Petro, Viktor, Felix, Kristine, Stephen and Alex.

The research presented in this dissertation was funded by the DFG under the Priority Program SPP-1243 “Quantum transport at the molecular scale”.

ABSTRACT

The field of molecular organic electronics is an emerging and very dynamic area. The continued trend to miniaturisation, combined with increasing complexity and cost of production in conventional semiconductor electronics, forces companies to turn their attention to alternatives that promise the next levels of scale at significantly lower cost. After consumer electronic devices based on organic transistors, such as TVs and book readers, have already been presented, molecular electronics is expected to offer the next breakthrough in feature size.

Unfortunately, most of the organic/metal interfaces contain intrinsic defects that break the homogeneity of the interface properties. In this thesis, the electronic and structural properties of such defects were examined in order to understand the influence of the inhomogeneities on the quality of the interface layer. However, the main focus of this work was the investigation of the local properties of a single molecule. Taking advantage of the Scanning Tunnelling Microscope's (STM's) ability to act as a local probe, a single molecular switch was realized and studied. Moreover, in close collaboration with theory groups, the underlying mechanism driving the switching process was identified and described. Besides the investigation of the switching process, the ability of the STM to build nanostructures of different shapes from large organic molecules was shown.

Knowing the parameters for realization and control of the switching process and for building the molecular corrals, the results of this investigation enable the reconstruction of the studied molecular ensemble and its deployment in electric molecular circuits, constituting a next step towards further miniaturization of electronic devices.

Contents

INTRODUCTION

Organic electronics has been a focus of interest for researchers over several decades. Nevertheless, only recently this field from being purely scientific has become industrially applicable. Although conventional materials such as silicon or GaAs will still be used in most electronic devices in the nearest future, organic electronics is making the first steps towards supplanting them in many areas. Experts estimate that by the year 2015 the share of organic electronics in the world market could reach 34 billion dollars [1]. The key factors determining the growth of electronics based on organic materials is its low cost, the rich functionality of organic materials and wide selection of them.

The full potential of the technology was not recognised immediately; until the mid-1980s manufacturers were still sceptical about the practical implications of the research studies in the field. However, the first demonstration of a highly efficient low voltage thin film light emitting diode (LED) gave hope to the researchers and aroused great interest from the manufacturing companies [2].

Since then organic thin film devices have been employed in a number of applications that have reached the consumer market. The biggest success belongs undoubtedly to organic light emitting diodes (OLEDs) which are now used in long-living and highly efficient colour displays [3-6]. Organic photovoltaic elements [7, 8] rank second to the OLEDs; materials containing electron and hole charge carriers, some or all of which are organic, produce voltages of 0.5–1 V and significant current in response to solar radiation, and can be assembled into multilayer thin film cells. Organic field effect transistors (OFETs) rank third in the list so far, but certainly have a lot of potential [9, 10].

All of the molecular devices created so far have been based on pure [11, 12] or doped [13] thin films of organic components, mostly with a layer(s) of π-conjugated organic molecules as an active component. Fabrication of devices based on a single molecule does not go beyond experiments in research laboratories [14-16]. Studies of the electron transport through such small channels require very delicate experimental preparations and complex theoretical analysis [17-20]. Experimentalists are faced with a problem of very small size and local properties of the system under investigation. Different parts of the molecules possess different electronic and structural properties. Miniaturization of molecular devices increases the influence of microscopic components of the system, such as electrodes. For theoreticians, a problem stands of developing an electronic structure method which can accurately describe a

system which consists of a finite molecule with localized wave functions connected to open, semi-infinite, metallic electrodes.

In experiments there are three techniques that can be used to contact a single molecule: mechanically controlled break junction (MCBJ) [17, 21-26], electromigration (EM) techniques [15, 27, 28], and scanning tunnelling microscope (STM) [29-40]. MCBJ provides mechanical stability that allows for the performance of the experiments at different temperatures, but lacks defined microscopic structure of the contacts. The EM techniques allow for the construction of three-terminal junctions, but the geometry of the contacts also remains unclear. Both techniques have no imaging ability; the location and bonding of a single molecule to the electrodes cannot be defined.

In contrast to MCBJ and EM, STM is very powerful with respect to the atomic junction structure. It allows not only for imaging before contacting, so that one knows the exact part of the molecule which forms the bond with the electrodes; the contacts also have a known shape: a flat surface and an edge tip apex atom. STM is not an perfect technique, however, and has its own deficiencies, such as mechanical instability and requirement of low temperatures to avoid drifts in the system. Realization of gating is almost impossible (in conventional one tip STM) due to the difficulty of mounting the third contact.

But in spite of its downsides, STM excels the other methods in the structural control of the junction, which is the most important component of transport measurements. In addition, it has the ability to manipulate molecules [37, 41-45] thus allowing for the building of nanostructures and measurement of their electronic responses. Finally, STM offers the opportunity of using the electric current through a single molecule to control switching between different conformations of the molecular junction [31, 32, 39, 46-51]. All of this makes the STM techniques the most appropriate for the investigation of transport through a single molecule.

The unique capabilities of STM allow the investigation of a variety of characteristics of organic-metal interfaces from conventional electronic properties to possible applications in single molecular devices.

In order to be used in molecular devices, the molecules must satisfy several requirements: they must be easy to position in a controlled way, and they have to be interconnected to a preformed electrical circuit [43]. Moreover, they ideally must provide at least one of the following functions: rectification [52], amplification [53], and switching [54]. Rectification

and amplification usually come as side effects of a molecular switch [54], and therefore the latter is of most practical interest to researchers.

As for a molecular switch, it can be realized by different changes in a molecule, such as rotation [43, 55], translation [56, 57], isomerization [58], and chemical interaction between the leads and the molecule [40]. Factors inducing a molecular switch may have different natures: light [59, 60], thermal activation [61], electric field [58], and flux of the current through the junction [62-64].

With the STM, a molecular switch can be realized by controlling the tunnelling current, with intramolecular conformation changes in the molecule ensuring either low or high conductance of the junction. Although many researchers observed molecular switch effects [57, 62, 65], the gain of the conductance is usually small; the current in the high conductance state is larger than the current in the low conductance state only by a factor of two. Among all reports, the largest conductance gains were demonstrated in the case of Cu-TBPP [43] and SnPc molecules [66].

Rotation of one of the legs of Cu-TBPP molecule on Cu(221) changes conductance by one order of magnitude. In this case, Cu-TBPP molecules switch between two stable molecular conformations on the surface. The reversible switch is performed by lateral displacement of the tip independently of the bias voltage. However, vertical movement of the tip leads to pushing of one of the legs towards the surface, and irreversibly switches the molecule to the state of low conductance.

Another switch with large difference of the conductance was observed in the case of SnPc molecules adsorbed on Ag(111) [66, 67]. Bistable conformational states of the molecules are attributed to the central tin atom either facing the surface or the tip. The switching was realized by resonant electron or hole injection into a molecular orbital, which led to up and down motion of the Sn ion through the frame of the phthalocyanine molecule. However this switch can be implemented only in the case of a Sn-Pc bi-layer, whereas with a single layer only irreversible switching was observed.

Both of these switches were suggested for use in molecular devices, however each of them has its problems. The first one (Cu-TBPP) involves lateral displacement of the molecule while rotating the leg, which is bad because the molecule requires free lateral space within the layer and every next switch has to be done after recording the constant current image defining the position of the moved molecule on the surface, which is time consuming. Although the second switch (Sn-Pc) can be performed much faster it requires much larger bias voltages

(several V) and the quantum conductance in the high conductance state does not exceed a few nS.

In this thesis the molecular switch of a PTCDA molecule deposited on the Ag(111) surface will be discussed. A reversible vertical switch was realized with the help of the low temperature STM. The switch does not require free lateral space and can be implemented with any single molecule in the layer. The carboxylic oxygen of the molecule can be controllably switched between the surface and the STM tip without destroying the molecule. The chemisorbtive interaction between the molecule and the substrate provides a wide channel for the electron transfer which leads to the high conductivity of the junction (few μS) in the high conductance state. In contrast to reference [66], the molecular switch was found to take place at quite low bias voltages (starting from 50 mV). The state of the molecule can be controlled by two parameters: tip height and bias voltage.

The molecular switch was considered from both experimental and theoretical points of view. On the base of qualitative (Chapter 2 and 3) and quantitative (Chapter 4) experimental analysis, a theoretical model for the process was provided (Chapter 5).

The controllability of the PTCDA molecular switch opens the possibility of its application in single molecule electronic devices, as depicted in Fig. 0.1. One can switch a molecule between two stable conformations (Fig. 0.1 a,b) by only applying electric current, achieving a one order of magnitude change in conductance making PTCDA a fully functional on-off molecular relay.

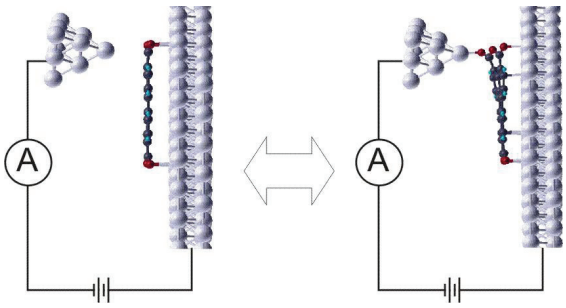

Figure 0.1. Experimentally realized STM-junction implementation of a molecular switch of a single PTCDA molecule on Ag(111). The tunneling current is passing through the molecule, resistance of which depends on the molecular conformation.

Beside the point of molecular switch applications, intrinsic structural defects in PTCDA layers were considered within this work. In spite of being well-ordered, PTCDA layers contain small concentration of point defects. The defects were found to have electronic and

structural characteristics different from normal PTCDA molecules. Despite a lot of interest in the PTCDA molecule, so far no reports concerning investigation of the defects were presented. In the section 2.3 of this work for the first time the origin of these defects was investigated together with their electronic properties.

CHAPTER 1.
PTCDA ON AG(111) AS A MODEL SYSTEM

1.1. INTRODUCTION

PTCDA (3,4,9,10-perylenetetracarboxylic-dianhydride) is a very well-known and extensively studied molecule [68-85]. Because there is an abundance of information about this molecule in the literature, this section will briefly introduce the properties of the PTCDA/Ag(111) interface which was used over a number of experimental studies.

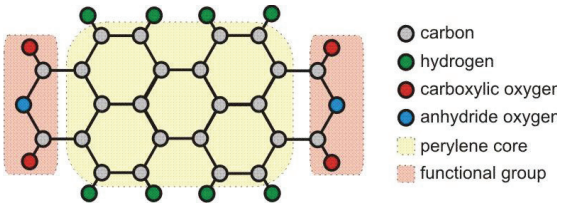

Figure 1.1. Ball and stick model of a PTCDA molecule. The bond between the molecule and the surface consists of two channels: electronically strong π-interaction between the perylene core and the surface, and mechanically strong Ag-O bonds between the carboxylic oxygens and the surface

PTCDA is a widely-used and model large π-conjugated organic molecule with functional groups possessing semiconducting properties (Fig. 1.1). It forms highly ordered structures on a wide range of substrates [73, 86, 87]. The planar stacking on the surface makes PTCDA perfect for investigation of the intrinsic optical and electronic properties. PTCDA is an intensive dye molecule[88] which can be used for optoelectronic applications. It can be easily synthesized and is stable under electron and phonon bombardment [84].

1.2. MOLECULAR ORDERING

Substrate temperature at deposition is important for the molecular ordering. The PTCDA molecules when deposited onto an Ag(111) surface kept at room temperature form a chemisorbed long-range ordered commensurate monolayer. The large size of the formed islands is a result of the high mobility of PTCDA molecules on the Ag(111) surface at room temperature [89]. The high mobility leads also to the observation of only a few domain boundaries, although the oblique symmetry of the unit cell implies the existence of the 6

mirror/rotation domains. The unit cell consists of two flat-lying molecules in a herringbone arrangement (Fig. 1.2 a) and has the following dimensions: *a = 18.96 Å, b = 12.61 Å, α = 89°* [90].

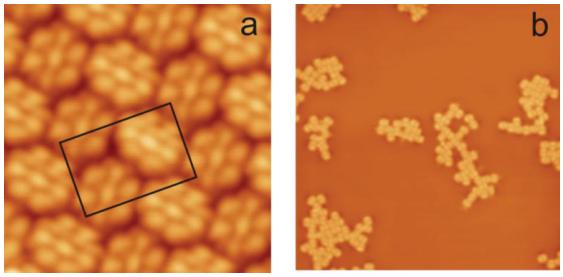

Figure 1.2. Constant current topography images of different phases of PTCDA/Ag(111) interface. a) Ordered phase, 5×5 nm², -340 mV, 0.1 nA. The unit cell dimensions: a = 18.96 Å, b = 12.61 Å, α = 89°[90] b) Disordered (low temperature of the sample during deposition) phase, 40×40 nm²,-340 mV, 0.1 nA.

The two molecules in the unit cell are not equivalent and have different orientations. One of them appears brighter in the images and is aligned along the $[10\bar{1}]$ direction of the Ag(111) surface, whereas the dimmer molecule is misaligned by 17° with respect to the same direction [80].

When deposited onto the cold surface (65 K) PTCDA molecules form disordered dendritic clusters of irregular shape and size (Fig. 1.2 b) [91]. Low temperature prevents the molecules from being diffused over large distances on the surface; however they tend to gather at the disordered islands. Although the molecular orientation is difficult to define by eye, statistical analysis tells that the orientations along the $[1\bar{1}0]$ and $[2\bar{1}\bar{1}]$ directions of Ag(111) are dominant [91].

Since the molecules in the island are disordered the intermolecular interaction is lower than for the molecules in the ordered monolayer. This happens as a result of the fewer hydrogen bonds which are established between the neighboring molecules. This effect together with different interfacial interactions leads to the change of the electronic properties (Fig. 1.3).

1.3. ELECTRONIC PROPERTIES AND ADSORPTION GEOMETRY

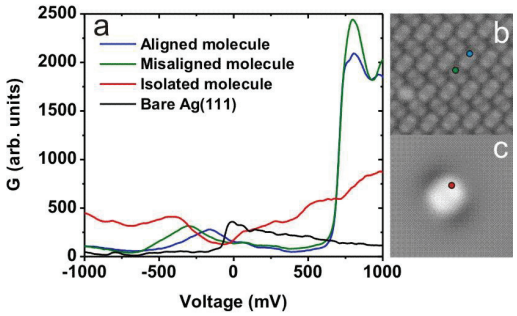

Figure 1.3. STS spectra of PTCDA on Ag(111), recorded with lock-in technique. a) Black line: surface state of bare Ag(111). Red line: isolated PTCDA molecule shown at c).Blue line: molecule aligned with the $[10\bar{1}]$ direction of Ag(111). Green line: molecule misaligned by 17° with the same direction. b) Constant current STM image of ordered PTCDA/Ag(111) monolayer with two types of the molecule (corresponding spectra are shown in a) as blue and green curves). 7.5×7.5 nm², -340 mV, 0.1 nA. c) Constant current STM image of a single isolated molecule (dI/dV spectrum corresponds to red curve in a). 5×5 nm², -340 mV, 0.1 nA.

PTCDA molecules are chemisorbed on Ag(111) surface, thus the lowest unoccupied molecular orbital (LUMO) becomes partially occupied and the position of this molecular orbital is shifted below the Fermi-level.

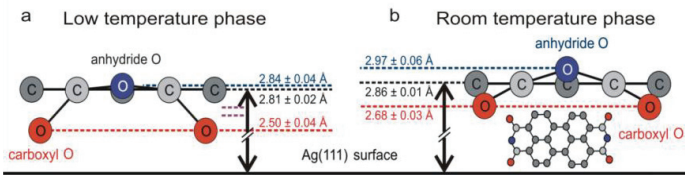

Figure 1.4. Adsorption height and vertical distortion of PTCDA molecule on Ag(111) measured with NIXSW. a) Disordered low temperature phase molecule. b) Ordered room temperature phase molecule. Taken from Ref. [91]

The electronic properties of the molecules do not only differ depending on the adsorption phase but also on the orientation of the molecules on the surface within the ordered phase. This difference in molecular orientation leads to the distinction in the electronic properties of the molecules belonging to the aligned or misaligned type [80]; this can be seen in the conductance spectra measured at the aligned and misaligned molecules (Fig. 1.3). As for the isolated molecules in the disordered phase, from the spectra one can see that the former lowest unoccupied molecular orbital (FLUMO) state is shifted further away from the Fermi-level. Thus stronger coupling to the surface takes place resulting in greater attraction between the molecule and the substrate. Further evidence for stronger bonding with the surface was

found by the normal incidences X-ray standing waves (NIXSW) studies [92, 93]. The vertical bonding distance of the perylene core of the PTCDA molecule in the low temperature phase is 0.06 Å smaller compared to the room temperature phase (2.80 Å compared to 2.86 Å, respectively). Additional proof for a stronger interaction with the substrate is greater vertical distortion of the molecules in the disordered phase, resulting in the carboxylic oxygens being located closer to the substrate and forming a chemical bond with the substrate (Fig. 1.4).

CHAPTER 2.
STRUCTURAL POINT DEFECTS AT THE PTCDA/AG(111) INTERFACE

2.1. INTRODUCTION

In this chapter, structural and electronic properties of the intrinsic point defects at the PTCDA/Ag(111) interface will be considered.

In spite of the usual high quality, the PTCDA/Ag(111) interface is not perfect and contains inhomogeneities. The presence of the inhomogeneities breaks the periodicity of the organic layer and changes the properties of the interface locally in the vicinity of such structural defects. For instance, for the delocalized state at the PTCDA/Ag(111) interface [1], one can expect to observe electron scattering effects similar to the well-known case of scattering at the surface state of Ag(111) [2].

All the experiments within this work were performed with a scanning tunneling microscope (STM), which is a very powerful technique in the field of surface science. Although it was invented almost three decades ago it is still one the most powerful instruments used for surface and interface investigations. Nowadays, apart from conventional imaging and spectroscopy, new applications of the STM are implemented such as atom manipulations [94] and molecular transport [95].

2.2. EXPERIMENTS PREPARATION

The experiments were performed with a low temperature scanning tunneling microscope (Createc GmbH) at 7 K in an ultra-high vacuum with a base pressure below 1^{-10} mbar. The Ag(111)surface was previously prepared by repeated sputtering-annealing cycles: the single crystalline metal surface was sputtered using an incident beam of Ar^+ ions (ion beam energy 0.8 keV) at room temperature, followed by subsequent annealing at temperatures of about 820 K. The surface quality was monitored *in situ* with low energy electron diffraction (LEED) optics. The PTCDA molecules were evaporated from a Knudsen cell with a temperature of 580 K onto the surface for 30 seconds, which was kept at room temperature in order to obtain submonolayer coverage for the experiments with switches. For the molecular displacement

experiments the disordered "precursor" phase was prepared (sample temperature is 80 K) [91].

An electrochemically etched tungsten wire was used for the STM tip after it was cleaned *in situ* by annealing at high temperature. The final atomic sharpening was done by indentation of the tip into the clean metal substrate and/or by application of voltage pulses. The tip quality was verified by measuring the surface state of Ag(111). The PTCDA material (commercial purity 99%) was purified by resublimation and outgassing in the UHV for 100 hours.

2.3. Properties of structural point defects at the PTCDA/Ag(111) interface

2.3.I. Appearance at the STM images

The herringbone pattern of PTCDA on Ag(111) is known to include molecules of two different orientations, similar to bulk PTCDA [90]. They belong to different sublattices and are referred to in literature as aligned and misaligned. In the experiments, the point defects in both sublattices with approximately similar portion were observed.

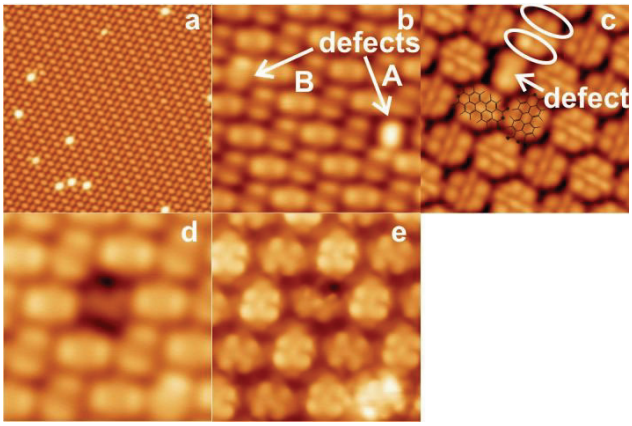

Figure 2.1. Constant current STM-images of PTCDA on Ag(111). a) 35×35 nm², 0.11 nA, 0.5 V, bright spots inside the PTCDA island correspond to point defects; b) 10×10 nm², 0.1 nA, -0.34V, topography of aligned (type A) and misaligned (type B) structural defects; c) 5×5 nm², 0.1 nA, -0.34V functionalized tip allows to resolve LUMO-contrast of molecules, whereas point defect does not possess the LUMO-structure; d) 5×5 nm², 0.3 nA, -0.34V B-type defect appears as a "dim" spot or vacancy, whereas with hydrogen-sensitized tip e) 5×5 nm², 1 nA, -0.29V reveals all rings present.

Figure 2.1 reveals the topography of the PTCDA layer, where difference of defects from the remaining normal PTCDA molecules can be easily defined. When positive bias is applied the defects look much brighter than the rest of the layer (Fig. 2.1 a). For STM images taken at negative bias, the normal molecules appear like two bright lobes with the same intensity

showing the LUMO of the molecule, whereas the point defects exhibit different structure. Misaligned defects may look similar to the normal molecules but with the LUMO-lobes having different intensities (Fig. 2.1 b). Aligned defects appear in the images as a single bright lobe in the center of the molecule (Fig. 2.1 b). Neighboring molecules next to both types of defects have the different intensity of LUMO-lobes thus look asymmetric (compare two ovals in Fig. 2.1 c).

The number of defects depends on growth conditions. Raising of the sample temperature during deposition from 293 K (for standard deposition resulting in a small (0.1 %[89]) portion of intrinsic defects) up to 373 K leads to a higher density of defects (0.7%) but does not influence the overall structure of the PTCDA islands. The percentage was calculated by counting the number of defects over the surface area of 400×400 $Å^2$. The unit cell size is known (*a = 18.96 Å, b = 12.61 Å, α = 89°*), as well as that it contains two molecules [90]. Thus by dividing the number of defects by the number of molecules, a value of 0.7% was obtained.

It is reported in literature [89] that the majority of the defects are vacancies, which is in agreement with the results of this work where imaging at certain conditions show the defects as the vacancies or "dim" molecules (Fig. 2.1 e,f).

Interestingly, the defects exhibit significantly different properties strictly depending on the sublattice they belong to. This was observed both in topographic imaging and local spectroscopic measurements and constant height dI/dV imaging. All further measurements were performed at A and B-type defects, which exhibit topography shown in Fig. 2.1 b.

2.3.II. ELECTRONIC PROPERTIES

The conductance spectra of the point defects exhibit more complicated electronic structure (Fig.2.2) in comparison with the normal molecules.

At the energy of FLUMO of the normal molecules (-340 meV and -180 meV for aligned (A-type) and misaligned (B-type) molecules respectively) no significant peaks in the spectra of defect molecules were found. As for the region where LUMO+1 and LUMO+2 states of normal molecules can be seen (above 700 meV) [81], there are also peaks in the case of defects. However, they are shifted relative to the ones belonging to normal molecules. Moreover, many additional peaks appear in the conductance spectra of B-type defects. The features belonging to both types of structural defects will be considered first.

A very strong resonance (V) can be observed at bias voltage 0.6 V. This peak is visible in both aligned (blue curve) and misaligned (green curve) defects, which are inhomogeneities with respect to the remaining layer of PTCDA. When inhomogeneities are strongly coupled to underlying surface, the scattering of the electrons from a point defect and the formation of a bound state, which splits off from the delocalized state [81] of PTCDA were observed. The effect of the influence of the coupling is discussed in Ref. [96]. The formation of a bound state was observed before by Cauyacq et al [97] between Cr and Ar adatoms adsorbed on the Cu(111) metal surfaces. However, there is only one paper in the literature concerning the observation of this effect for organic molecules was found in the case of C_{60}/Au(110) interface. Nevertheless, the electronic and structural properties were not considered.

The bound state can be seen at both A and B-type defects and is localized over the structural defects (Fig. 2.3 h). This resonance is not related to the electronic structure of the defect itself and is only due to the scattering of the two-dimensional electron gas off the inhomogeneities [98].

The small peak below the Fermi-level (I), which belongs to the spectrum of misaligned defect (green curve) could be either a superposition of B-type defect electronic state and neighboring normal A-type molecule's LUMO-state, as can be clearly seen from the coincidence of positions of the peaks with LUMO of the normal molecule (black curve) or can be the LUMO+1 state of the defect itself. Peak I was not observed in the spectra of A-type defects because the spectroscopic measurements were performed in the center on the aligned defect. It is the position of the highest intensity of brightness (see Fig. 2.2) and the neighboring molecules were further away from the points of measurement. However, peak I could be a signature of the former LUMO+1 state, which will be discussed later.

Since the spectra of A-type defects have no additional peaks, only the electronic structure of B-type defects will be discussed from here onwards, with the exception of the cases which will be mentioned specifically.

2.3.III. Conductance peak at the Fermi-level

Peak II seems to be related to LUMO-state of the PTCDA molecule, which is indicated by the topography image recorded in vicinity of the Fermi-level (Fig. 2.3 c) where the defect looks almost identical to the normal molecule (imaged at the LUMO-bias). This peak can be detected only within the bright areas of the defect which coincide with the LUMO-maximum

of the normal molecule. The resonance at the Fermi-level was observed before in many cases: PTCDA [40], C_{60}[99, 100] and NTCDA[101]. According to Ref. [40] PTCDA may exhibit a Kondo-resonance when it is peeled from the surface. The Kondo-effect can only be observed if the orbital is occupied by a single electron with unpaired spin.

This state is well-known for magnetic impurities situated at nonmagnetic surfaces [102]. There are also a few examples where non-magnetic particles acquire magnetic properties, however this is not associated with a Kondo-nature. Charged gold adatoms have a peak close to Fermi-level due to partially occupied molecular orbitals (SOMO and SUMO) [103]. An enhancement of intensity of the peak was obtained in the case of C_{60} when the molecules were adsorbed onto a K precovered Cu(111) surface[100]. It was explained by half-filling of the LUMO by the donating of electrons from the K atoms below the C_{60} molecule.

If the peak at the Fermi-level is a LUMO-derived Kondo-state one can expect a split of the LUMO into three peaks [104, 105]. A singly occupied level at energy ε_0, a doubly occupied level at the energy ε_0+U, and the Kondo resonance at the Fermi-level (ε_0 and U are the energy of the molecular level and Coulomb repulsion respectively) [40]. This agrees well with the conductance spectra (Fig. 2.2). However, spectroscopic images taken at the energies of 0 meV and ±200 meV show the electronic structure of the different shapes (Fig. 2.3 b-d).

2.3.IV. Conductance peaks I, III and IV

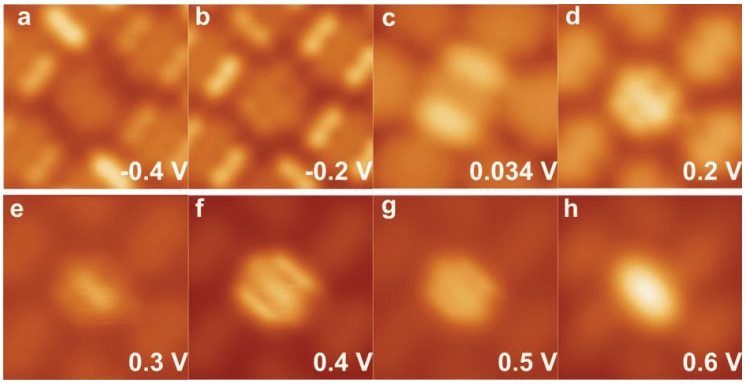

Figure 2.3. dI/dV images recorded at constant height regime (a,b,d-h) and topography (c) of B-type defect: 2.5×2.5 nm², 20 nA (a,b,d-h) and 0.2 nA (c). The image reveal similar to calculated for the bulk PTCDA LUMO-like structure of the defect (see Fig. 2.4).

The second model used to explain the nature of the peaks I and III is the formation of singly occupied states (SOMO) [104]. When a molecule contains an odd number of electrons, there

is an orbital which has only one electron making the orbital half empty (half filled). Thus, an additional electron can be either taken from this orbital or inserted into it, which gives peaks in the dI/dV spectra which are symmetric with respect to the Fermi-level. Peaks I and III in fig. 2.2 are also almost symmetric with respect to the Fermi-level. As for the odd number of electrons in the system, PTCDA in bulk has 200 electrons per molecule. Deposition onto Ag(111) substrate brings an additional 0.5 electrons to the system [83, 106]. However, due to the unclear structure of the defect, the exact number of electrons is difficult to define.

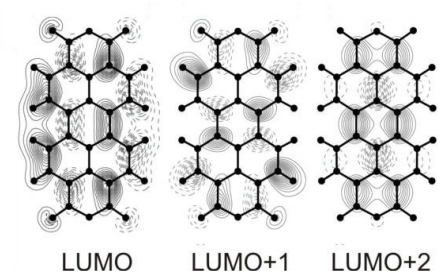

Figure 2.4. DFT Calculated wavefunction probability amplitudes of the lowest unoccupied molecular orbital LUMO, LUMO+1 and LUMO+2 of PTCDA. Images are courtesy of M. Rohlfing, taken from the ref. [83].

The constant height dI/dV mapping at bias voltages +0.2 V and -0.2 V reveals that the electronic structures of the defect are the identical to each other at these energies (Fig. 2.3 b,d), which could indicate that the states are similar in nature. The shape of the defect orbitals is similar to that calculated for LUMO+1 (Fig. 2.4) [83]. This contrast vanishes with changing the bias further away from the Fermi-level (Fig. 2.3 a,e,g,h).

Another possible explanation for the origin of peak III can be a split LUMO, one part of which pinned to the Fermi-level (peak II). This behavior was observed in the case of C_{60} molecules [99, 107] and NTCDA [101]. The split of the molecular orbital was explained as derivative of adsorbate-substrate interaction.

The next feature which is attributed to the B-type defect is a peak (IV) at 0.4 V. This resonance is most likely to be the LUMO+2 state of the point defect, since the spectroscopic image recorded at this voltage shows very similar shape (Fig. 2.3 f) to the theoretically calculated image of the LUMO+2 of the PTCDA molecule in the gas phase (Fig. 2.4) [83].

2.3.V. SPECTROSCOPIC MEASUREMENTS AT DIFFERENT TIP HEIGHTS

The tunneling current has an exponential dependence on vertical tip position, which implies the intensity of the peaks should have the same dependence. However, in contrast to expectations, the resonances III and IV move towards the Fermi-level, reduce their intensities, and become broader with tip approaching (Fig. 2.5 b). The similar amount of the shift infers that the nature of the process is the same.

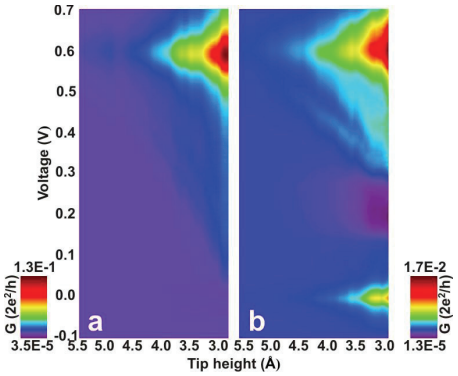

Figure 2.5. A map of the conductance spectra of PTCDA measured above a B-type defect (a) at the center of the defect and (b) at the LUMO-lobe maximum intensity as a function of tip-surface separation. Stabilization point: -340 mV, 0.1 nA. Modulation frequency 618Hz, modulation amplitude 4 mV.

These observations can be explained by reducing the Coulomb repulsion via tip screening or by Stark shift. Reducing the Coulomb repulsion leads to a smaller amount of energy needed to fill the SUMO with the second electron, and as a result the SUMO-state shifts towards the Fermi-level. The dependence on tip height can be related to the Stark shift, which is the influence of the electric field between the STM tip and the surface on the STS spectra [108]. It was reported recently that the Stark shift takes place in STS spectra of the Ag(111) [109], Au(111), and Cu(111) [110] surface states and was suggested to be a general feature of scanning tunneling spectroscopy [110]. In our case, vertical tip movement by 1 Å leads to a shift of the LUMO+2 state of the defect PTCDA molecule by 0.09 V, which is of the same order as the shifts reported in the literature.

All peaks related to molecular orbitals states are subject to influence by lateral tip movement (Fig. 2.5 b) and become negligibly small with respect to bound state in the center of defect (Fig.2.5 a).

2.3.VI. MANIPULATION OF THE DEFECTS

The origin of the defect formation so far remains unclear. In order to understand it, the method of manipulation of the molecules was used.

The molecules were first picked up by an STM tip, laterally displaced to another position and put down (detailed procedure will be presented in section 3.4). Firstly removal of molecule from the layer will show what is underneath (Ag(111) structural defect, CO molecule…). Secondly, the captured molecule can be deposited back to the surface to see whether it has the same properties as in the compact layer.

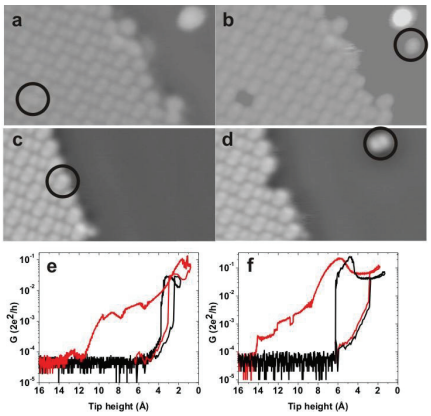

Figure 2.6. Displacement of the defect (a,b,e) and normal (c,d,f) molecules. Constant current STM images (a-d) 15×7.5 nm², 0.1 nA, -340 mV. At e) and f) black curve corresponds to pulling resulted in molecule falls back, red curve - molecule is on a tip. Modulation amplitude 618 Hz, modulation frequency 4 mV.

The molecule was displaced from the PTCDA layer to a new position on bare Ag(111) surface (Fig. 2.6 a,b). The manipulations were also carried out with normal PTCDA molecules and showed the molecules staying intact after the procedure. However, none of the experiments with manipulating the defects show entire molecules after displacement (Fig. 2.6 c,d). This observation indicates that the defect molecule reacts differently with the tip than normal molecules, leading to the breaking of molecular skeleton during manipulation procedure. However, it could also be the case that the defect is a molecule which was destroyed from the beginning (damaged chemical skeleton) or during evaporation from the Knudsen cell.

In addition, the spectra of approach and retraction of the tip during pulling and dropping of the normal molecules and the defects are significantly different (Fig. 2.6 e,f) from the measured spectrum at defects. The behaviour of both A and B-type molecules under pulling

was discussed in detail in the literature [40]. As for the pulling of structural defects, due to a combination of operating at almost zero voltage and the presence of the LDOS at the Fermi-level, the current jumped to the maximum immediately after the tip-molecule contact formation. In contrast, with a normal molecule the maximum current is achieved after 2 Å retraction. The dropping spectra of normal molecule and defect are difficult to analyze since they are not always reproducible.

2.3.VII. Hydrogen sensitization of the STM tip

In order to expose the chemical structure of the defects, the mechanism of hydrogen-sensitized STM-junction [111] was applied. It turned out that the defect molecule of both types (A and B) may have different chemical skeletons even if they belong to the same type as far as electronic image is concerned (Fig. 2.7 a,b). The defects are usually brighter than normal molecules and have either the same chemical structure or are missing one of the rings, containing oxygens (Fig. 2.7 a,b).

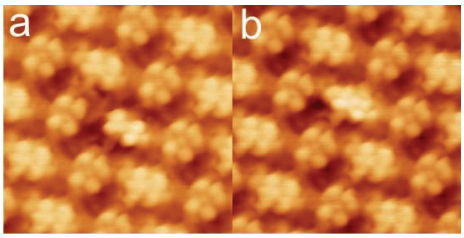

Figure 2.7. dI/dV images of A-type defects (a,b) taken with a use of hydrogen sensitized tip reveal different number of rings. At a) the ring containing anhydride oxygen disappears, whereas at the b) it is present. 2.5×2.5 nm², 0.1 nA, 10 mV.

In the case of B-type defects one of the rings of the perylene core can switch its contrast and becomes dark (Fig. 2.8 c); moreover, the an additional bright feature appears in the image when measuring at positive bias (Fig. 2.8 e).

These observations show that electronic property modifications can be caused by changes in defect chemical structure.

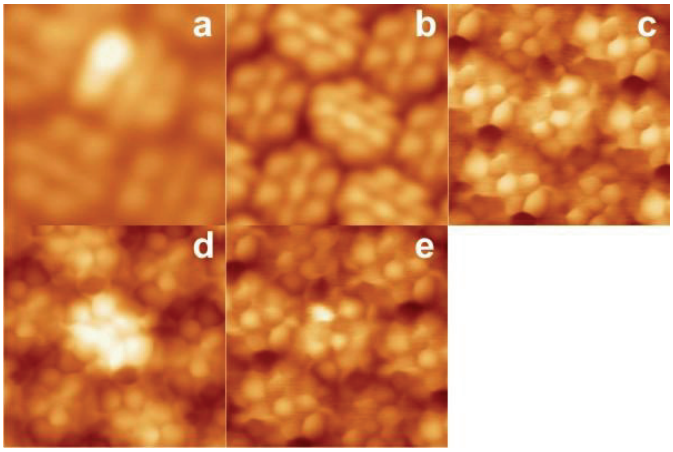

Figure 2.8. Topographic images of PTCDA layer containing structural defects of both types recorded at different voltages with functionalized (a,b) and hydrogen-sensitized (c-e) tip: a,b) -340 mV, c,d) -600 mV, e) 600 mV, (a,c,e) - B-type defect, (b,d) - A-type defect. The spectroscopic images reveal different structure of defect molecules. 2.5×2.5 nm², 0.1 nA.

Besides, one can see the rotation of the B-type defect molecules by ~3° relative to the other B-type molecules (Fig. 2.9). The rotation may lead to rearrangement of the defect molecule - surface bonding and endows the molecule with the uncommon electronic properties discussed above.

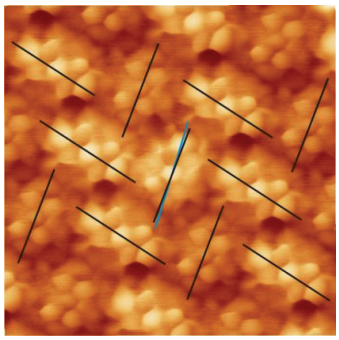

Figure 2.9. Rotation of a B-type defect (in the middle) relative to other normal B-type molecules. Constant current STM image: 5×5 nm², 0.1 nA, 10 mV.

2.3.VIII. MODELS.

Differences in the electronic properties of the defects with respect to normal molecules indicate that electron transport through the defects goes in a different way: since there are more peaks in the STS spectra, there are more molecular states which the electrons can tunnel

to. Changing of the bonds between the normal PTCDA molecule and the Ag(111) surface seems to be the likely explanation for structural defect formation. These changes can be the result of different influences. Two models will be used to explain the change, along with their advantages and shortcomings.

2.3.VIII.I. Ag adatom

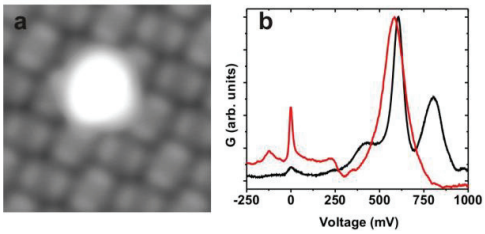

Figure 2.10. Constant current STM image (a) and spectrum (b) of PTCDA layer covered with Ag cluster. a) 5×5 nm², 0.1 nA, -340 mV. b) black curve - spectrum of B-type defect measured before the cluster deposition; red curve - spectrum measured above the cluster. Modulation frequency 816 Hz, modulation amplitude 4 mV.

The existence of an Ag adatom underneath the molecule may explain the presence of particular electronic properties. The distinction between type A and B defects can be due to different positions of adatoms relative to defect molecule since type A and B defects belong to different sublattices. It is known that the LUMO-state of normal B-type molecules is shifted further from the LUMO of bulk PTCDA compared to the LUMO of A-type. This is the evidence for less charge transfer between A-type molecules and the surface. Since the bonds have different strengths, different influences on the defect properties can be expected. In addition, several PTCDA molecules were covered by silver, including the B-type defect (Fig. 2.10). The following redistribution in the conductance intensities was observed (Fig. 2.10): the resonance at the Fermi-level increases ten times over the covered area irrespective of whether there is a type A, type B or defect molecule underneath and the intensity becomes comparable with a bound state. At the same time as resonance IV vanishes, an additional peak at -0.12 appears, which could be the shifted SOMO-state (peak I in Fig. 2.2). The topography images of the PTCDA island after the removal of a defect sometimes reveal a bright spot remaining in the area of the former defect site; nevertheless, it could be a fragment of broken molecule, which goes together with the second model.

2.3.VIII.II. Reaction with water molecule(s)

The PTCDA molecules are hydrophilic: the anhydride groups react with water molecules very easily under atmospheric conditions and form a carboxylic acid [112]. It is also known [113] that water is combined with PTCDA and can be released together with evaporated PTCDA. As a result, decomposition of the PTCDA molecules leads to the loss of carboxylic or carboxylic and anhydride groups, and these fragments of PTCDA (with lost groups) stick onto the surface. The established "broken" molecule can be either symmetric or asymmetric (which is seen in the images as well). The asymmetry may lead to a tilt of the compound relative to the surface and a situation similar to the lifted PTCDA molecule [40] may happen. These compounds are positively charged (+2 or +4), which may play a role in the formation of the two types of defects. Different compounds can be responsible also for the presence or absence of the rings at "hydrogen"-images.

2.4. CONCLUSION

Properties of the intrinsic structural defects in the PTCDA/Ag(111) interface were investigated. Two types of defects were observed depending on the sublattice of the surface they belong to. The structural properties of both types of defects can be either the same to the normal molecules or different. The difference can consist of missing one of the rings by the defect molecule or the acquisition of additional end groups; in addition, the B-type defects have a rotation of ~3°, which results in a stronger interaction with the surface. The electronic structure of the defects is significantly different from the normal molecules. The 2D electron gas scattering from the defects leads to formation of a bound state at 0.6 V. The split LUMO state or formation of the SUMO and SOMO state from former LUMO+1 were observed only at the B-type defects and were dependent on the lateral tip positioning. The possible nature of the defects was discussed but still remains unclear. Two models were suggested to try to explain the nature of defects: Ag adatom underneath the normal molecule or breaking of the normal molecule due to reaction with water.

CHAPTER 3.
MOLECULAR MANIPULATION

3.1. INTRODUCTION

Since the early 1990's when Eigler and Schweizer first used the STM tip to position individual atoms on the surface [114], a number of studies have been reported aiming to understand the underlying physical mechanism from experimental and theoretical points of view. The displacement can be realized by both lateral movement [37, 38, 41, 57, 115-133] of the adsorbate (Fig. 3.1 a) and vertical manipulations [134-140] (Fig. 3.1 b).

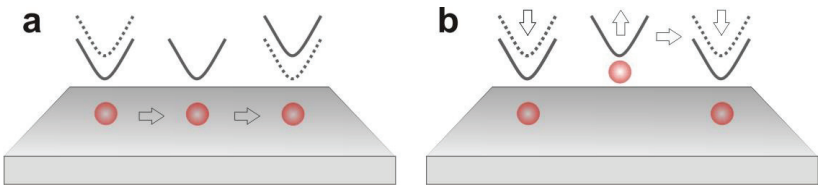

Figure 3.1. Lateral (a) and vertical (b) manipulations of an adsorbate with an STM-tip

Both attractive and repulsive interactions can be involved in a process of lateral manipulation [120]. In the case of attractive nature of the force, the adsorbate follows the STM tip, being pulled by it. For the repulsive case, the STM tip pushes the adsorbate across the surface. Vertical manipulation can be realized only when an attractive interaction takes place between the tip and the adsorbate. The tip and surface binding sites can be considered as a double well potential. The tip-side potential minimum is deeper because the tip apex has fewer neighboring atoms than a surface atom, thus the tip-adsorbate binding is stronger than surface-adsorbate [94].

In this chapter, realization of vertical and combined (vertical and lateral) manipulations of the PTCDA molecules will be discussed.

3.2. CONTACTING A SINGLE PTCDA MOLECULE

3.2.I. CAPTURE AND UNCONTROLLED DETACHING

Recently the possibility of contacting a PTCDA molecule with an STM-tip was discovered [40, 85, 141]. A molecular wire between a surface and a tip can be formed via approaching

the tip to one of the carboxylic oxygens and breaking the chemical bond between it and substrate. A new chemical bond is established with the tip apex atom. A molecule cannot be only contacted but also peeled from the surface continuously by increasing the tip-surface separation. Transport through the single molecule for different geometries can be measured in a controlled way by measuring the dI/dV spectra during the pulling procedure. These measurements reveal a change of the electronic properties of the junction during stretching. For example, the effect of reverse chemisorption was observed [40, 85, 141].

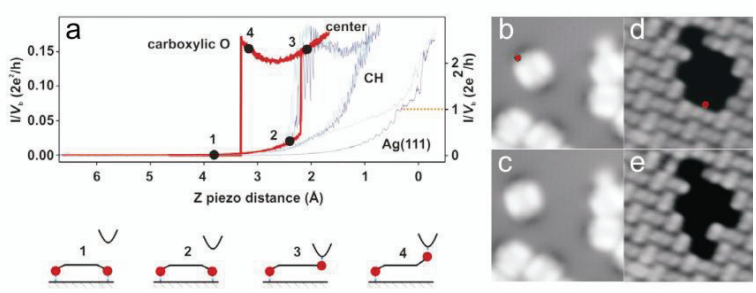

Figure 3.2. Contacting a PTCDA molecule. a) Approach and retraction spectra recorded above various parts of a molecule and bare Ag(111), as labeled (2 mV) with a schematic view of the contact formation process. Taken from Ref. [38] b-e) Constant current STM image of the uncontrolled lateral displacement of an isolated and edge molecule during pulling procedure (0.1 nA, -340 mV, b,c - 5×5 nm², d,e – 7.5×7.5 nm²)

In previous work [40], it was shown that a PTCDA molecule establishes a bond with an STM tip via substitution of one of the Ag(substrate) – O chemical bonds to Ag(tip) – O bond. The exact part of the molecule which interacts was determined by comparison of the current spectra taken above the different parts of the molecule recorded during tip approach. Two abrupt jumps in the current curve corresponding to capture and detaching of the molecule from the tip were observed only when approaching to the carboxylic oxygen atom (Fig. 3.2 a). Detaching of the molecule from the tip leads to uncontrolled molecular deposition back to the surface to the same or different position depending on the molecular surroundings in the initial state.

When performing the experiments on the molecules inside the ordered layer, the molecule occupies the same position in the PTCDA layer after being detached from the tip. However, the lateral displacement of the isolated molecule and the molecule at the edge of the island was observed (Fig. 3.2 b-e). The influence of the molecular surroundings on the behavior of the molecule under tip approach and retraction will be discussed in section 3.7.

3.2.II. STRETCHING OF A MOLECULAR JUNCTION

Besides the situation when the molecule is detached from the tip and flips back to the surface, there is the possibility to remove the molecule from the substrate. The molecule can follow the smoothly retracted tip and end up being completely peeled from the surface.

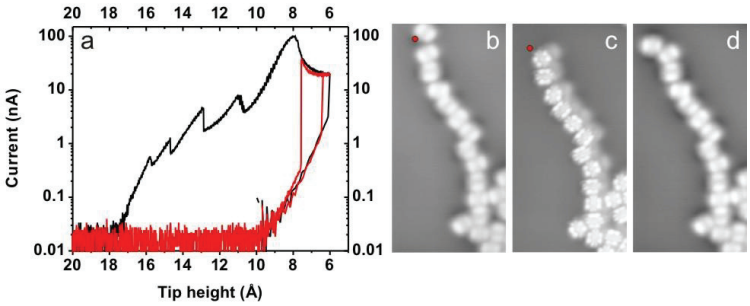

Figure 3.3. a) Approach and retraction spectra of STM-junctions measured at 4 mV with different outcomes after the stretching of the junction. Black curve – the molecule remains on the tip. Red curve - the molecule falls back to the surface. b-d) Constant current STM images of an artificially created chain of the PTCDA molecules: -430 mV, 0.1 nA, 7.5×15 nm². b) The clean STM tip approaches to the red point where the carboxylic oxygen of a molecule located in order to capture a molecule. c) The STM tip is functionalized by the molecule being captured (see b). d) After release of the molecule to the desired position on the surface the tip has conventional resolution

From the *I(z)* curves measured during approach and retraction, the outcome of the stretching process can be predicted (Fig. 3.3 a). During retraction of the tip, a sudden drop of the current corresponds to the jump of the molecule out of contact. The molecule is detached from the tip and flips back to the initial position on the surface. The current drop occurs at tip-surface distances (*z*) which are about 1-2 Å larger than for a capture, meaning that the molecule is slightly peeled from the surface when it falls back. Absence of the current drop at the small *z* indicates the molecule remains attached to the tip. Additional current jerks appeared at larger *z* (12-20 Å) corresponding to the sliding of the molecule over the surface. The sliding of the molecule can result in two situations: the entire molecule stays on the tip or it flips back to the surface [40].

These two outcomes are difficult to distinguish from the *I(z)* curves. However, in the topographic images recorded right after retraction of the tip one can see whether the molecule is on the tip or on the surface.

If the molecule is connected to the tip, the resolution of the STM increases ('functionalized tip'). In the former place of the molecule, nothing can be found (Fig. 3.3 b,c). However, in the

case of displacement the resolution remains normal and only the molecule changes its position on the surface (Fig. 3.2 c-e).

3.3. CONTROLLED DEPOSITION OF A SINGLE MOLECULE WITH THE STM TIP

Removal of the molecule from the layer does not give any advantage of molecular manipulation (such as transport measurements or building nanostructures), and it contaminates the STM tip. Approaching to the surface with the molecule on the tip does not result in a deposition of the molecule onto the substrate when the same parameters as for capture are used. One has to either dip the tip into the bare surface or to apply a high voltage pulse to get rid of the molecule which leads to destruction of the surrounding area (normal tip cleaning procedure, see section 7.3). Also one does not know whether the molecule is broken by stretching or remains intact. Thus the possibility of controlled deposition of the molecule to a definite position on the substrate can answer questions about molecular structure after stretching and open the gate to building nanostructures.

The controlled molecular deposition of a PTCDA molecule onto a defined position on Ag(111) surface turned out to be possible. By varying the bias voltage and the tip height, suitable parameters for molecular deposition were found. The molecules remain intact (Fig. 3.3 c) confirming the harmlessness of the transport measurements to the molecular properties.

3.4. PROTOCOL FOR CAPTURE AND CONTROLLED DEPOSITION OF A MOLECULE

3.4.I. CAPTURE

A very small bias voltage was used to contact the molecule. Actually, bias is needed only for recording a current and monitoring the junction behavior, because the formed molecule-tip bond is strong enough to remove the molecule from the surface.

The process of capture was performed with a bias voltage within the range ±5 mV. The bias polarity as well as its value does not influence the character of the current curves. The only necessary condition for the process to occur is for the tip to be brought into close vicinity of carboxylic oxygen. After stabilizing above the oxygen (-340 mV, 0.1 nA) the STM tip is moved vertically by 5 Å towards the surface with the feedback switched off so that the contact between the tip and the molecule can be formed. While lowering the tip, the abrupt increase of the current occurs when the tip is moved by approximately 4 Å from its

stabilization point. This jump corresponds to the jump of the molecule into the contact with the tip.

3.4.II. DEPOSITION

The STM tip, with a captured molecule attached to it, was stabilized at a height above the definite position on the surface where the molecule should be deposited (-340 mV, 0.1 nA). A bias voltage of 600 mV was applied to the sample with the feedback switched off. The tip was moved vertically towards the surface by 5 Å and then retracted by 15 Å in order to stretch the molecule. Current spectrum during the tip movement was recorded. The success of deposition was checked by subsequent imaging of the surface (the tip is clean, the molecule is on the surface (Fig. 3.3 d)).

3.5. BUILDING OF THE MOLECULAR STRUCTURES

Knowledge of the protocol for capture and deposition of a molecule allows for manipulation of them and for building molecular structures of a desired shape on the surface. Two parallel chains, a quadrate and a circle were built on the Ag(111) surface (Fig. 3.4).
In principle, nanostructures of different forms can be built from PTCDA molecules. The only limiting factors for the shape are molecular orientation on the surface and bonding to the surrounding molecules, which will be discussed in the next section.

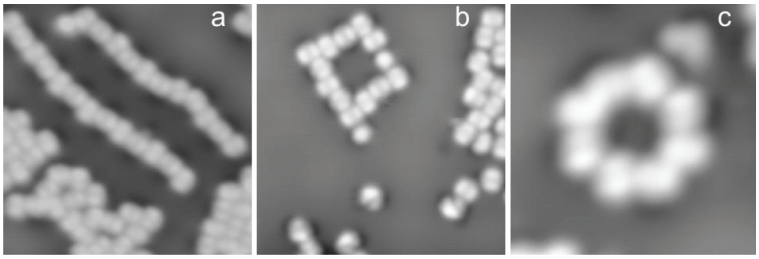

Figure 3.4. Constant current STM images of the artificially made molecular structures: -340 mV, 0.1 nA. a,b) 15×15 nm², c) 7.5×7.5 nm²

3.6. MOLECULAR ORIENTATION ANALYSIS

The same applies as for the ordered or low temperature phases when depositing the molecules on the surface; they tend to be located perpendicular to each other. This orientation is dominant because of the hydrogen bonds which are responsible for the molecular ordering on

the surface [83]. The hydrogen bonds are established between the carboxylic oxygens of one molecule and the hydrogen atoms (one or two) of the neighboring one. The relative position of two molecules can be different which leads to a small shift of the molecules with respect to each other (Fig. 3.4 and 3.5).

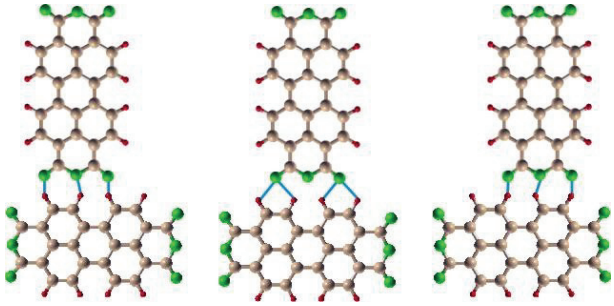

3.5. The hydrogen bonds between two PTCDA molecules corresponding to the molecular ordering observed in the manipulation experiments

The tendency of the molecules to be connected to each other can be examined by weak diffusion of the molecules over the surface even at very low temperature (7K). This agrees with the result of the formation of the PTCDA molecules in a "precursor" phase when deposited onto a cold substrate [91].

By applying high voltage while depositing a molecule the energy can be spread over the surrounding area leading to the "heating" of it and thus inducing the reorganization of the hydrogen bonds between the molecules. The released energy seems to be enough not only to move one molecule but a chain of them. A relative shift of the position of several molecules caused by deposition of a new one can be seen in Fig. 3.6.

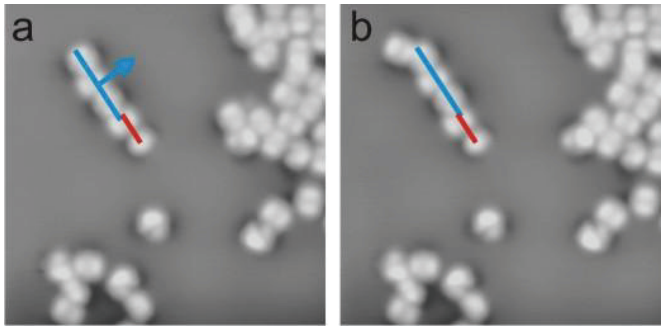

Figure 3.6. Rearrangement of the hydrogen bonds after high voltage was applied. A group with three molecules is shifted with respect to the bottom edge molecule after depositing a new molecule at the top of the chain. -340 mV, 0.1 nA, 15×15 nm²

However, perpendicular arrangement is not a necessary condition for molecular building. A molecular chain can be bent on purpose in order to construct a molecular circle, for example (Fig. 3.4 c).

The molecules can be deposited on the bare surface or attached to an existing island. However, if there are molecules in close vicinity of the place of deposition, the trapped molecule attaches to other molecules rather than remain isolated. This happens due to strong intermolecular interaction resulting in the presence of the attractive field, which forces a molecule to bond to its neighbors [83]. The interaction is so strong that during building of the two parallel chains they tended to be bent towards each other. Due to the large strength of the hydrogen bonds the molecule is much harder to remove from the inside of the island than from the edge. This observation brings us to the next section.

3.7. Role of the molecular surroundings in the success of the capture procedure.

To realize the manipulation process, four types of the PTCDA molecule were probed to be captured by a tip: single isolated molecules, non-isolated molecules in the disordered phase (Fig. 1.2 b), molecules at the edge of an island, and molecules resided in a compact PTCDA island. All four types reveal a different disposition towards being removed from the substrate by the STM tip.

The molecules residing in a compact layer are the most difficult to remove due to the hydrogen bonds to the adjacent molecules which prevent it from being captured by the tip.

The percentage of successful removals from the layer is much lower than 1%. In most of the cases the molecule flips back to the surface while the tip is retracted (Fig. 3.3, red curve). The molecules at the edge of the island and the molecules in the disordered phase exhibit similar behavior because both types have less order in the hydrogen bonding than the “island” molecules. Although they can be more easily removed from the surface, they still tend to stay on the surface. The percentage of successful removals reaches 1-50 %, depending on the tip state.

A single isolated molecule is very unstable due to the absence of intermolecular interactions which in-turn prevents a molecule from being displaced. So this molecule can be easily trapped by the STM tip because it has no neighbors and thus no hydrogen bonds.

The strength of one hydrogen bond is about 5 kcal/mol for the $C - H \cdots O$ bonds [142], which is approximately 200 meV (1 kcal is equal to $2.6*10^{22}$ eV and 1 mol contains N_a number of

atoms). This means that to remove a molecule from inside the island one needs to overcome approximately a 1eV higher potential barrier than for an isolated single molecule.

The *I(z)* spectrum (black curve in Fig. 3.3) of an isolated molecule has only one jump of the current corresponding to the capture of the molecule. After the tip is retracted the molecule stays on it. This behavior agrees with the density functional theory (DFT) calculations which predict that the molecule remains on the tip [141] which will be presented in the next section.

3.8. THE REASONS FORCING A MOLECULE TO SWITCH: THEORY AND EXPERIMENT

3.8.I. JUMP INTO THE CONTACT (UPWARD TO THE TIP)

According to DFT calculations, the spontaneous upward switch of the oxygen atom by 1.4 Å occurs when the tip is within 6.2 Å from the surface [141]. This value agrees very well with the experimental results where the most likely distance, *z,* for the capture of the molecule is 6.65 Å [40]. The DFT calculations were performed for a fully relaxed single isolated molecule on Ag(111) surface. The calculations were done for the silver tip with a pyramid shape apex. Silver material was taken because this case is more likely in the experiments. The tip was indented into the silver surface for sharpening which leads to the tip being covered by silver. Also calculations performed for a silver tip show better agreement with the experiments than tungsten [141].

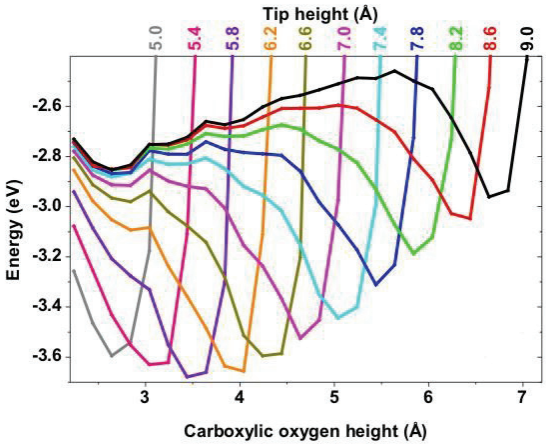

Figure 3.7. Calculated potential energy of the fully relaxed single isolated molecule as a function of the height of one of the carboxylic oxygen atoms. The tip height scale is shown at the top. The shallow minimum belongs to the potential energy of the oxygen at the surface side. The deep potential is for the oxygen on the tip side

The upward switch of a carboxylic oxygen atom happens when the total energy potential changes from a double well to a single well due to approaching of the tip (Fig. 3.7). At heights, *z,* smaller than 6.2 Å the energy barrier separating the two wells on the tip and on the surface sides disappears leading to the sliding of the oxygen to the local energy minimum on the tip side.

Experimentally the upward switch was detected in the *I(z)* spectra during approaching to all types of the molecules (isolated, edge, island). The only difference observed was the tip height *z* when the switch occurs. According to the NIXSW studies [92, 143] the distance between the substrate and the oxygens of a single isolated molecule is smaller by 0.18 Å in comparison with ones belonging to a molecule residing in the compact layer (see section 1.3). In agreement with this, the flipping of the oxygen atom to the tip occurs at larger values of *z* with the isolated molecule. Jump into contact of the "island" molecule (Fig. 3.8 red curve) occurs 0.2-0.3 Å earlier than for the isolated one which tells that transition from a double well situation into a single well happens at smaller *z* for the isolated molecule.

3.8.II. JUMP OUT OF THE CONTACT (DOWNWARD TO THE SURFACE)

3.8.II.I. Uncontrolled molecular detaching

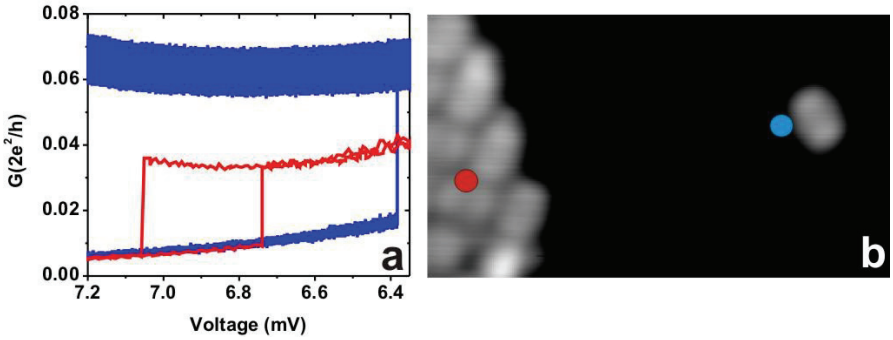

Figure 3.8. a) Spectra of the pulling of the PTCDA molecules from the surface (black curve - molecule at the edge of the island, red curve – molecule inside the island, green curve – isolated molecule). Modulation frequency 816 Hz. Modulation amplitude 4 mV. b) STM image (-340 mV, 0.1 nA, 10×5Å²) of PTCDA island and a single artificially isolated molecule with the points where the spectra a) were measured. -340 mV, 0.1 nA, 10×5 nm²

After the tip side is occupied by the oxygen, the tip can be moved both directions (toward and backward). According to the DFT calculations, it does not lead to the oxygen switching back

to the surface side, because as one can see from the Fig. 3.7 the tip site is energetically more preferred for the oxygen.

In spite of theoretical predictions there are experimental cases when the bond established between the oxygen and the tip breaks and the molecule flips back to the surface. Frequency of this event depends on the type of the molecule under manipulation. Thus, a single molecule stays attached to the tip much more often (90%) than a molecule in the island (<1%).

As was previously mentioned, the calculated potentials are valid for the situation of a single isolated molecule; therefore the calculations illustrate behavior of an isolated molecule only. The rare cases of uncontrolled detaching of the molecule from the tip during retraction can be explained by the tip apex shape modification. Flipping of the molecule to the tip may cause to the altering of the pyramid form of the tip apex thus changing the potential diagram.

The potential energy surface of a molecule residing in the compact layer can be significantly modified due to the changing of the molecular environment. Therefore, Fig. 3.7 should not be applied to the "island" molecule. Apparently, bonding to the neighboring molecules deepens the potential well on the surface site. However, the switch of the oxygen back to the surface cannot be explained only by potential deepening. Further calculations of a potential energy diagram should be performed for a molecule residing in the compact layer.

3.8.II.II. Controlled molecular deposition

Controlled deposition (see Section 3.3 for details) takes place when a bias voltage of 600 mV is applied to the junction. In Fig. 3.7 one can see that the depth of the potential on the tip site is smaller than 600 mV at large *z*. Thus if the whole energy caused by bias is released on the excitation of a vibration of the oxygen atom, it can overcome the potential barrier and the molecule can be dropped from the tip. The question of vibrational excitations will be discussed in greater detail in Chapter 6.

3.9. IMAGING THE OXYGEN SWITCHING

In the previous sections (3.6 and 3.7), the stability of the PTCDA molecule residing in the compact layer was shown to be against removal from the surface. Nevertheless, the jumps of the oxygen atom in and out of contact occur when the tip is moved down and up respectively. Such observation brought the idea of the possibility to detect the molecular switches during imaging of the PTCDA island.

According to the spectroscopic measurements, when the tip is brought close enough to the surface, the carboxylic oxygens of a molecule react with the tip showing a higher conductance. Indeed white speckles in the image can be seen at the positions of the corner oxygen atoms if the tip scans the surface at a very low height (4 mV, 10 nA) (Fig. 3.9).

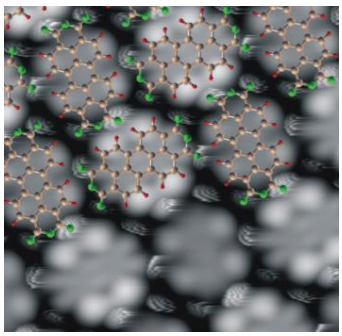

Figure 3.9. Constant current image of PTCDA layer recorded with functionalized tip. White speckles correspond to flipping of the carboxylic oxygen atoms into and out of the contact with an STM tip. -4 mV, 10 nA, 5×5 nm²

The difference in the reactivity of the oxygen atoms can be seen depending on the number of hydrogen bonds they are involved in [83] and molecular orientation [40]. Oxygens which have two hydrogen bonds reveal a higher reactivity in the images.
In the next section another factor which influences the reactivity of oxygens will be discussed.

3.10. SINGLE SWITCHES AT LOW BIAS

In all of the experiments described in the previous sections, very low bias voltage was applied to the junction (with the exception of molecular deposition). This was done in order to compare experimental results with theoretical calculations which were performed for zero bias. Thus the question of voltage influence to the switching process remained unanswered. In order to fill this gap in the investigations, additional measurements were done. The *I(z)* spectra for approach and retraction were measured at different bias voltages. The same was observed as for very small biases within the voltage region of (-45… 45 mV), only spontaneous single switches were observed during approach and retraction of the tip, independent of the bias polarity. This is reflected in the current spectra by the two steps corresponding to the capture (step upwards) and detaching (step downwards) of a molecule from the tip (Fig. 3.10).

The smaller the voltage, the larger the difference in the position of these two steps. At very small biases, it reaches a value of 0.6 Å (Fig. 3.10). Capture of the molecule happens closer to the surface than when it is detaching.

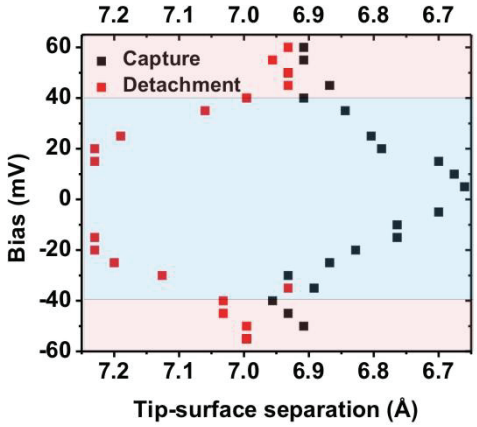

Figure 3.10. The tip heights corresponded to capture and release of a molecule from a tip as a function of bias voltage. Hysteresis is observed at low bias region and disappears with increasing voltage together with turning a system to the repeated switches regime.

When the voltage is increased, the positions of the steps start to approach each other until finally, at voltages above 45 mV, they coincide with each other, moving the system into the repetitive switching regime.

3.11. Conclusion

Realizations of manipulations of single PTCDA molecules were shown to be possible on an Ag(111) surface. Capture of the molecule happens during approach of the STM tip, independent of the bias value and polarity, due to a transition of the potential energy surface from a double well situation to a single well. Release of the molecule from the tip can happen in two ways: uncontrolled detaching of the oxygen and controlled molecular deposition. Reasons for the detaching remain unclear, while controlled deposition (600 mV) can be explained by the excitation of the oxygen vibrations and sufficiency of the bias to overcome the potential barrier. Analysis of the oxygen response to the tip movement and of molecular orientation leads to the conclusion that the molecular environment plays an important role in the process of manipulation. The bias voltage applied to the junction defines the distances at

which the jumps of the oxygen into and out of the contact with the tip occur. Molecular manipulations can be used for building molecular nanostructures.

CHAPTER 4.

MOLECULAR SWITCH

4.1. INTRODUCTION

The experiments described in the previous chapter show that the transfer of the oxygen atom from the surface to the tip and vice versa is possible. However, the underlying mechanism of such manipulation was not completely understood. Particularly unclear was the detaching of oxygen from the tip being in contradiction to DFT calculations of the potential surface.

In this chapter detailed quantitative experiments performed in order to understand the nature of the switching process will be considered.

In contrast to the previous chapter, all measurements will be realized by applying a high bias voltage *(V)*. Current spectra *I(t)* were measured above carboxylic oxygen at different tip heights, *z,* and *V*. At certain *z* and *V* the current spectra revealed two level fluctuations between two states with different conductance values.

These two states are associated with the two positions of the carboxylic oxygen atom of a PTCDA molecule. The high conductance state corresponds to the oxygen being bonded to the tip. Note that the rest of the molecule remains connected to the surface [141] so that the system is in the transport regime. The low conductance state corresponds to the conventional tunneling situation when all oxygens are bound to the surface. Transition between the two states will be called a molecular switch.

The frequency of the switches as well as the fractional occupation of the states depend on *z* and *V*. In order to plot a 2D map displaying dependence on both variable parameters two methods of measurements were used, which are fixed tip height/ variable bias voltage and fixed bias voltage/ variable tip height.

Very careful measurements were performed for many bias voltages and tip heights leading to a large quantity of recorded data. Programming in Mathematica software was used to reduce the amount of processing data.

4.2. PROCESS OF MEASUREMENTS: TECHNICAL DETAILS AND DATA DESCRIPTION

4.2.I. TECHNICAL DETAILS

Most of the analysis was done for the data obtained with the additional data acquisition module from National Instruments NI USB-6211. However, part of the data was recorded without the data acquisition device with the best resolution obtained being equal to 0.8 ms.
For the spectra recording, the variable-gain low-noise Femto DLPCA-200 preamplifier was used. The gain of 10^9 allows a bandwidth of 1.2 kHz, which is sufficient for the conventional spectroscopy but not enough for detection of the fast switches. For the switching recording, a gain of 10^6 was needed (bandwidth is 200 kHz). However, the STM software allows the recording of data with a maximal frequency of 25 kHz. In order to increase this value, an additional data acquisition module with a characteristic resolution of 8 μs (125 kHz) was introduced to the system to record the data independently from the STM program.
The experiments were done on two types of molecules: molecules residing in the compact layer and at the "free" oxygens of the motecules in the edge of the island. Without the data acquisition module the "island" molecules were probed, whereas the measurements on the "edge" molecules were performed with the use of it.

4.2.II. METHODS

4.2.II.I. The first method: fixed tip height, variable bias voltage

The tip was positioned above a carboxylic oxygen at the stabilization point (-340 mV, 0.1 nA). The feedback was switched off, the tip brought close to the surface and the current spectra were measured as a function of bias. The measurements were started with a tip-surface separation of 7.8 Å and finished with 6.6 Å with steps of 0.05 Å. The bias voltage was changed from -200 mV to 200 mV and back to -200 mV during 120 seconds. The bias was changed with a step of 5 mV meaning that for each of the 81 different bias voltages (-200, -195, -190…0…190, 195, 200 mV) the time spectrum duration is about 1.5 seconds.
At large z (7.8 Å…7.35 Å) no switches were observed and the junction was in the low conductance state. When the tip approaches closer to the surface (7.25 Å), fluctuation of the current appears in the spectra (Fig. 4.1 a). One can notice that there are many more switches

at negative bias, which will be discussed later. Further approach leads to the increase of the number of switches for both voltage polarities (Fig. 4.1 b). When the tip is brought very close to the surface (6.85 Å) the high conductance state is prefered for the junction (Fig. 4.1 c) and finally at 6.6 Å the configuration where the molecule is bound to the surface and the tip becomes stable in the whole range of measured bias voltages (Fig. 4.1 d).

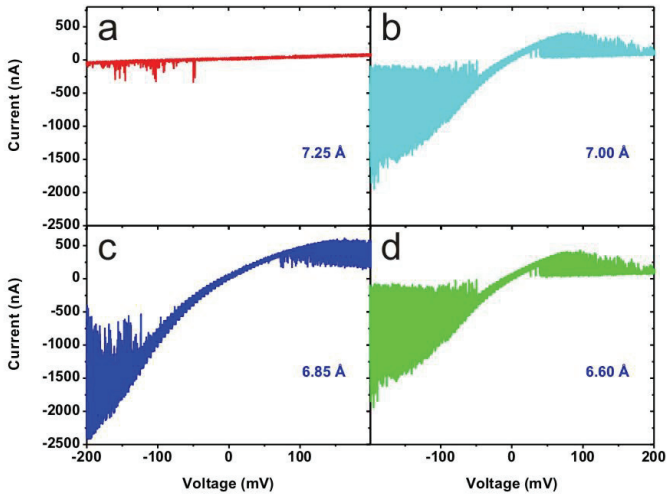

Figure 4.1. Current spectra of the STM-junction as a function of bias voltage taken at different tip heights. The transition of the junction during the tip approach from the low conductance state for the whole measured bias range (a) to the high conductance state (d) can be clearly seen. At the intermediate heights the junction switches between two states depending on the bias applied. Measurements without data acquisition module

4.2.II.II. The second method: fixed bias voltage, variable tip height

The same as for the first method, the tip was positioned above a carboxylic oxygen at the stabilization point (-340 mV, 0.1 nA). The feedback was switched off, the chosen bias voltage was applied to the sample, and the tip was moved slowly towards the surface starting from the tunneling regime until it reached a distance lower than where the tip-oxygen bond is established and was then retracted (Fig. 4.2). The *I(t)* spectra as a function of distance were measured for both negative and positive biases. Current spectra measured at low biases ($|U|$<50 mV) always reveal at least two steps (up and down) in the current corresponding to the jump of the junction into and out of contact with the tip (Fig. 4.2 red and green curves). Raising the bias leads to (i) an increase of the number of switches and (ii) a change of the tip

height where the repeated switches region starts and ends (Fig. 4.2 black and blue curves). The spectra were measured during approach and retraction of the tip in order to check the influence of the direction of movement to the switching behaviour.

In Fig. 4.2 one can see that after switching to the high conductance state the junction exhibits a tendency to decrease in conductance. This effect is caused by pushing the oxygen atom towards the surface. The charge transfer between the molecule and the substrate occurs mostly via the LUMO-level of the molecule [40]. This level shifts towards the Fermi-level

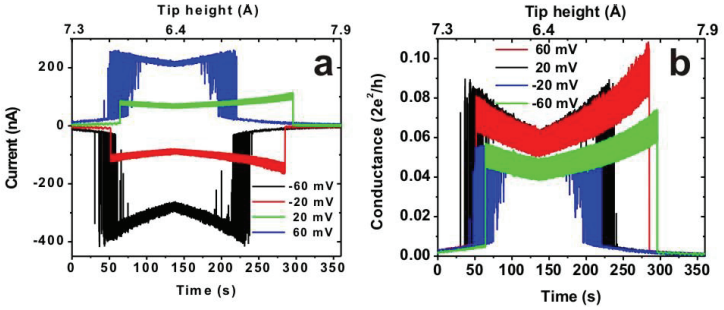

Figure 4.2. Approach and retraction spectra of current (a) and conductance (b) of the STM-junction measured at positive (blue and green curves) and negative (black and red curves) bias voltages. At low biases (red and green) only two steps corresponded to the jumps of the molecule into and out of contact have been observed whereas at higher biases (black and blue) the junction is unstable revealing repeated switches. Measurements without data acquisition module

when the molecule is peeled from the surface (reverse chemisorption) [141] and moves from the Fermi-level when the molecule is pushed towards the surface. Thus pushing on the molecule leads to reducing the LUMO intensity at the Fermi-level and as a result decreasing the conductance near zero bias.

It should be noted that the distance region where the junction turned from one stable state (oxygen is bound to the surface) to another (oxygen is bound to the tip) via an intermediate (switches) state lays within the region of less than 1 Å.

The tip state influences the rate of the switching process so that for some tips no switches were observed. The tip height at which the switches start also varies from one tip to another. To have better statistics the spectra series were measured several times for the different tip states.

The method of measurement was found to be of little consequence for the switching process and the switching behavior of the junction, which is nearly the same independent of tip approach or retraction (will be discussed in Section 5.4).

4.2.III. MEASUREMENTS WITH THE DATA ACQUISITION MODULE

Due to the similarity of the results from both methods the second one was used for data recording with the additional data acquisition module. With the use of the module, five series of measurements were performed: four series for positive bias voltages (I – from 45 mV to 100 mV (tip height was changed from 7.9 Å to 7.0 Å), II – from 50mV to 120 mV (tip height was changed from 8.1 Å to 7.3 Å), III – from 70 mV to 250 mV (tip height was changed from 7.9 Å to 7.3 Å), IV – from 60 mV to 130 mV(tip height was changed from 7.7 Å to 7.1 Å)) and one for negative (from -50 mV to -140 mV(tip height was changed from 8.1 Å to 7.3 Å)). The bias voltage was increased with a step of 5 mV from one spectrum to another.

Each spectrum was measured for 15 minutes with the tip velocity less than 0.1 pm per second, which gives 112.5 million points per spectrum (about 2 Gb of memory). The tip states for the negative series and for the second positive series were the same, whereas for the three other positive bias series different tips were used. The starting tip height was chosen in such a way that the oxygen atom does not yet react with the tip, which was determined from a short test spectrum measured before recording the to-be-analyzed one. During the spectra the tip was linearly lowered by 0.7 Å towards the substrate. Due to the similar behaviour of the junction during retraction of the tip, only the approach spectra were recorded to reduce the amount of data to analyse. The difference between the junction behaviour during approach and retraction for positive and negative bias voltages will be discussed in the next sections.

4.3. DATA PROCESSING

4.3.I. EMPLOYING MATHEMATICA SOFTWARE

When the measurements were performed, the questions of access to the data and analysis were raised. One spectrum consists of 112.5 million points and requires 2 Gb of memory. Far from analysing the data, none of the commonly used programs (Origin, Excel, Access) could manage to open such a huge file.

At first MatLab software was used to try to access the data. However, it turned out to be unsuitable for the analysis because it does not allow one to see the raw data; due to that the accuracy of the analysis could not be checked. Because of these reasons MatLab was excluded from the list of possible solutions.

As an alternative, Mathematica software, which is based on the C programming language, was used. The latest version of Mathematica (7.0) allows the use of parallel computing. On any multicore computer system it is automatically set up to be able to run multiple parts of a computation concurrently. So Mathematica 7.0 seemed to be more suitable for the switching analysis.

In order to be able to look at the data in the file and to check the accuracy of the computation after analysis, the files were split into smaller parts (25 Mb each) using Total Commander. The partitioned file may contain the erroneous numbers in the first and in the last lines because Total Commander counts number of bytes in the file but not number of points. Therefore, the edge points will be deleted but this will be taken into account during the analysis.

Every file contains two columns of data. The first one is the piezo voltage corresponding to the tip height and the second one is the voltage corresponding to the current. The voltage (distance) value is not absolute and cannot be recalculated uniformally for all of the files, so this value cannot be taken as a reference. Current also changes from file to file due to the change of the bias applied. Therefore, the serial number of the string (i.e. the row number of the point in the original raw data) was taken as a reference because all of the points in the spectra within one series were measured for the same differencies in the tip height during equal time intervals. The tip height was adjusted at a constant rate, and thus the n^{th} string in every file corresponds to a constant height difference to the same point in every other file. Hence, the tip height for each data point can be worked out. However, to check the accuracy of this assumption one needs to access the raw data file. From this it is clear that one cannot use a program which only makes the analysis without allowing access to the raw data.

In order to reduce the amount of data, a program in Mathematica was written in such a way that only “important” points were included into a new file (the body of the program see in Appendix I). These “important” points are the points when the switch of the STM junction between two states occurs and will be used for statistical analysis of residence time.

For one full switch (up and down or down and up) 4 points are written down (Fig. 4.3) with the four significant values: the tip position where the switching starts and ends, and the current at the high and low states.

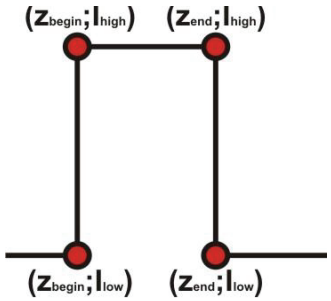

Figure 4.3. The significant points for the data processing. To every switching event correspond four important parameters: the tip heights where the switch starts and ends and the current values at the high and low states.

Due to the huge amount of the data produced by the data acquisition module the raw spectra cannot be shown. The spectra analysed by Mathematica program show similar behaviour to the one discussed in Section 4.2.II.II. At low biases there are only a few switches and at high biases the number of switches increases (Fig. 4.4).

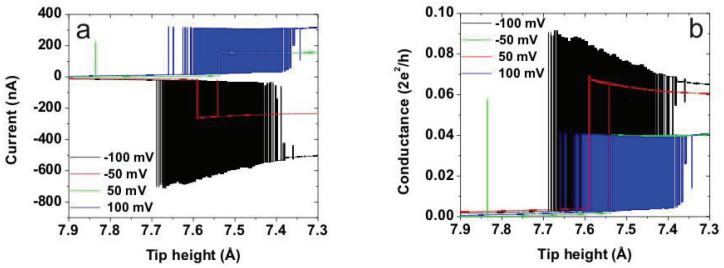

Figure 4.4. Approach spectra of current (a) and conductance (b) of the STM-junction measured at positive (blue and green curves) and negative (black and red curves) bias voltages. At low biases (red and green) only two steps corresponded to the jump of the molecule into and out of contact have been observed whereas at higher biases (black and blue) the junction is unstable revealing repeated switches. The spectra were processed with Mathematica program; the initial ones were taken with a data acquisition module. Input data for the processing procedure were taken from the results of series II.

Further analysis of the switching process was done using the processed spectra in the following way. The *I(t)* spectrum was cut into small pieces such that the tip height does not change significantly ($\Delta z \leq 0.05$ Å). In the parted spectra the assumption of a constant tip height was made. Within the spectrum two situations are possible: either there are switches of the current or there are none. The second case is not interesting for a switching analysis. If the spectrum contains switches then the distribution of the fractional occupation of the two conductance states differs from spectrum to spectrum. At large tip heights the junction is

mostly in the low conductance conformation (Fig. 4.5 a), changing to the equal fractional occupations when the tip moved closer to the substrate (Fig. 4.5 b) and ending up with a situation where the high conductance state is more favourable for the junction (Fig. 4.5 c).
The behaviour described above is common for every spectrum. The differences are in the number of switching events and the tip height where the switches start and end, both of which vary depending on the bias applied. Because the distance range during each spectrum was kept constant, this led to the situation where at high biases (>150 mV) the region where the oxygen spends most of the time attached to the tip could not be reached. Also, the duration of time the oxygen spends in the specific site becomes very small at high biases making it impossible to detect within an 8 μs time resolution, which is the characteristic resolution of the data acquisition module. The limitation of time resolution leads to all the switches which are shorter than 8 μs being written as a single switch with an 8 μs duration. This can influence very much the quality of the analysis if the residence time in the specific state is shorter than 8 μs. However, at the biases used in the experiment there is a sufficient amount of data points corresponding to the switches with longer residence times allowing the performance of good quality analysis.
Increasing the bias leads to an increase of the number of switches thus providing more statistics for careful analysis (Fig. 4.5 d-f).
As was mentioned before, the data acquisition device does not record the time corresponding to the spectra, so that the 'number of points to time' recalculation should be made. This was done automatically by the Mathematica program. Translation of the time value to the absolute tip height above the surface was performed later, with the Origin program in agreement with the tip height rescaling.

4.3.II. TIP HEIGHT CALIBRATION

The values for the tip height were calculated in the following way: it is known that the acquisition time for 1 point is 8 μs. The initial and final tip heights are set by the STM program. Knowing the difference between these heights and the time the tip has to travel it, one can calculate the tip velocity, which gives the possibility to determine the tip height as a function of time at every point with a simple equation:

$$z(t) = z_{start} + \frac{z_{end} - z_{start}}{t_{spectrum}} \cdot t \qquad (4.1)$$

Where t can be defined as $t = i/125000$ (i – number of point in the raw spectrum), z is the relative tip height defined by the STM program, and $t_{spectrum}$ is the spectrum duration.

In order to determine the absolute value of this coordinate, two types of additional experiments have been performed. The first one is contacting the bare silver surface (described in the supplementary information of Ref. [40]). In this method the STM-tip touches the surface, which corresponds an the increase in the conductance to a value larger than the quantum of conductance.

The second method for absolute tip height estimation is based on the measurement of a current above the molecule as a function of tip height. The tunnelling current decays exponetially with increasing distance between the tip and the surface:

$$I = I_0 e^{-2kz} \tag{4.2}$$

Where k is a decay constant and related to the local barrier height Φ by:

$$k = \frac{\sqrt{2m\Phi}}{\hbar} \tag{4.3}$$

However, the decay constant cannot be derived from the formula due to the unknown local barrier height (apparent work function), which is:

$$\Phi = \frac{\Phi_{\text{tip}} + \Phi_{\text{surface}}}{2} \tag{4.4}$$

The work functions of Ag(111) and PTCDA/Ag(111) interface are known to be 4.74 eV [144] and 4.75 [145], respectively. The work function of the tip, Φ_{tip}, is difficult to define due to the combination of two materials (tungsten covered by silver for the tip and PTCDA and silver for a surface) and the uncertain shape of the tip. To define the absolute tip height above the surface the decay constant values should be calculated. This should be done within the low bias region in order to exclude the influence of the bias on the electronic structure of the junction. Current was measured as a function of the distance above the carboxylic oxygen of the molecule. The current at 4 mV is plotted in Fig. 4.6a. Fitting the current curve with the exponential growth gives a value of 0.98 for the decay constant.

The current as a function of distance can also be calculated theoretically. The current was calculated with the help of the non-equlibrium Green's function formalism [146]. The value for a decay constant for 4 mV is 1.1 which is comparable with that obtained experimentally.

From the equation (2) and theoretical results the prefactor I_0 is equal to 0.0013 A. Using this value for fitting experimental data, the formula for absolute height calculation can be derived:

$$z_{tip\ height} = 10.8 - z_{STM\ program} \tag{4.5}$$

The comparison of the conductance of the junction obtained experimentally and theoretically is shown in Fig. 4.6 b.

Both methods (tip crash [40] and current measurements) give similar values for the tip heights where the switches occur. The disagreement between them is about 0.2 Å.

Although good agreement of the results obtained by different rescaling methods is obtained, the error of the distance estimation is relatively large (±0.5 Å) due to several factors: tip state,

the error of the distance estimation is relatively large (±0.5 Å) due to several factors: tip state,

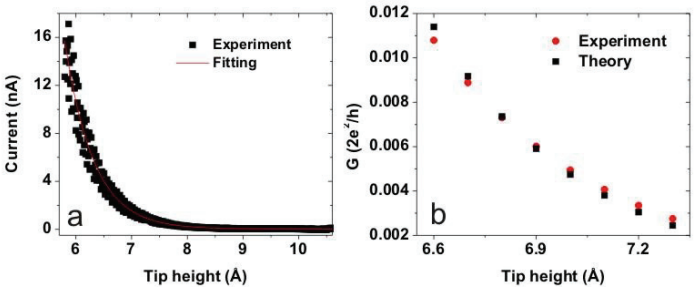

Figure 4.6. a) Current spectrum of the STM junction as a function of tip height (black points – measured data, red curve – exponential decay fitting) measured during approach to a carboxylic oxygen. b) Conductance spectra of the STM junction as a function of tip height (red points – experimental results based on a), black points – calculated values) measured/computed for the approach of a tip to a carboxylic oxygen. The tip heights are scaled according to the performed fitting procedure (see text for details)

STM program set-point reproducibility, etc. However, since the tip does not change during one series of experiments, the influence of the tip state can be excluded leading to smaller errors within one series of the measurements.

4.3.III. PROGRAM DESCRIPTION

As was said before the idea of the data processing is to reduce the amount of data by excluding the points that are not essential for residence time analysis. In every spectrum there are regions where no switches take place and where the junction switches recurrently between

the two states. At the beginning of the spectrum, no switches occur and the program averages the value of current for the given number of points (10000 for this particular case). The program applies the same averaging procedure every time when no switches take place within one file. The presence of switches in the file was checked for by comparing the maximum and the minimum values of current. If the difference between them is larger than the given value, then switches take place in the file and additional analyzing procedures are required to define the type of a switch (up or down), when does it happen, and how long does it take. Moreover the program should remember the "important" points attributed to the switches and write them down into a new file "Output".

After the finding that the file contains switches, the program starts to work on the identification of the switches within it. This is done by comparing the current value for the concerned point with the maximum (switch to down-state) and minimum (switch to up-state) current values, taking into consideration the variable given by the user together with a definition of the state which the previous point belongs to plus considering the difference in the currents for the two nearby points. If the current exceeds the minimum current by more than a given value, and current at the next point is higher than current at the concerned one, and the previous state was a down-state, then the junction switches from the low conductance state to the high conductance. If the current is less than the maximum current by more than a given value, and current at the next point is smaller than current at the concerned one, and the previous state was an up-state then the junction switches from the high conductance state to the low conductance state. The average values of the current for the high and low conductance states are defined for every file separately by averaging the current values within one file. For obtaining the average current for the high conductance state, the values when the current is larger than the maximum current minus α (where α is a variable parameter in the program) were taken into account. The same was done for the average current calculation at the low conductance state with the difference that the current should be smaller than the minimum current plus α.

The most difficult part of the data processing is to join the partitioned analysed files into one because there are files with switches and without. The switches may start in one file and end in the next one, which should be taken into account. One also should not forget that the edge points in the files are cut so that each file misses one or two points depending on how the file was partitioned. Assuming that usually the two points at the beginning and end of every file are missing, the program adds 2/125000 second to it when the local file time is computed. In order to bring the whole files together, the absolute time for a spectrum was calculated. The

final spectrum was saved into "Output" file. It is much smaller in size and thus possible to open, as shown in the Fig. 4.7 a.

Summarizing, the Mathematica program performs with raw files the following operations:

- Defining whether the partitioned file contains switches;
  - If not, averaging the current;
  - If yes, going to the next step;
- Finding the "important" points of the spectrum and writing them down;
- Joining the partitioned files into one;
- Calculating the residence times in high and low conductance state.

4.3.IV. CHECKING THE ACCURACY OF THE FINISHED DATA

The check of the accuracy for the performed analysis was done for one of the partitioned files. The program turned out to give a good agreement between the raw data and modified files with respect to the positions of switches and their duration (Fig. 4.7 b).

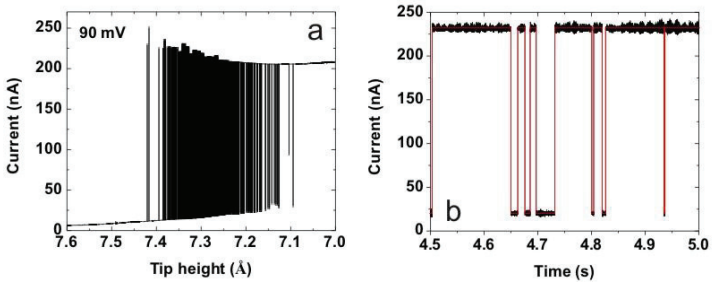

Figure 4.7. The analyzed data. Behaviour of the STM junction during a tip approach with 80 mV bias applied. a) The full analyzed spectrum. b) Checking the accuracy of the performed analysis. Black curve – raw data, red curve – finished spectrum. Input data for the processing procedure were taken from the results of series III.

The coincidence of the calculated points with the measured ones gives the opportunity to use the modified file to perform the residence time analysis. The residence time analysis is the most important part in the computing process because it is a starting point for performing the further analysis of the behaviour of the STM-junction. By the residence time, the time which the molecule stays in the certain (low conductance or high conductance) state is considered, namely: residence time in the low conductance state and in the high conductance state. The residence time computing was done by substracting the times corresponding to the adjacent

points. Comparing the current values for these two points defines what type of switch takes place: up or down. The residence time associated with a switch up was written down to "TimeUp" file, and that for a switch down to the "TimeDown" file, together with the current values and the time when the switches occur.
In order to check the accuracy of the residence time analysis another approach was used with a slightly modified Mathematica program (the program's body is in the Appendix II). The difference is that the times now were calculated for every partitioned file separately and later joined together. This turned out to play a negligible role in the final result and thus can be neglected.

4.4. CONCLUSION

Careful investigations of the switching process performed by different methods required a lot of time, not only for measurements, but mostly for processing of the data.
The switching process turned out to be dependent on bias voltage *(V)* and tip height *(z)*. The switching rate increases with bias and has a maximum at ~ 7 Å tip height. In order to investigate this dependence two methods of measurements were suggested. In both methods the *I(t)* spectra were measured varying only one parameter within one spectrum (V or z). Similar results were obtained with both methods, therefore the detailed investigation of switching process was done using only one of them. An additional data acquisition module was introduced to the system in order to increase time resolution of the experiments.
The quantity of measured data was reduced with a help of Mathematica program which allowed the performance of further quantitative analysis of the switching process, which will be presented in the next section.

CHAPTER 5.

SWITCHING PROCESS: ANALYSIS OF THE EXPERIMENTAL RESULTS

5.1. INTRODUCTION

After performing different kinds of experiments involving manipulating PTCDA molecules, attention was shifted to the understanding of the underlying physical mechanisms.
The adsorbate transfer can be caused by many reasons: coherent phonon process (for low bias) [147], vibrational heating (intermediate bias) [148-152], electronic excitations (high bias) [153], thermal activation[154], and by quantum tunneling (if the adsorbate mass is not too large) [56].
In this chapter, quantitative analysis of the measured data will be presented. The characteristic features of the switching process will suggest the theoretical model which can be applied to explain the observed behaviour.

5.2. SWITCHING RATE

From the experiment of the previous chapter, it is known that high voltage is needed to observe repeated switches. This energy can be gained from the inelastically tunneling electrons which travel through the molecule when the bias voltage is applied. The electric field accompanying the bias can influence the direction of the molecular motion [155]. During the manipulation, the STM tip is positioned over a molecule and tunneling electrons are injected. The energy of tunneling electrons is transferred to the molecule leading to the excitation of vibrations of the molecule which can result in switching, hopping, rotation, and even chemical reactions on the surface [61, 140, 156].
In the case of PTCDA on Ag(111), the transferred energy goes towards inducing the switching of the oxygen atom of a molecule between two sites: surface and tip. The number of switches depends on the bias voltage applied to the junction. The dependence of the switching rate as a function of the tunneling current and junction conductivity is shown in Fig. 5.1. Note that here, in contrast to the transfer rate which will be discussed later, the switching rate is just the number of switches independent of direction of the transfer (up or down).

Interestingly, the slope of the switching rate curve before the maximum rate is the same for all measured biases and is equal to 20. Whereas after passing the maximum, the switching rate decays with a different slope (7-13). This effect can be clearly seen in the Fig. 5.1 c where the switching rate is presented as a function of the junction conductance. The slope of the switching rate curve reflects the number of electrons involved in the process [46]. However, a value of 20 is very large in comparison to what was found in the literature [65, 157]. The switching rate decay with current increase was not observed before.

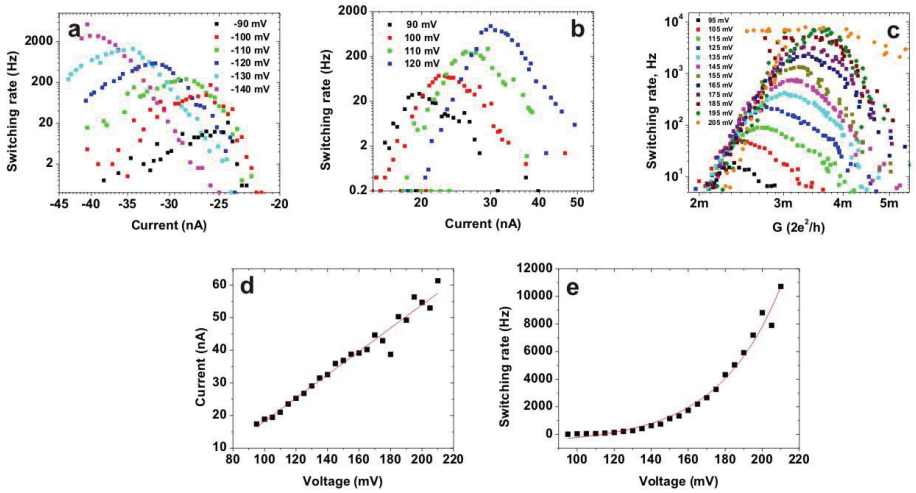

Figure 5.1. Number of switches as a function of tunneling current and junction conductance. Tunneling current implies the junction being switched down (low conductance state). The switching rate increases with increasing bias up to a certain value and then decays. Behaviour is common for both bias polarities (a,b,c). d) Current corresponded to the maximum switching rate as a function of bias voltage; e) Switching rate as a function of bias voltage. Input data for the processing procedure were taken from the results of series II (a,b) and III (c-e). m = 10^{-3}.

The current at which a switching rate has a maximum has a linear dependence on the bias voltage applied to the system (Fig. 5.1 d). With increasing voltage, the maximum of the switching rate increases exponentially (Fig. 5.1 e).

As one can see from the figures and as it was shown in the previous chapters the two level fluctuations strongly depend on the applied voltage. At low bias voltages single spontaneous fluctuations were observed, whereas at higher voltages the current fluctuates between the two states very frequently. From this observation, two regimes of the molecular junctions can be defined: single spontaneous switches in the low bias region and repeated switches in the high conductance region.

5.3. DEFINING THE PARAMETER WINDOW WHERE THE SWITCHING OCCURS

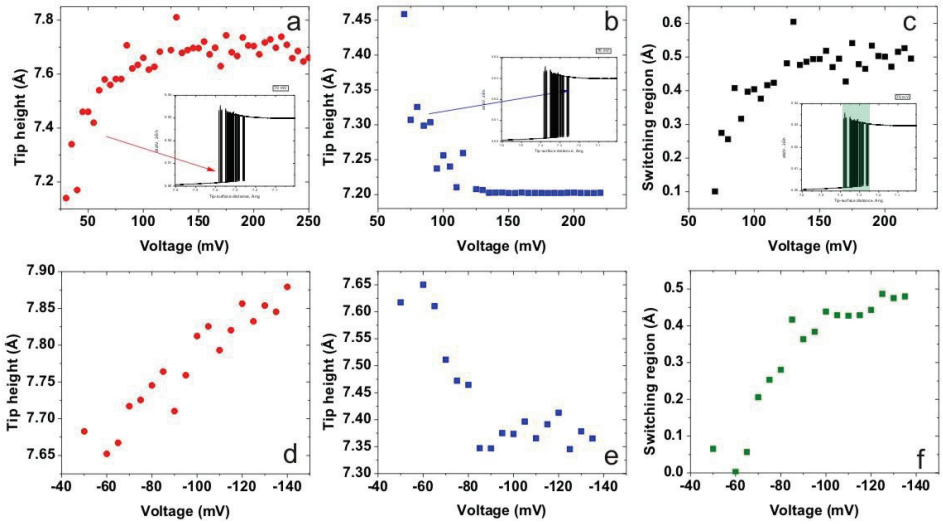

Figure 5.2. Tip height where the first (a,d) and the last (b,e) switch of a molecule between an STM tip and a surface occur and as a function of positive (a,b) and negative (d,e) bias voltage; c,f) The width of a tip heights window where switches were observed as a function of bias voltage (c – positive, f – negative). The maximum width of 0.5 Å were reached at 140 mV and stayed constant with further bias increase. Input data for the processing procedure were taken from the results of series II.

The applied bias influences the number of switches as well as the tip height at which they start and end. The lower the bias the closer the tip should be brought to reach the region of repeated switches. However, after 120 mV the tip height where the switches start reaches a value of 7.7 Å and remains constant with further bias increase (Fig. 5.2 a). As for the tip height where the junction stops switching, it goes down to 7.2 Å at 130 mV and stays constant for higher biases (Fig. 5.2 b). By subtracting the two heights from each other, the distance region where the switching takes place can be obtained (Fig. 5.2 c). It develops from the very narrow region (0.1 Å) at small voltages to approximately 0.5 Å for the voltages larger than 130 mV. The same analysis was made for the negative voltages and reveals similar behaviour with the only difference being that the switching window is situated further away from the surface, namely: approximately 0.15 Å higher (Fig. 5.2 d-f). For all series of measurements, slightly different tip-surface separation limits of the repeated switches were observed due to the influence of the tip state on the switching process and thus on the absolute tip height rescaling. However, the repeated switches region lays within the distances 6-8 Å of a tip above a surface.

For negative bias, the repeated switching region can be reached at greater tip heights than for positive bias. This may be explained by the fact that the PTCDA molecule is negatively charged, with a large charge density on the carboxylic oxygens [143]. They have lone pair electrons, which, due to the electrostatic forces appearing when a bias voltage is applied, can lead to a difference in the tip heights for the switches at negative and positive bias (Fig. 5.2). Another difference regarding the bias polarity one can notice from looking at the switching maps in Fig. 5.3 is that the switching rate at the positive bias region reaches its higher value faster than at negative voltages. However, for some tip heights, an absolute increase of the voltage leads to further rise of the switching rate at negative bias, whereas at positive bias it passes through a maximum and then decays (can be seen also in Fig. 4.1).

5.4. SWITCHING MAPS

The switching process was observed during both approach and retraction of the tip, showing similar behaviour apart from the tip height difference discussed above (Fig. 5.3 a). Due to this reason, further analysis regarding the approaching procedure will be considered.

As was mentioned before (cf. Section 4.2.II) the switching process can be monitored by two methods: with the bias voltage fixed at a certain value and the tip approaching the surface (Fig. 4.2) or with the tip height fixed within the window where repeated switches were observed and the voltage being changed (Fig. 4.1). The switching maps corresponding to both methods are shown in the Fig. 5.3 a,c (first method) and in the Fig. 5.3 b (second method). One can see that the course of the experiment does not influence the switching map results. This indifference provides the opportunity to stick with only one method of measurements: namely, to keep the bias voltage fixed within one spectrum.

The switching maps display well-defined regions the molecule switches repeatedly. When the proper tip height is chosen the repeated switching process starts from ±45 mV. The threshold voltage that is needed to induce two level fluctuations is independent of bias polarity. This is possibly due to the fact that the switching behaviour has a vibrational nature, and the electron energy produces the transfer of the molecule from one state to another independent of the direction of current. This will be discussed later in more detail.

The two level fluctuations were found to take place within the measured bias voltage regions up to 250 mV. However, further increase of bias might bring stability to the junction because in Fig. 4.1 b one can see that at high positive bias the junction tends to be stable on the surface

side. Unfortunately, the voltage values required for junction stabilization were not reached in the quantitative experiments due to the breaking of the PTCDA molecules at high bias. One should also not forget about the time resolution limit of 8 μs of the data acquisition module, thus, the fast switches attributed to the high voltages cannot be detected.

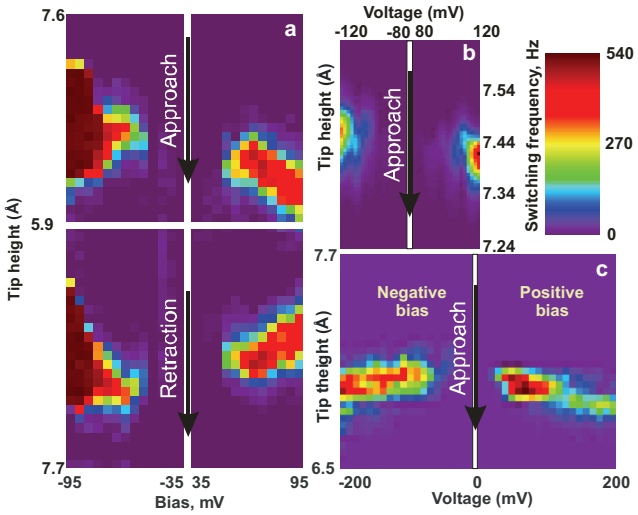

Figure 5.3. The switching rate maps as a function of bias voltage and tip height obtained from the different types of measurements. a,b) Bias voltage was fixed, tip height was varied; c) tip height was fixed, voltage was varied. All maps show similar behaviour of a junction. Map at a) includes also number of switches during retraction of a tip. Measurements were performed without (a,c) and with (b) a use of data acquisition module

From the definition of the voltage and tip height limits of the repeated switching, let us now turn to the quantitative analysis of the switching behaviour. One should note that the switching rate analyzed above is for the number of switches during a finite time and does not take into account the different type of switches: namely, switches of the molecule into and out of the contact with an STM tip. Thus, a small number of switches does not imply that a molecule prefers to be on the surface rather than on the tip. In order to understand the nature of the two level fluctuations the high and low conductance state should be separated and the analysis of both of them should be made.

5.5. TWO STATES ANALYSIS

So far, the switching rate characterizing the number of switches of the junction was considered. In this section the focus will be put on the differences of the states which the

oxygen atom occupies on the tip and on the surface sites respectively. The analysis of the residence times and fractional occupation as well as the transfer rate will be performed for two states separately.

5.5.I. RESIDENCE TIME ANALYSIS

The performed data processing gives access to the *I(t)* spectra of the STM junction. The residence times which oxygen spends in the each specific site were calculated. In order to perform further analysis the distribution of the residence time intervals should be considered. However, in order to perform the analysis, a sufficient number of switches are required to have better statistics. From Fig. 4.5 only the *I(t)* spectrum at 7.62 Å (Fig.4. 5b) can be used for residence time calculations because the other two have too few switches. Longer measuring of the spectra could solve the insufficient number of switches, however this brings the problem of thermal drift of the STM tip and sample in the experiment. The "time up" and "time down" residence time distributions of the spectrum are shown in the Fig. 5.4. At higher bias (140 mV) the spectrum reveals significant increase of the switching events in comparison with the time spectrum at 90 mV at the same tip-surface separation distance (Fig. 5.4 a,b). This leads to much better statistics and smaller errors during the following quantitative analysis of the residence times (Fig. 5.4 c,d).

When the switches of the PTCDA molecule take place, the behaviour of the STM-junction can be described by three situations: (i) low conductance state is favoured, (ii) the molecule spends equal time in both configurations, and (iii) the high conductance state is preferred. These outcomes are reflected in residence time distributions as (i) residence time at the low conductance state is significantly larger than at the high conductance state, (ii) they are almost equal (iii) residence time at the low conductance state is significantly smaller than at the high conductance state.

The residence times distributions obey the exponential decay of the first order. This tells that the process has no memory of the state it was in before. According to Markov's equation [158] the residence time probability density is given by:

$$P_{0,1}(t) = R_{0,1}(t) \cdot \exp(-R_{0,1}(t) \cdot t) \tag{5.1}$$

The transfer rate $R_{0,1}(t)$ is the power of the exponent and can be obtained from the residence time histogram.

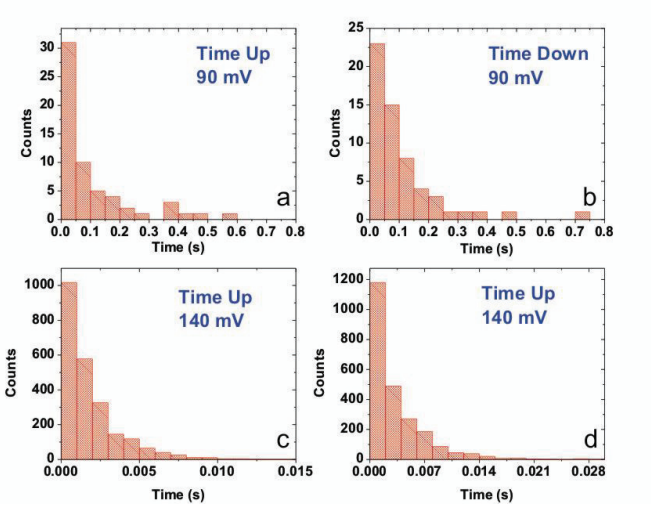

Figure 5.4. The first order exponential decay distribution of the residence times at low (Time Down) and high (Time Up) conductance states for two different voltages: 90 mV (a,b) and 140 mV(c,d). Increase of the bias leads to significant decrease of the residence times. Input data for the processing procedure were taken from the results of series III.

5.5.I.I. Oscillations in the residence time spectra

After passing through a voltage of 150 mV, switches with a residence time shorter than the time resolution of the data acquisition module take place, limiting the accuracy of the measurement. However, the number of switches with larger residence times is large enough to perform the analysis. Another problem the analysis faced with is the presence of oscillations in the exponential decay of the residence time (Fig. 5.7a).

Having a closer look at the curve, one can see the periodicity in the fluctuations. The period of the oscillations is 0.5 ms which is equivalent to 2 kHz and constant for all voltages and tip heights (Fig. 5.5 b). The state of the molecular junction does not influence the presence of the oscillations and they were observed for both high and low conductance states.

A Fourier transformation was applied to the time spectra of tunneling current to decompose the signal into the frequencies and amplitudes:

$$\hat{f}(\omega) = \int_{-\infty}^{\infty} f(t)\, e^{-2\pi i t\omega}\, dt = \frac{1}{\sqrt{2\pi}} \int_{-\infty}^{\infty} f(t) e^{-it\omega}\, dt. \qquad (5.2)$$

The transformation of segments of the time spectra in which the junction remain in either a low or high conductance state reveals a huge amplitude peak at 2 kHz (Fig. 5.7 c). It has several satellite peaks, and although their positions are slightly different depending on the junction state, the position of the main peak remains unchanged. The amplitudes of the two sets of peaks differ by a factor of 10 which is equal to the difference in the junction conductance in the tunneling and transport regimes (Fig. 5.5 c).

The peak around 2 kHz in the frequency spectrum is not surprising because the noise spectra of the STM always show a peak at this frequency (cf. Section 7.5). As will be shown later, the origin of the peak is most probably the eigenfrequency of the piezo-elements of the STM, which typically lies in this frequency region.

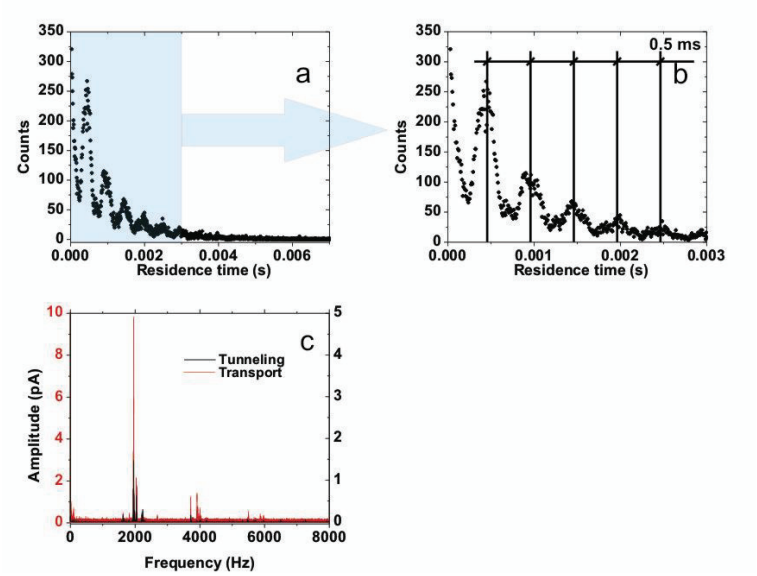

Figure 5.5. The residence time probability as a function of time (a,b). According to the Markov equation the residence time probability should follow an exponential decay. However, oscillations of the curve with 2 kHz frequency were observed during all measurements. They were connected to the eigenfrequency of the piezo-elements which was always present in the time spectra (Fig. 4.4). The Fourier transformation (c) of the time spectra measured with a molecule in and out of contact with a tip also reveals a huge peak in the amplitude at the frequency of 2 kHz. Input data for the processing procedure were taken from the results of series III.

The oscillation of the STM tip leads to the deviation of the residence time distribution curve from the exponential behaviour. Instead of the smooth exponential decay, fluctuations in the function between two exponents which correspond to the boundary states were observed. In

order to confirm the idea of the "noise" nature of these oscillations, the following analysis was performed.

5.5.I.II. Residence time distribution modeling

The equation applied for Markov process assumes that the residence times are measured with the experimental parameters kept constant in time. However, in the case of measuring the switches with the STM tip, it follows a sine curve with a period of 0.5 ms in time due to the presence of the 2 kHz frequency piezo-oscillations. Moreover, during the spectra the tip moves linearly towards the surface thus the final trajectory of the tip movement can be presented as a superposition of both types of motion (Fig. 5.6 a), and can be described by the formula:

$$z(t) = At + Bsin(\omega t + \varphi). \tag{5.3}$$

Here A is the velocity of the linear motion (0.01 Å/s), B ($1.5 \cdot 10^{-3}$ Å) is the amplitude of the tip oscillation, $\omega = 2\pi f$ is the angular frequency, φ is the phase of the oscillation. The transfer rates, $R_{up \to down}(t)$ and $R_{down \to up}(t)$, have a strong dependence on the tip height value. Within 0.5 Å distance the system changes from being in one state to another (Fig. 5.6 c). As one can see from the experiment at constant bias voltage, lowering the tip towards the surface leads to the exponential growth of the transfer rate from tip to surface, whereas the transfer rate value for a switch from surface to the tip decays exponentially. Summarizing, the residence time probability has a complex dependence on the time; however, the formula to describe it can be derived as follows:

$$R(t) = Cexp\left(-\frac{z(t)}{D}\right). \tag{5.4}$$

Using equation (5.1) and (5.4):

$$\begin{aligned} P(t) = R(t)\exp(-R(t)t) = Cexp\left(-\frac{Z}{D}\right)\exp\left(-Cexp\left(-\frac{Z}{D}\right)t\right) = \\ = Cexp\left(-\frac{At+Bsin(\omega t+\varphi)}{D}\right)\exp\left(-Cexp\left(-\frac{At+Bsin(\omega t+\varphi)}{D}\right)t\right). \end{aligned} \tag{5.5}$$

Where *C* and *D* are the constants to be fitted. They differ depending on the bias voltage and the tip height. With reasonable values for these constants this formula gives a residence time distribution curve of the same shape as was obtained after analyzing of the experimental data (see Fig. 5.5 b and Fig. 5.6 b).

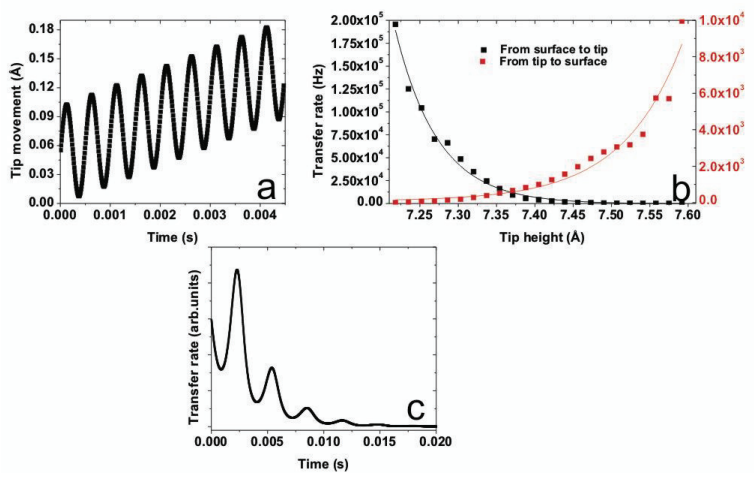

Figure 5.6. Residence time distribution modeling. a) schematic view of the tip trajectory during manipulations; b) residence time distribution as a function of time (compare to Fig. 4.7b) obtained numerically by using formula (1.13); c) the transfer rate depends exponentially on the tip height bringing the second exponent to the Markov equation. Constants: A = 0.01 Å/s, B = 1.5·10-3 Å, C=-300; D=3 Å. Input data for the processing procedure were taken from the results of series III.

A good fit of the modeling of the residence time probability to the one taken from the measurements allows us to conclude that the oscillations in the residence time curves are indeed due to the influence of the piezo-elements' fluctuations. For further transfer rate analysis, the exponent obtained from averaging over one measurement will be used.

5.5.II. Fractional occupation and time-average conductance as a function of bias voltage and tip height

The frequency of the two level fluctuations has a strong dependence on the bias. Besides this the voltage influences the occupation of the two conductance levels in such a way that at a fixed tip height, one can change the junction from one state to the other by altering the bias. This effect can be seen in Fig. 5.5. With increasing bias, the conductance of the junction

changes gradually from the high conductance state (oxygen is on the tip side) to the low conductance state (oxygen is on the surface side). For a given tip height and bias voltage, the time-averaged conductance as a function of the fractional occupation and conductance of the junction in both states can be obtained from the formula:

$$G = n_{up} \cdot \sigma_{up} + n_{down} \cdot \sigma_{down} \tag{5.6}$$

Here n_{up} and n_{down} are the fractional occupation numbers of the high and low conductance states with the conductance σ_{up} and σ_{down} respectively ($n_{up}+n_{down}=1$). Using this formula, one can calculate the time-averaged conductance as a function of applied voltage for every measured tip height (Fig. 5.7). The threshold bias voltage below which the system remains in the high conductance state ($n_{down} \approx 0$) depends on the distance between the tip and the surface. Larger tip-surface separations lead to a smaller threshold voltage. The junction is more stable in the high conductance state when the tip is brought closer to the surface.

Above the threshold voltage, the system starts to change to the low conductance state and saturates there. When the tip is far from the surface, this saturation happens at smaller voltages than for the close distances (see evolution in Fig. 5.7).

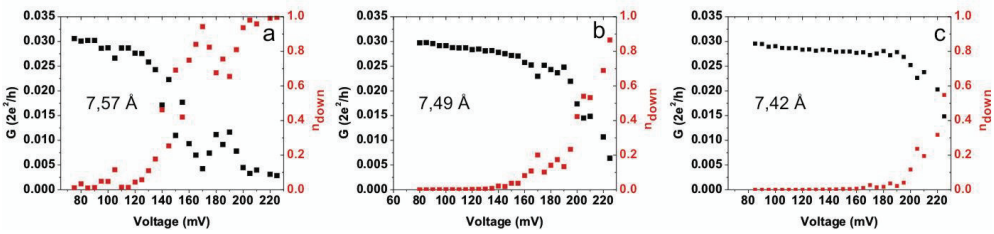

Figure 5.7. Fractional occupation (red points) and time-averaged conductance (black points) as a function of bias voltage calculated for different tip heights. The intersection of the two curves moves towards higher biases with lowering of the tip. Input data for the processing procedure were taken from the results of series III.

The two level fluctuations were investigated by changing the tip height above the surface with a fixed bias voltage. The inversion of the states occurs at different tip-surface separations depending on the voltage applied (Fig. 5.8). Higher biases shift the inversion height to smaller distances. This observation confirms the conclusion made before about the preference for the high-conductance state when at small biases and close distances (Fig. 5.8 c,f). The smaller the bias, the smaller the tip height at which the junction inverts its state. Therefore, in order to keep the system in the stable transport regime one should use small bias voltages.

The low noise level of the graphs in Fig. 5.8 and quite large noise level in Fig. 5.7 is due to the manner in which the experiment was done. The data points for both figures were taken from the same initial spectra, which were measured with the bias voltage being kept fixed while the tip height was changed. When one spectrum is measured, the tip is retracted to the set-point position. Although in the next spectrum it is sent to the same starting distance, the tip height might change slightly leading to a small shift in the z-scale. Since the two level fluctuation process is very sensitive to the tip heights, even a tiny difference in the altitude results in increasing roughness of the conductance curves. The data points for every curve in Fig. 5.7 were taken from 30 spectra, whereas in Fig. 5.8 (a,b,d,e) all points within one curve were taken from one spectrum.

By changing the bias voltage and tip height, the potential landscape of the system can be altered. It can be changed from being in one conductance state to another either by tuning the bias voltage or the tip-surface separation or both.

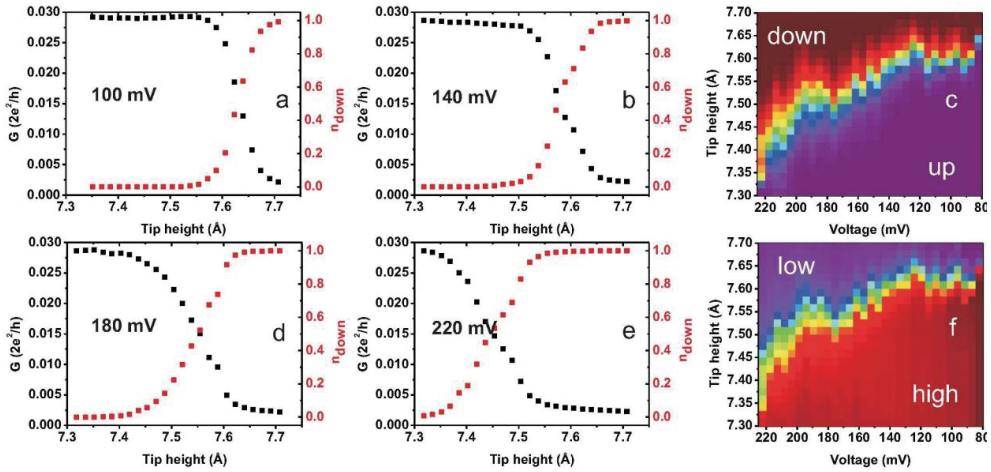

Figure 5.8. a,b,d,e) Fractional occupation (red points) and time-averaged conductance (black points) as a function of tip height calculated for different voltages. The intersection of the two curves moves towards smaller tip heights with bias increase; c,f) map of the fractional occupation (c) and time averaged conductance (f) as a function of bias voltage and tip height; c) dark red area – oxygen is bound to the surface, purple – to the tip, which affects to the time-averaged conductance f), where dark red is an area with a high conductance, blue – with low. Input data for the processing procedure were taken from the results of series III.

5.5.III. TRANSFER RATES

The transfer rates were calculated for every bias voltage and tip height. The range of bias voltages covered was from -140 mV to 250 mV, depending on the series. The tip height was varied within a window of 6-8 Å above the surface. Single transfer rate refers a single time spectrum of the tunneling current measured at fixed bias voltage during a period of 25 seconds. During this time the tip height was changed by approximately 0.017 Å, which allows us to say that the tip height was kept also constant. The exponential fitting was performed with Origin software.

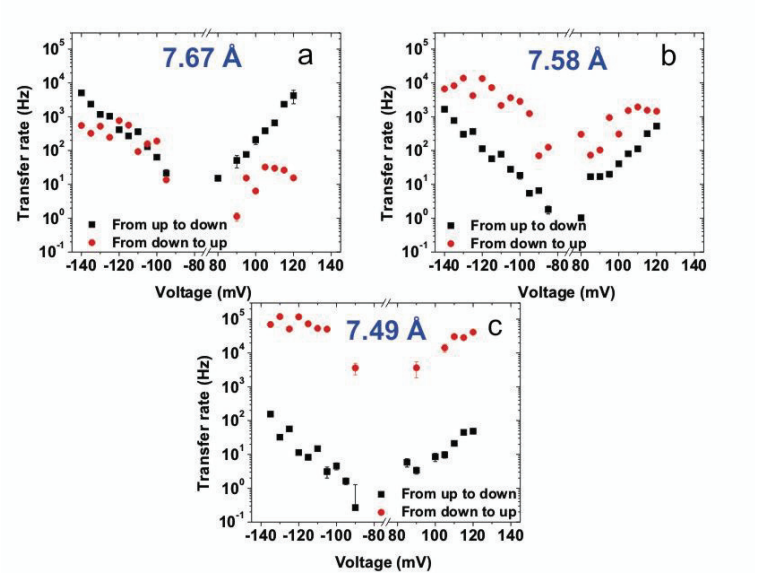

Figure 5.9. Transfer rates of the molecular junction as a function of bias voltage measured at different tip heights at negative and positive bias voltages. The black points correspond to transfer rate from the high conductance state to the low conductance state, and the red ones to the opposite direction. The transfer rates are nearly symmetric with respect to bias polarity. Input data for the processing procedure were taken from the results of series II.

Spectra taken from the different measurements (different tips) at both positive and negative bias voltages were analyzed. The whole set of produced graphs for four series of measurements is included into Appendix III.

Several of the transfer rate curves are shown in Fig. 5.9 and 5.10. All sets of the calculated transfer rates can be found in Appendix III and IV. The difference between the two figures is that the tip state was changed by dipping and applying a voltage pulse from one series to another. In total four series of measurements were done.

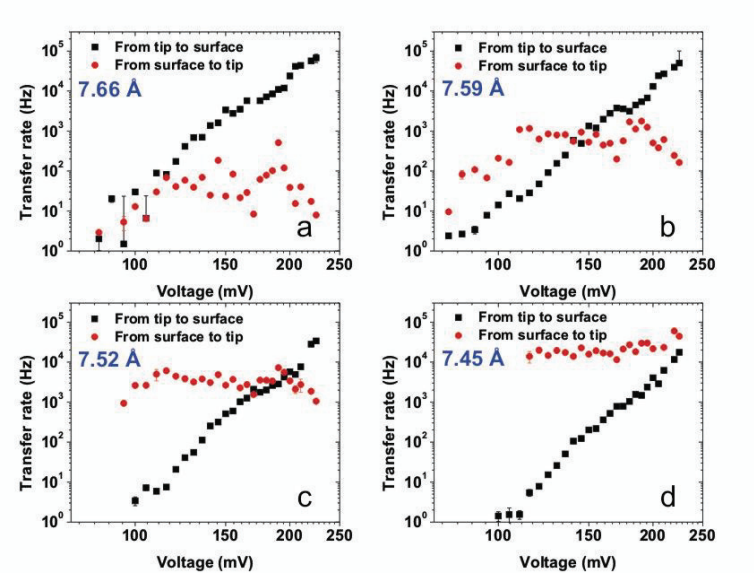

Figure 5.10. Transfer rates of the molecular junction as a function of bias voltage measured at different tip heights. The black points correspond to transfer rate from the high conductance state to the low conductance state, red ones – to the opposite direction. High to low transfer rate seems to follow the power law dependence with bias, whereas low to high transfer rate has a clear saturation at about 120 mV. Input data for the processing procedure were taken from the results of series III.

Analysis of all of them led to similar results independent of the polarity of the voltage and the tip states; the following observations are common for all of them:

- At large tip heights, the transfer rate of an oxygen atom from the high conductance state (from the tip) to the low conductance state (to the surface) is larger than the transfer rate in the opposite direction.
- At small tip heights, the transfer rate of an oxygen atom from the high conductance state (from the tip) to the low conductance state (to the surface) is smaller than the transfer rate of the opposite direction.
- The transfer rate from the high conductance state to the low conductance state increases with rising voltage within the whole range of measured biases. It seems to follow a power law with respect to bias voltage.

- The transfer rate from the low conductance state to the high conductance state growth with voltage up to 120 mV. After passing this value the transfer rate saturates and remains constant until the highest measured bias.
- Both transfer rates are nearly symmetrical with voltage polarity.
- The slope of the transfer rate (high→low) changes by a factor of 2 (from 8 to 16) with an altering of the tip height, whereas the change of the slope of the transfer rate in the opposite direction is significantly larger, although the exact values are difficult to determine due to the lack of number of points.

At large tip heights (Fig. 5.9a) one can notice the asymmetry of the red curve with respect to the bias polarity. The asymmetry most probably comes from the influence of the bias polarity on the shape of the potential well, which will be discussed in the next theoretical chapter. However, it disappears when the tip is brought close to the surface.

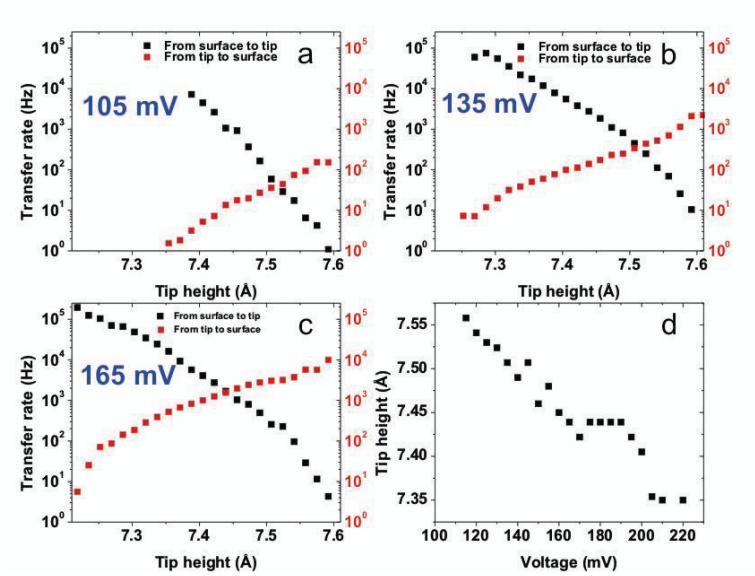

Figure 5.11. a-c) Transfer rates as a function of tip height measured at different voltages. The black points correspond to transfer rate from the high conductance state to the low conductance state, red ones – to the opposite direction. d) Tip height where inversion of the preferred state occurs as a function of bias voltage. Input data for the processing procedure were taken from the results of series II.

The transfer rates computed from the tunneling current spectra not only depend on the bias voltage applied but also on the tip heights. The transfer rates grow (from tip to surface) or decay (from surface to tip) with the tip height (Fig. 5.11). This behaviour was observed in all measurements, irrespective of bias polarity or tip state.

The position of the transfer rate intersection corresponds to the bias voltage and tip height where the preferred state of an oxygen atom changes from being on the surface site (low conductance) to being on the tip site (high conductance). The tip height for this inversion is inversely proportional to bias voltage (Fig. 5.11 d), however, it changes only by 0.2 Å with a change of bias of 100 mV.

5.6. CONCLUSION

The two level fluctuating PTCDA molecule turned out to be an ideal two-state switch, with clearly defined states with one order of magnitude difference in conductance. The high and low conductances are related to the different conformations of the molecule (in the high conductance state the molecule is connected to the tip and the surface, in the low conductance state the molecule is bound to the surface). The preferred state depends on the parameters of the system such as bias voltage and tip height. Changing one of the parameters one can switch a molecule into a definite state. The tip height window corresponding to the repeated switching region was found to be within 0.6 Å for all measured bias voltages. Investigations of the two level fluctuations show a power law dependence of the transfer rate on the bias voltage. However, some deviations from the power law were observed. The possible reason for them can be a shape and a position of the molecular level which will be discussed in the next chapter together with consideration of the theoretical model which can explain the switching mechanism.

CHAPTER 6.

THEORY OF THE SWITCHING PROCESS

6.1. INTRODUCTION

In this chapter, theoretical models for the experimentally observed behavior of the PTCDA molecule on Ag(111) will be discussed. The transfer of the oxygen atom will be treated as a potential barrier crossing process. The models consider a double well potential formed by the interaction of the atom with the STM tip and the surface. Among the many possible mechanisms, the vibrational heating model turned out to be the most appropriate for description of the switching of the molecule.

6.2 THEORETICAL MODELS FOR THE ADSORBATE TRANSFER

To understand how an adsorbate can be transferred between a surface and an STM tip, detailed calculations of the potential energy surface have been performed by different groups using different methods [137, 141, 159].

The results of these calculations show that when the tip is far away from the surface (imaging mode), the adsorbate has two stable bound positions: on the surface and on the tip. The double well potential obtained from the calculations reflects that the transfer process is very unlikely when the tip is far from the surface. The barrier height separating two wells is about 1 eV and moreover the potential minima are spaced laterally (Fig. 3.7).

There are two ways to reduce the height of potential barrier: by applying an electric field or by reducing the tip-sample separation. In the case of applying the electric field the double well potential will be modified [160]. However in order to remove the 1 eV high barrier high voltages (few V) should be applied which are not appropriate for the PTCDA molecule as it disintegrates when a voltage higher than 250 mV is applied. The second way to reduce the barrier height and thus transfer the adsorbate is to reduce the tip-sample distance (Fig. 3.7). When the tip is brought close to the surface the double well potential acquires a saddle point and the adsorbate can slide to the local minimum at the tip site.

Nevertheless, the absence of a potential barrier is not a necessary condition for a transfer event. The switching of an adsorbate between two states can be induced by several

mechanisms such as atomic quantum tunneling [161, 162], thermal activation [59, 163], coherent phonon processes [147], electron excitation [164], and vibrational heating [152].

6.2.I. ATOMIC QUANTUM TUNNELING

Atomic quantum tunneling implies tunneling of the atoms. In the presence of a potential barrier there is a certain probability for the atom to cross the barrier even if its energy is smaller than the barrier height. For small tip-surface separations (1-2 Å), low barrier heights, and light atoms the probability of atomic quantum tunneling is significant. However, there are additional requirements for quantum atomic tunneling to happen, which include a weak potential corrugation and a small adsorbate mass [162].

As for the adsorbate mass, it is known from the DFT calculations that it is not just the oxygen atom which flips up and down [141]. The molecule is "soft" and neighboring atoms follow the oxygen (Fig.0.1), increasing the mass which has to tunnel thus making the probability of atomic quantum tunneling less likely. Moreover, at the distances where repeated switches were observed the double well potential is very asymmetric (Fig. 3.7) and the barrier separating two wells is quite high (100 meV) for the transfer from the surface to the tip. This implies that in the case of elastic tunneling transfer even if the adsorbate tunneled from the surface potential minimum to the local minimum on the tip site, the back transfer cannot be explained by atomic quantum tunneling. In the case of highly asymmetric potential there is no state in the surface potential at the same energy as the bottom of the tip potential, so that the law of conservation of energy prohibits tunneling from the tip to the surface.

The applied bias voltage influences the potential depths of each of the two wells in opposite ways: if one potential becomes deeper, the other one gets shallower. Thus while one bias polarity will make the double well potential more symmetric, the opposite polarity will make it even more asymmetric. Increasing the asymmetry makes the atomic quantum tunneling process even less likely, whereas the symmetric situation could still involve tunneling in the transfer process. However, similar behaviours of the transfer rates were observed for both bias polarities (cf. Section 5.5.III), whereas the opposite influence of the applied bias on to the potential depths means that the probability for the adsorbate to tunnel will increase in one direction and decrease in the other. This was not observed in the experiments where both transfer rates increased with increasing magnitude of the voltage.

Therefore, the atomic quantum tunneling mechanism can be excluded from the list of appropriate theoretical models for describing PTCDA switches.

6.2.II. THERMAL ACTIVATION

Thermal excitations of the adsorbates may provide sufficient energy for the molecule to cross the potential barrier. Thermally induced conformational changes of the molecules [59] and chemical reactions [163] have been reported in literature for quite low temperatures.
The temperature dependence of the rate constant can be described by Arrhenius formula:

$$R = \upsilon \cdot \exp\left(-\frac{E_a}{kT}\right), \tag{6.1}$$

where υ is the vibrational frequency, and E_a is the activation energy.
From the DFT calculations for PTCDA the height of the potential barrier is about 100 meV and the experiments were performed at 7 K. From the experiment we know that the threshold energy for repeated switching is about 50 meV, which gives the vibrational frequency of about 10^{13} s^{-1}. Thus using formula (6.1) one can estimate the transfer rate to be almost zero (10^{-59} Hz).
Thus, thermal activation as a mechanism to explain the PTCDA switching can also be excluded.

6.2.III. COHERENT PHONON PROCESS

When low bias voltages are applied the electrons do not have enough energy to emit or absorb real phonons. Nevertheless, it can emit one and adsorb it again, but this must happen over a very short time scale. As soon as the electrons have sufficient energy to excite real phonons incoherent phonon processes take place, which will be discussed in Section 6.2.V. The energies at which the PTCDA switching process occurs are much higher than those needed for coherent phonon excitations. Therefore, the influence of the coherent phonon processes can be neglected.

6.2.IV. *ELECTRONIC EXCITATIONS*

The tunneling current passing through the STM junction can transfer the atom or molecule into an excited state. The electronic excitations enable the molecule to be excited into far-from-equilibrium conformations resulting in very rapid processes [165]. Usually the process takes place within a bias region of several volts which suggests one of the molecular orbitals (e.g. the HOMO or LUMO) is involved in the excitation mechanism. For example, in the case of the biphenyl molecule on the Si(100) surface the HOMO energy which is between 2 and 3 eV coincides with the threshold energy for the electronic excitation process [164].
When a resonant process takes place the electron from the molecular orbital can be transferred to the tip or vice versa so that it obtains a net charge. In this case, the electron lifetime and the shape of the potential energy surface play a dominant role in the molecular dynamics [166]. However, the PTCDA molecules are chemisorbed on the Ag(111) surface and the electron residence time becomes small excluding the probability of the resonant electron excitation process. Moreover, the energies used to excite the switching of PTCDA molecule is smaller than needed for the resonant electron excitation process to happen. The FLUMO of PTCDA is at about -300 meV, depending on the molecular orientation, whereas the bias voltages in the experiments did not exceed 250 mV.
When "off-resonant" process [167-169] takes place the coincidence of the molecular levels with the threshold energy is no longer required, the molecule is not necessarily charged and the lifetime and potential energy have no influence on the electronic excitation process. Thus only the "off-resonant" excitation can only occur; the electron-hole pair can contribute its energy to vibrational excitation of the molecule as will be discussed in the next section.

6.2.V. *VIBRATIONAL HEATING MODEL*

The final model which can be used to describe the switching behaviour is the vibrational heating model, which involves inelastic electron tunneling processes. It was suggested independently by two groups [152] and [170] in order to explain the reversible switch of a Xe atom on a Ni(111) surface [134], which was the first switch realized with the STM.
When electrons tunnel inelastically, they are scattered into states with lower energy and thus the energy difference between the initial and final state can be released. Although part of the

released energy can dissipate to the substrate phonons and electron-hole pairs, most of it goes to the excitation of the adsorbate vibrations.

The theory is based on the local polaron model [147] and a truncated harmonic oscillator model [171]. A key ingredient of the theory is the presence of a resonance close to the Fermi-level, which is a characteristic feature of many adsorbates on metal surfaces [172]. Electrons tunnel via such a resonance, providing the dominant channel for the current in STM [134]. The local polaron model implies this resonance to be coupled to a local phonon mode of the electrodes [173].

The idea of the mechanism is depicted in Fig. 6.1.

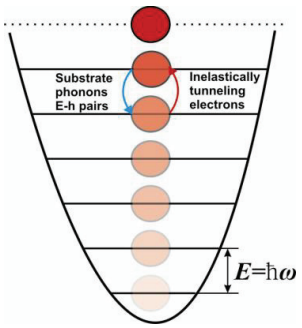

Figure 6.1. Truncated harmonic oscillator model for vibrational heating mechanism. Atom climbs the vibrational ladder up to the last level and escapes from the potential well through a competition between gaining energy form the inelastically tunneling electrons and losing it to substrate phonons and electron-hole pairs.

Being either at the surface or at the tip, the atom can be considered to be located in the potential minimum. Reaching the top of the potential well allows the atom to escape from it (i.e. to switch). There are several energy levels in the well corresponding to vibrationally excited states of the adsorbate. The bottom level corresponds to the ground state. This is the so-called truncated harmonic oscillator model which was adopted to describe the transition rates of the adsorbate. The atom motion is assumed to be harmonic and the transfer occurs irreversibly as soon as the atom reaches the highest level.

The main assumptions of the vibrational heating model are:

- $k_BT << |eV|$ and $\hbar\omega << |eV|$, which excludes the possibility of thermal activation process (see Section 6.2.II); this is true in the PTCDA experiments which were performed at 7 K and at quite high bias voltages;
- $\rho_a^{s,t}(\varepsilon)$ is constant over an energy scale eV around the Fermi-level which implies that the current is linear in the bias, thus the elastic tunneling component is constant. This is not the case for the PTCDA molecule and the influence of this factor on the

deviations from the vibrational heating model will be discussed in sections 6.4 and 6.5.

In the situation of inelastic electron tunneling there are three main sources which influence the transfer process: inelastically tunneling electrons, substrate phonons and electron-hole pairs. In the next section contributions from all of these will be considered.

6.3 INELASTIC TRANSITION RATES.

In the vibrational heating mechanism, the atom crosses the potential barrier separating two wells by vibrational activation through a competition between gaining energy from the inelastically tunneling electrons and losing energy to electron-hole pairs and substrate phonons. Although energy is gained mostly from the tunneling current, the phonons of the electrodes (incoherent phonon process) and electron-hole pairs (off-resonant electronic excitations) may also participate in increasing the energy. However, the loss of energy to phonon and electron-hole pair excitations is much larger than the gain from them, so they will be considered as energy damping sources.

The tunneling process in the case of a surface-molecule-tip junction can be described by a standard transfer Hamiltonian:

$$H_e = \sum_s \varepsilon_s c_s^\dagger c_s + \sum_t \varepsilon_t c_t^\dagger c_t + \varepsilon_a c_a^\dagger c_a + \sum_s \left(t_{sa} c_s^\dagger c_a + H.c.\right) + \sum_t \left(t_{ta} c_t^\dagger c_a + H.c.\right) \tag{6.2}$$

where *s, t* and *a* label the one-electron states $|s\rangle$, $|t\rangle$ and $|a\rangle$of the surface, the tip and the adsorbate level, respectively, with the corresponding energies ε_s, ε_t and ε_a, and c_i and $c_i^\dagger$ are the creation and annihilation operators. The first three terms are the Hamiltonians of the substrate, the tip and the adsorbate, respectively. The hopping between the surface and the tip via the adsorbate level is defined by the last two terms in Eq. (6.2).

Starting from an effective transfer Hamiltonian approach, the vibrational excitation and damping rate by inelastic electron scattering in the tunneling current can be derived. In addition to the electron-hole pair process, coupling to substrate phonons provides another contribution to the damping and thermal excitation of adsorbate vibrations. At 7 K the thermal excitation can be neglected while de-excitation due to phonon emission gives efficient damping.

The assumption of a linear shift of the adsorbate level ε_a with the vibrational coordinate results in a linear dependence of the Hamiltonian on q. Thus only the excitation and de-excitation rates ($\Gamma_\uparrow$ and $\Gamma_\downarrow$) between the vibrational ground state and the first excited state needed to be calculated. All the transitions between nearest neighboring levels can be expressed in terms $\Gamma_\uparrow$ and $\Gamma_\downarrow$.

Thus the total transition rates between the first excited state and the ground state are [152]:

$$\Gamma_\downarrow = [1 + n(\hbar\omega)]\gamma + \Gamma^{iet},$$
$$\Gamma_\uparrow = n(\hbar\omega)\gamma + \Gamma^{iet}, \tag{6.3}$$

where $n(\hbar\omega) = \frac{1}{\left[\exp\left(\frac{\hbar\omega}{k_B T}\right)-1\right]} \ll 1$ and $\gamma=\gamma_{eh}+\gamma_{ph}$ and γ_{ph} and γ_{eh} are the full width at half maximum of adsorbate vibration determined by a single phonon emission or adsorption and electron-hole pair, respectively. Note that the assumption $n(\hbar\omega)<<1$ implies that the upward transfer is caused by inelastically tunneling electrons ($\Gamma_\uparrow \approx \Gamma^{iet}$) while the downward transfer is defined by electron-hole pairs and substrate phonon excitations ($\Gamma_\downarrow \approx \gamma$).

According to the Boltzmann distribution for the population of the vibrational level n-1 and the transition rate from this level to level n, the Arrhenius-like expression for the transfer rate has the form:

$$R \cong n\Gamma_\uparrow \exp(-\frac{\bar{V}_B}{k_B T_v}), \tag{6.4}$$

where $T_v = \frac{\hbar\Omega}{k_B \ln\left(\frac{\Gamma_\downarrow}{\Gamma_\uparrow}\right)}$.

Taking into account the main assumptions of this model and the linear dependence of Γ^{iet} on V one gets:

$$R = n\Gamma_\uparrow \left(\frac{\Gamma_\uparrow}{\Gamma_\downarrow}\right)^{n-1} \approx n\Gamma^{iet} \left(\frac{\Gamma^{iet}}{\gamma}\right)^{n-1} \propto V^n. \tag{6.5}$$

The power law dependence of the transfer rate with applied voltage is the main characteristic feature of the vibrational heating model.

As one can see from the experimental plots the power law has been observed in most of the cases. Nevertheless, there are some deviations from such a dependence (especially for the transfer rates from the surface potential), which will be discussed in the next section.

6.4. APPLYING THE VIBRATIONAL HEATING MODEL TO THE EXPERIMENTAL RESULTS

In Fig. 5.10 one can see the transfer rates from the low conductance state to the high conductance state (red points) and also the transfer rate for the opposite direction (black points). According to the vibrational heating model, they both should follow the power law dependence on the bias which would correspond to a straight line behaviour in the double logarithm plot. However, only the transfer rate in the tip to surface direction follows the power law within the measured bias region (Fig. 6.2).

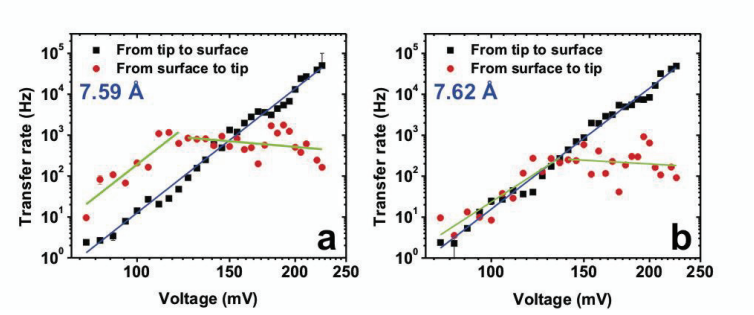

Figure 6.2. Fitting the experimental results to the vibrational heating model. Scatters – transfer rates calculated from the experiments. Solid lines – linear fitting of the experimental points. Input data for the calculating procedure were taken from the results of series III of the experimental measurements.

A strong deviation of the transfer rate from the low conductance state to the high conductance state is common for measurements at all tip heights (see Appendix III). Instead of expected monotone linear increase over the whole range of measured bias voltages the transfer rate increases with voltage up to 120 mV, and then slowly decays linearly. Moreover, the transfer rate curves change their slope significantly even with tiny alterations of the tip height (Fig. 6.2a and 6.2b), which according to the model implies that the tip height drastically changes the shape of the potential well on the substrate side. The change in the transfer rate is due to both of the model parameters which are defined by the depths of the potential well: the vibrational frequency of the adsorbate (which determines the spacing between the levels) and the number of vibrational levels in the well.

As for the transfer rate from the tip to the surface, its linearity in a double logarithm scale allows for the characterization of the potential well on the tip site. First of all, it should be noted that the shape of the potential well does not depend on the bias voltage V but only on the tip height z. The graphs of the number of vibrational levels as a function of z are presented

in Fig. 6.3 (black points) showing that the closer the tip is to the surface the deeper the potential well on the tip side will be, similar to the DFT calculations (Fig. 3.7).
If one assumes that the depth of the potential well to be equal:

$$E_{pot} = (n + \frac{1}{2})\hbar\omega \tag{6.6}$$

then fitting equation (6.6) to the results would imply that lowering the STM tip by 0.4 Å would lead to an increase in the potential barrier for the atom travelling from the tip to the surface of 0.39 eV (Table 6.1), independent of the bias voltage applied. This fitting procedure uses a vibrational energy ($\hbar\omega$) of 46 meV, which was chosen according to the theoretically calculated in-plane vibrational mode of the carboxylic oxygen. However, according to the zero-bias DFT calculations, the change in the potential should only be 0.1eV for a 0.4 Å reduction in tip height [141]. Moreover, the number of levels changes by a factor of two, which implies significant change in the double well potential, which was not the case for theoretical calculations.
Although the vibrational heating model can explain the linearity in the double-log plot of the transfer rate of the oxygen atom travelling from the tip to the surface side, it fails trying to describe the transfer rate in the opposite direction with a power law. However, the theory underlying the vibrational heating model implies a strong deviation from the power law in a few extreme cases. In the case of strong electron-phonon coupling ($\Gamma^{iet} \approx \gamma$) Eq. 6.5 breaks down. Another extreme case is the non-constant DOS near the Fermi-level which leads to nonlinearity of Γ^{iet} with V. According to experimental conductance spectra [80] the second case is relevant to PTCDA therefore the theoretical model should be modified.

6.5. MODIFIED THEORETICAL MODEL

The vibrational heating model was extended by the theoretical group from Dresden Technical University (group of Prof. Cuniberti) in collaboration with us as part of the project "Quantum Transport on the Molecular Scale" [64]. The experimental results for checking the reliability of the model were taken from the experimental investigations of the switching process of PTCDA on Ag(111) described in Chapter 4 of this thesis. The DFT calculations were partially performed by the same group and in University of Osnabrück (group of Prof. Rohlfing) [141].

As was mentioned at the end of previous section, the PTCDA molecule adsorbed on Ag(111) has non-constant density of states in vicinity of the Fermi-level (Fig. 1.3) due to the presence of the former lowest unoccupied molecular orbital (FLUMO). This level is hybridized with the silver surface and has a broadened Lorentzian line-shape so that the tail of the FLUMO passes through the Fermi-level. Moreover, according to experiments and DFT+NEGF calculations, the position of the molecular level shifts with changing tip height due to reverse chemisorption [40, 85, 141] (Fig. 6.4), thus introducing the dependence of Γ^{iet} on z into the total transition rates.

In addition to the tip height, the bias voltage also influences the position of the FLUMO level. The non-equilibrium Green's function (NEGF) calculations show that the molecular level moves with bias, following the surface potential [141]. For negative bias, the chemical potential on the surface is higher than that of the tip, so that electrons enter the FLUMO from the surface and leave via the tip. The FLUMO of the molecule is more strongly bound to the substrate than to the tip, so that the electrons can travel more easily between the FLUMO and the substrate than between the FLUMO and the tip. Therefore, for negative bias, electrons enter the FLUMO more rapidly than they leave, resulting in an accumulation of charge on the orbital, thus increasing its energy (Fig. 6.4d). When positive bias applied, this process occurs is the opposite direction, reducing the charge on the orbital and lowering the energy of the level.

Moreover, bias voltage plays a role in the depths of the potentials. Although the tip is grounded in the experiments, the electric field due to applied bias makes the surface potential either shallower or deeper depending on the bias polarity. The stronger the field, the more appreciable the shift of the potential well bottom on the surface side will be. However, for the switching process, what is important is not the absolute depth of the potential, but rather the distance from the bottom of the well to the top of the barrier. If the barrier is assumed to in the center between the potential wells, in the simplest case applying a bias voltage of V would change the surface potential by eV and the position of the top of the barrier by $eV/2$. Thus barrier height is changed by $eV/2$ on both sides, but in the opposite directions, which is the same effect as if the bias was applied symmetrically to the tip and substrate, as it is in the theoretical calculations. The change in barrier height alters the transfer rates, where the direction of the change is determined by the sign of the bias.

In the experiment, no influence of the bias polarity on the transfer rate from the high conductance state to the low conductance state was observed, whereas the transfer rate in the opposite direction is asymmetric with respect to bias polarity (Fig. 5.9). At negative bias the

transfer rate out of the surface potential well is higher than that at positive bias, because negative bias makes the potential well on the surface side shallower, and thus easier to escape from.

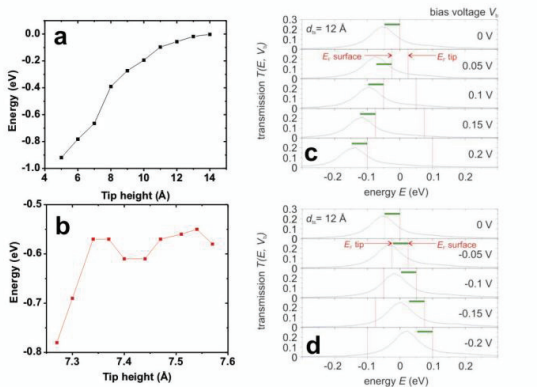

Figure 6.4. Position of the FLUMO molecular level as a function of tip height (a,b) and applied bias voltage (c,d) calculated with DFT and NEGF. The position shifts towards the Fermi-level with tip retraction, taken from [141]. a) DFT+LDA+NEGF calculations, b) values obtained with modified vibrational heating model [63] on the results of series III of the experiments.

Summarizing, the following observations have to be taken into account in the extended vibrational heating model:

- presence of the molecular level (FLUMO) with a Lorentzian line-shape close to the Fermi-level;
- dependence of the FLUMO position on the tip height;
- dependence of the FLUMO position on the bias voltage (including bias polarity);
- dependence of the potential energy surface on the bias.

The new model was based on the vibrational heating model developed in Ref. [152] in which all the effects listed above are introduced into the transfer rate calculations [64]. The total transfer rate can be expressed by the same formula (first part of the Eq. 6.5) but the excitation and de-excitation rates ($\Gamma_{\uparrow}$ and $\Gamma_{\downarrow}$) between the vibrational ground state and the first excited state are different in the extended model and Γ^{iet} is not linear with V. The equations for them can be found in Ref. [64].

The additional fitting parameters of the new model are:

- vibrational frequency (ω), which defines the spacing between the vibrational levels in the well;

- tip height (z), which influence the position of the molecular level and the potential energy surface[141];
- DOS of molecular level ε_a: $\rho_a(E)=\Delta/((E-\varepsilon_a)^2+\Delta^2$, where $\Delta=\Delta_s+\Delta_t$ is the coupling between the molecular level and the electrode electronic states;
- number of vibrational levels (n).

6.6. APPLYING THE EXTENDED VIBRATIONAL HEATING MODEL TO THE EXPERIMENTAL RESULTS

A molecule has several energy levels, with those above and below the Fermi level being the lowest unoccupied and highest occupied molecular orbitals. The molecular level used for the theoretical calculations described here was the one which is the closest to the Fermi-level, because it is the main component of the DOS of the molecular junction at the Fermi-level, and thus provides the primary channel for the inelastic electron tunneling. As a starting point, the molecular level was fixed to the value obtained from DFT and the calculations for the transfer rates were run. The results gave an approximate range for the values of the parameter of the system (vibrational energy, number of levels). The vibrational energy $\hbar\omega$ obtained via fitting is expected to be similar to the energy of one of the vibrational modes corresponding to the in and out of plane vibrations of a carboxylic oxygen [174]. The position of the molecular level as a function of z and V was calculated using NEGF combined with DFT-LDA [141].

A more sophisticated fitting procedure of the new model gave a good agreement with the experimentally observed behaviour (Fig. 6.5). However, in order to fit the transfer rate out of

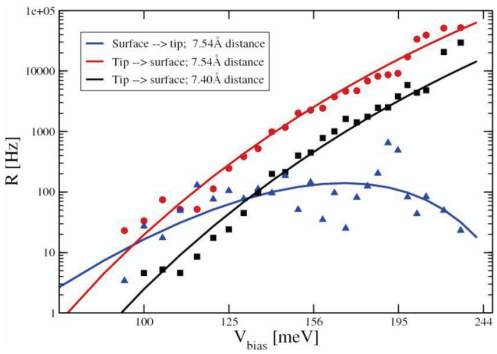

Figure 6.5. Double logarithm plot of the transfer rates for PTCDA switching from the tip to the surface (black and red) and in the opposite direction (blue). Solid lines - theoretical calculations [63], scatter points - experimental results. Input data for the calculating procedure were taken from the results of series III of the experimental measurements.

the surface potential the position of the molecular level was chosen to be at the positive bias region, which contradicts with the experiment. The transfer rate calculations for the molecular level being at the negative bias region did not give a good agreement with experimental results.

The fitting parameters used for the curves shown in the Fig. 6.5 are presented in Table 6.1:

Table 6.1. Fitting parameters for the calculated transfer rates shown in Fig. 5.5, according to Ref. [63]. Input data for the calculating procedure were taken from the results of series III of the experimental measurements.

	z (Å)	*ħω (meV)*	*ε $_m$ (meV)*	*n*
Black	7.54	35.14	-550	12
Red	7.40	37.71	-610	12
Blue	7.54	14.05	260	13

The curvature of the plots of the calculated transfer rates as a function of bias is the major difference to those obtained using the model of Gao [152]. It stems from the non-linear dependence of the current induced transition rate I^{iet} on V, which is due to the fact that the position of the FLUMO level moves with bias and has a Lorentzian shape.

In contrast to the conventional vibrational heating model, the modified version can fit the transfer rates of both switching directions: from tip to substrate and substrate to tip. The parameters used for the fitting procedure agree with the previous *ab initio* theoretical calculations [40, 85, 141, 174, 175]. As was expected from the DFT+NEGF calculations, the molecular level (FLUMO) shifts towards the Fermi-level with increasing tip-surface distance (Fig. 5.4a). As for the vibrational energies, they lie in the energy region of 12-60 meV where several in plane and out of plane vibrations of the carboxylic oxygen are found. The number of vibrational levels in the potential well on the tip side (n) was found to be independent of the tip height (z) and to be equal to 12; while on the surface side n changes from 13 to 11 on lowering the tip by 0.3 Å. In comparison, a fit with the Gao model gives significant change of n (from 16 to 8) with z (Fig. 6.3). If one assumes that one electron excites the switching of the atom from level (n-1) to level n then the total number of electrons needed to induce a single full switching (from the tip to the surface and back or vice versa) of the adsorbate is equal to 23-25. This value agrees with the slope of the switching curves calculated in the section 5.2.

Raising the tip by 0.3 Å reduces the well depth by 370 meV, but also reduces the energy of the vibrational level from 60 to 35 meV [64], while the number of levels remains equal to 12.

This implies that, when connected to the tip, the vibrational modes resulting in a switching process are different depending on *z*. However, in the case of the potential well on the surface side the alteration in the potential depth (by 30 meV) is caused mostly by changing the number of vibrational levels, because according to calculations the vibrational frequency is almost constant (14 meV).

In the model proposed by Gao [152], the alteration of the potential well depth causes changing *n.* This would imply that the same vibrational modes are involved in the adsorbate transfer in both directions, which is unlikely in the case of the large PTCDA molecule.

The fact that the number of vibrational numbers ($n \approx 12$) in both potential wells and different vibrational frequencies (14 and 60-35 meV for surface and tip potential, respectively), which are responsible for vibrational ladder climbing, implies that the potential on the tip side is significantly deeper than that on the surface side which agrees with Fig. 3.7.

Thus, all of the fitting parameters used to describe the experimentally observed curves do not contradict those obtained previously by both theoretical and experimental methods.

6.7. CONCLUSION

Among the many possible mechanisms used to describe transfer of an adsorbate between two electrodes, the vibrational heating model turned out to be the most appropriate for the case of PTCDA adsorbed on Ag(111).

However, the conventional vibrational heating model proposed by Gao and co-workers [152] had to be modified in order fit the experimentally observed behaviour. Movement of the Lorentzian-form FLUMO level with tip height and bias voltage turned out to be significant for the transfer rate calculations.

The behaviour of the transfer rates cannot be described by simple power law due to the curvature of the plots observed in a double logarithm scale. The degree of the curvature depends on the molecular level position ε_a, the number of vibrational levels in the potential well *n*, the frequency of the vibrational mode responsible for a switching process ω, and the tip height *z*, which are the fitting parameters used in the modified vibrational heating model.

The theoretically calculated curves agree very well with the experimentally measured results. In contrast to the conventional model, which could describe the transfer of the adsorbate only in one direction (from the tip to the surface), the modified one could explain the transfer in both directions.

CHAPTER 7.

METHODS

7.1. BASICS OF SCANNING TUNNELING MICROSCOPY

In 1981 two researchers from IBM, Gerd Binning and Hans Rohrer, developed the scanning tunneling microscope (STM) which significantly advanced surface science (Nobel Prize of Physics in 1986). This technique is based on quantum tunneling, which is a physical phenomenon which has been known about since the early stages of the development of quantum mechanics.

In classical mechanics an electron moving in a potential *U(z)* can overcome a potential barrier only if the electron has an energy *(E)* which is greater than *U*. Whereas in quantum mechanics, the electron is described by a wave function *ψ(z)* which has a nonzero probability of tunneling though a barrier if that the barrier has a finite height (Fig. 6.1).

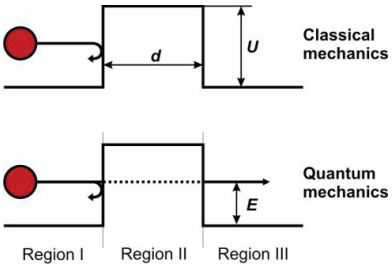

Figure 7.1. Representation of the classical and quantum mechanical point of view of an electron moving in a potential well

In each region the electron wave function satisfies the time-dependent Schrödinger equation:

$$-\frac{\hbar^2}{2m_e}\frac{d^2}{dz^2} + U(z)\psi(z) = E\psi(z) \tag{7.1}$$

where m_e is the electron mass and E is the electron energy.

The respective solutions for the different regions are:

I: $\psi_1 = e^{ikz} + Ae^{-ikz}$,

II: $\psi_2 = Be^{-\kappa z} + Ce^{\kappa z}$,

III: $\psi_3 = De^{ikz}$,

where $k = \frac{\sqrt{2m_e E}}{\hbar}$ and $\kappa = \frac{\sqrt{2m_e \Phi}}{\hbar}$, Φ=*U-E* is the work function of an electrode.
The transmission coefficient is given by:

$$T = \frac{1}{1+\frac{(k^2+\kappa^2)^2}{4k^2\kappa^2}\sinh^2(\kappa d)}, \tag{7.2}$$

where *d* is the width of the potential.
When $\kappa d \gg 1$ the transmission coefficient can be simplified to:

$$T \approx \frac{16\kappa^2 k^2}{(\kappa^2+k^2)^2}\exp(-2\kappa d) \tag{7.3}$$

Thus the tunneling probability decays exponentially relative to tip-surface separation (barrier width) times the square root of the work function. This explains the high sensitivity of the tunneling current to the tip-surface separation.
In order to explain the electron tunneling between two electrodes, for example between the tip and surface of an STM, Bardeen suggested first order time dependent perturbation theory [176] which was later used by Tersoff and Haman to appropriately describe the tunneling process in STM [177]. The tunneling current is produced via an applied bias voltage, *V*, the potential barrier is formed by the workfunctions Φ_{tip} and $\Phi_{surface}$ of the electrodes. Thus, the transmission probability *T* can be described by (6.3) where $\kappa = \frac{\sqrt{2m_e(\Phi_{tip}+\Phi_{surface}-eV)}}{\hbar}$.
For low temperatures and small *V,* the current can be described by

$$I \propto \int_0^{eV} \rho_t(\epsilon - eV)\rho_s(\epsilon)T(\epsilon, V)d\epsilon, \tag{7.4}$$

where ρ_t and ρ_s are the density of states of the tip and surface, respectively.
With a small increase of the voltage, *dV,* the tunneling current changes by *dI*. The first approximation becomes:

$$\left.\frac{dI}{dV}\right|_{V=V_0} \propto \rho_t(0)\rho_s(eV_0)T(\epsilon = 0, V_0) \tag{7.5}$$

Assuming the density of states (DOS) of the tip and the transmission coefficient are independent of the voltage, the differential conductance can be defined as

$$\frac{dI}{dV} \propto \rho_s(eV). \tag{7.6}$$

However, in order to satisfy assumptions which were made in obtaining the final equation (7.6) one should minimize the dependence of the tip DOS on the bias voltage. Thus a tip with a featureless DOS has to be used in order to get the best correspondence between the experiments and Eq. 7.6. The process of tip preparation will be discussed in section 7.3.
Thus the differential conductance is a signature of the sample density of states.

7.2. Low temperature beetle type STM.

In 1986, in Jülich, K. Besocke invented the so-called beetle-type STM which had better stability and was simpler to operate [178]. In the present work a commercial STM setup of a beetle-type was used (from Createc ®). The design was slightly modified by G. Meyer. It consists of three piezoelectric tubes mounted on a base plate (Fig. 7.2). These piezos are used for coarse approach and XY-scanning. Balls are fixed at the ends of the tubes. On top of the balls is a ramp ring which is divided into three spiral sectors. In the center of the ramp ring an additional piezo-element is mounted for Z-scanning and the main approach. A tip is fixed to this piezo. Finally, a sample is situated on the base plate. By applying an appropriate voltage to the outer piezos, the ramp ring can be rotated moving the tip towards the surface of the sample.

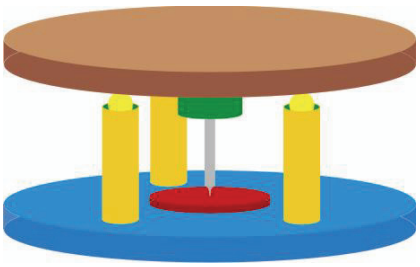

Figure 7.2. Sketch of the beetle-type Createc LT-STM head. Blue - base plate, brown - ramp plate, red - sample, grey - tip, yellow - balls, orange and green – piezoelements. Orange ones are responsible for course approach and XY movements, green one – for main approach and Z-movement.

The vertical stability of the tip was 1-3 pm. After stability was reached, which took several hours at temperatures near that of liquid helium, the lateral and vertical drift was 1Å/hour. The ramp ring had a maximum movement of 300 nm.

7.3. STM TIP PREPARATION

The success of experiments in scanning tunneling microscopy strongly depends on the shape of the tip. For all measurements a tungsten tip was used.

A W wire with a 0.5 mm diameter was electrochemically etched according to the following procedure. (In order to avoid contamination of the vacuum system, cleaning of the whole wire, not just the tip, was very carefully completed in ambient conditions.): First the 25 mm long wire was etched in a NaOH solution (5g of NaOH per 50 ml of distillate water) for 30 seconds and then cleaned in distilled water and ethanol to remove the solution. The wire would glitter when sufficiently cleaned. Next, a cleaned part of the wire was lowered into the NaOH solution to an immersion depth of 1.5-2 mm for approximately 10 min and the etching electronics were turned on. The initial and final values of the current were 14 and 4 mA, respectively. When the tip is ready, a part of the wire would fall down and the electronics would stop the etching process. Next, the etched part was cleaned in hot (near boiling) distilled water and ethanol several times. Finally, the wire was cut to the appropriate length and the quality of the tip was checked with an optical microscope (Fig. 7.3).

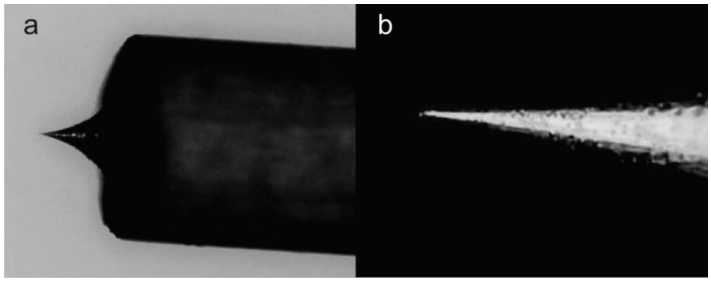

Figure 7.3. Microscopic image of a good quality freshly etched tungsten tip

The etched wire was fixed to the tip holder, loaded into the vacuum chamber and cleaned *in situ* by annealing to a high temperature with a high current. Afterwards the tip was loaded into the STM chamber and fixed to the magnets. The tip was then brought close to the bare Ag(111) surface and a series of voltage pulses (from -10 to 10 V for 1 s durations) was applied to the tip. The current spectra was monitored during the cleaning procedure and the pulses were stopped after a stable configuration of the tip was obtained (e.g. there were no sudden jumps and drops of the current). If the voltage pulses did not help one could also try dipping the tip into the clean surface by 10 to 100 Å for a time duration of 1 s.

In order to check the stability of the tip the topography image of the surface was recorded. The presence of molecular islands was desirable. This indicated there was not a double tip situation. If the topographic image was homogeneous and lacked any speckles and there was not a double tip, then the quality of the tip would be sufficient for imaging. However, these steps did not necessarily indicate the suitability of the spectroscopic measurements. The final check of the tip state was made by measuring the dI/dV spectrum of a clean surface. The surface state at -55 meV was used as a sign of tip quality. In most cases having a clear step in the conductance curve without additional peaks in the negative bias region in is a guarantee of the reproducibility of the measurements of the electronic properties.

7.4. SUBSTRATE PREPARATION AND MOLECULAR DEPOSITION

An Ag(111) single crystal was cut from a single monocrystalline silver wire and then polished under ambient conditions. After that the crystal was fixed to the sample holder, transferred to the load-lock of the STM and then to a preparation chamber with a base pressure of 10^{-10} mbar. The freshly made crystal required a longer cleaning procedure than for the used ones because it has a very rough surface with many terrace steps. When a sample is loaded from a non-vacuum, one has to flash it for a short time at about 200 ºC in order to bake off the water and other contaminants which can be pushed into the surface during the annealing. This was followed by the sputtering procedure. Sputtering was performed with Ar^+ ions (beam energies of 800-1000 eV) at room temperature for 15-30 min depending on the contamination of the surface. Subsequently the surface was annealed at temperatures of about 650 ºC for 0.5 – 1 hour. The sputtering-annealing cycle was repeated several times until one could see clear reflection spots in the LEED (Fig. 7.4).

After verification of the surface cleanliness, deposition of the molecules was started. The PTCDA molecules were deposited from a Knudsen cell by sublimation. Before deposition, the oven with the organic material was baked for several hours at about 200 ºC. During the deposition the temperature of the Knudsen cell was 300 ºC while the sample was at room temperature. In order to get sub-monolayer coverage one has to deposit the molecules for less than 1 min because the usual deposition rate is about 1 ML/min. After the deposition the sample was flashed at 150 ºC for a minute and subsequently cooled down to the temperature of liquid nitrogen. After cooling, the sample was transferred to the STM chamber and released

from a manipulator to the STM table. During a period of 5-10 hours it was cooled down to the liquid helium temperature (7K), which makes it ready for STM investigations.

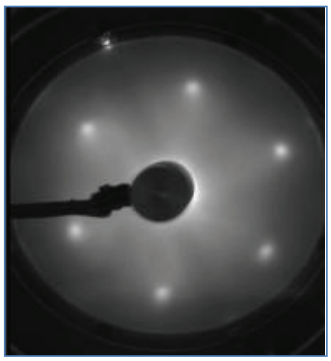

Figure 7.4. Low energy electron diffraction image of a clean Ag(111) surface. Beam energy 70 eV.

7.5. NOISE CHARACTERIZATION

Some of the experiments were done with an STM located in a special ultra-low vibration laboratory; however, measuring with this specific equipment did not lead to a significant difference. The signal to noise ratio was about 20 in both cases. The noise spectra are presented in Fig. 7.5.

As one can see from both the graphs, peaks of the frequencies of about 2 kHz are present in the spectra. This frequency region corresponds to the eigenfrequency of the piezo-elements of the STM. One could expect peaks at lower frequencies to appear in the measurements taken outside of the low vibration laboratory; however, no additional peaks were observed.

For spectroscopic measurements, the lock-in technique with a typical modulation of 4 mV and a modulation frequency of 618 Hz was used. The ratio between the modulation of the bias voltage induced by lock-in and the noise level characterize the quality of the measurements. Fig. 7.6 illustrates the noise spectra of the STM junction at the same parameters as in Fig. 7.5 but with modulation of the current introduced to the junction.

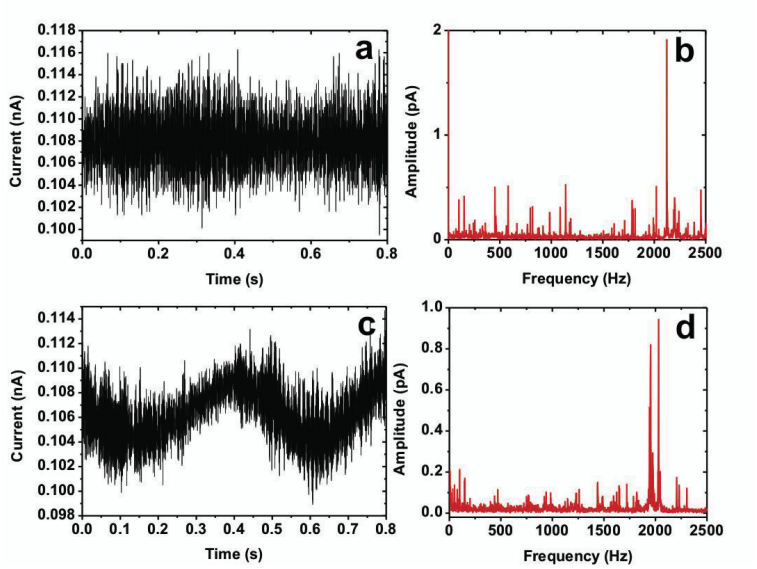

Figure 7.5. Noise spectra of the STM junction in the tunneling regime with lock-in modulation of the current turned on. 0.11 nA, -340 mV, feedback switched off (integrator = -0.1), modulation frequency 618 Hz, amplitude 4 mV. a) Time spectrum of the tunneling current, measured in the ultra-low vibration laboratory. b) Fourier transform of the time spectrum shown in a. c) and d) same as a) and b)but measured outside of the low vibration laboratory.

From Fig. 7.6 one can see that the oscillation of the current induced by the lock-in is more than 10 times larger than the highest peak corresponding to the noise. This value indicates the good quality of the spectroscopic measurements.

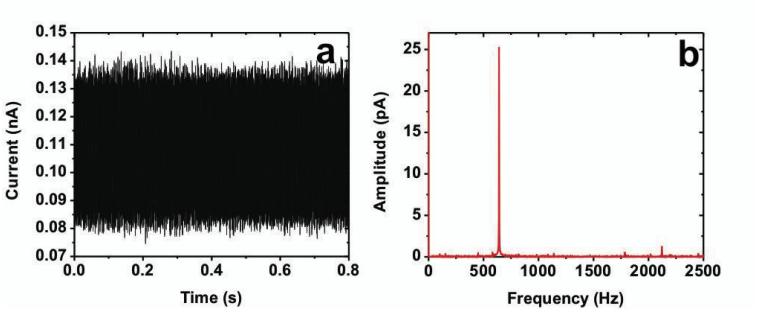

Figure 7.6 Noise spectra of the STM junction in the tunneling regime with lock-in modulation of the current turned on. 0.11 nA, -340 mV, feedback switched off (integrator = -0.1), modulation frequency 618 Hz, amplitude 4 meV. a) Time spectrum of the tunneling current. b) Fourier transform of the time spectrum shown in a.

7.6. PREPARATION OF THE ELECTRONICS OF THE STM FOR SPECTROSCOPIC MEASUREMENTS.

One of the most fascinating aspects of the STM measurements is the capability to obtain spectroscopic data at atomic resolution. However, to get spectra of this quality, one has to adjust the parameters of the lock-in amplifiers such as modulation frequency and amplitude, phase, sensitivity, and acquisition time.

7.6.I. MODULATION FREQUENCY, AMPLITUDE, AND PHASE

In this work two external lock-in amplifiers of type SRS830 (Stanford Research Systems) were used. One of them provided the synchronization sinusoidal signal of a specific frequency with amplitude of 100 mV. The second one provided a bias modulation signal with the same frequency and an amplitude of 4 mV. The modulation signal was added to the bias voltage provided by a voltage supplied by the STM.

The frequency of the lock-in modulation should be chosen in an appropriate way so as to avoid possible interference from the frequency of the electronics, eigenfrequency of the STM and noise. The frequency of 50 Hz is very often present in the measurements due to the noise of the power network, thus modulation frequencies with a value which is a multiple of 50 are not recommended. In the case of IETS measurements the second harmonic of the modulation frequency also should not coincide with the parasite frequencies.

A noise spectrum of the STM sheds the light on all frequencies which are present in the system and helps to find the optimal modulation frequency (Fig. 5.4). The effect of the modulation signal to the time spectrum can be seen in Fig. 5.5.

The modulation amplitude used in all spectroscopic measurements was 4 mV which is the smallest possible modulation voltage. The lowest value was defined by noise conditions of the system. Higher modulation amplitudes reduce the resolution of the tunneling spectra. However, they might be required in the case of high noise level in the STM. When high resolution spectroscopy is needed in the vicinity of the Fermi-level one can use a voltage divider (1/10) which leads to the modulation amplitude to become ten times smaller (0.4 mV).

The STM system contains a parasitic capacitance which can influence the measurements and thus should be minimized. This goal can be achieved by setting the phase of the lock-in amplifier to the appropriate value. This can be done by retracting the tip out of tunneling

contact and switching on the modulation signal. Presence of the parasitic capacitance results in the oscillation of the current signal induced by the modulation. To get rid of the capacitance one should adjust the lock-in phase to the maximum signal intensity and shift the phase by 90º.

7.6.II. ACQUISITION TIME AND SENSITIVITY

A proper choice of the acquisition time is one of the important tasks needed for getting reproducible spectra with high resolution. The time constants can be varied from one experiment to another depending on the bias range scanned within one spectrum. Conventional STS measurements of the PTCDA layer were performed in the bias window [-2; 2] V, whereas for the IETS a range a quarter of this size is enough.

The limiting parameter for the acquisition time is the minimum voltage step in the STM software which is 1 mV. This means that the maximum number of points that can be recorded during ramping the bias from -2 V to 2 V and back to -2 is 4001. A backward change of the bias assures that the tip state in the beginning and in the end of a spectrum is the same and allows one to better determine the lock-in time constants.

The acquisition time can be calculated from the time constant of the preamplifier. If the acquisition time is less then what is allowed then the spectra will appear shifted if you scan within the same bias range but in different directions. Generally, an appropriate acquisition time can be determined from the time constant and the number of points in the spectra. It should be chosen within the time interval:

$$1 \times T_{lock-in} \times N < T_{acqusition} < 3 \times T_{lock-in} \times N$$

where $T_{lock\text{-}in}$ is the time constant of the lock-in amplifier and N is the number of points in the spectrum.

The sensitivity of the lock-in amplifiers should be set to the minimum possible value in order to obtain the best resolution.

GENERAL CONCLUSION

SUMMARY

In the first part of this thesis, a detailed experimental investigation of the structural point defects of the PTCDA/Ag(111) interface was carried out. Monolayers of PTCDA were found to contain intrinsic defects of two dominant types, each of which appears in only one type of sublattice (A or B, corresponding to the aligned and misaligned orientations of PTCDA molecules in the commensurate herringbone layer [80]). A difference in the electronic structure of point defects from the PTCDA layer surface was observed. Additional resonances of various nature were found in the dI/dV spectra of PTCDA/Ag(111) interface. The strong resonance at 0.6 V derives from electron scattering by the point defects and formation of a bound state split off from the interfacial state. This feature appears in both types of defects. In contrast, a resonance at the Fermi level, which may be a spectroscopic sign of the Kondo-effect observed earlier in magnetic particles [179], pertains only to misaligned (type B) defects. Two additional peaks in between the alleged Kondo-resonance and the bound state are also resolvable only at misaligned defects. The positions and intensities of these two peaks depend on both the lateral and vertical tip position. Spectroscopic images recorded in the range of ±0.4V expose the LUMO, LUMO+1 and LUMO+2-structures of the defects, which provide an evidence that of all three peaks are associated with unoccupied molecular orbitals.
Besides the difference in the electronic properties, the geometry of the defects was also found to differ from the geometry of normal molecules. The mechanism of hydrogen sensitization of the STM junction [111] was used to resolve the geometrical structure of the molecules. Rotation of the defect molecules by 3º was found to take place. Heterogeneousness in the molecular skeleton was also found: namely, one of the rings was missing. Detaching of one of the rings from the molecules is in agreement with the hydrophilic property of PTCDA; water molecule could attract part of the PTCDA molecule resulting in ring removal. However, a damaged geometrical structure was not always the case; therefore such interaction cannot fully explain the nature of the defect. Another explanation for the defect formation was the presence of a silver adatom underneath the molecule. Indirect verification of this hypothesis was provided by depositing a silver cluster on top of the PTCDA monolayer. Similar to what was observed for the defects an additional peak in the dI/dV spectra appeared at the Fermi-

level. Also, in some cases the hydrogen-sensitized tip showed a small particle located underneath the defect molecule after displacing it from the layer.

In the second part of this dissertation a molecular switch was constructed and studied, with the advantage of local probing provided by the STM, which was used to contact the molecules. The PTCDA molecule deposited on Ag(111) surface was found to be an ideal two-level fluctuator; a part of the molecule following the carboxylic oxygen can switch between the STM tip and the surface without destroying the molecular skeleton. An ultra-fast chemical reaction occurs when the tip is brought in the vicinity of the molecule: the covalent bond between one of the carboxylic oxygens of the molecule and the surface breaks in order to establish a chemical bond with the apex of the tip. In the case of the oxygen being switched up to the tip, a molecular wire is formed between the tip and the surface, and transport measurements can be performed. The two states of the system are associated with the different bonding sites of the molecule and have different levels of conductance. In the standard situation with the oxygen atom bound to the silver surface, the conductance is the normal conductance of the PTCDA/Ag(111) interface in the tunnelling regime. Substitution of the surface-oxygen bond with the tip-oxygen bond leads to increase of the conductance by the factor of ten, moving the system into the transport regime.

A single spontaneous molecular switch or repeated switching process can occur, depending on the bias voltage applied to the system.

At low bias voltages (below 50 mV), a single switch to the tip takes place as the tip approaches. Retraction of the tip results in two scenarios: either the molecule falls back, or it follows the tip and can be removed from the layer.

In the cases when the molecule was trapped by the tip after retraction, molecular displacement was performed. As a result, molecular corrals of different shapes were built. However, only displacement of isolated molecules or molecules at the edge of the molecular island was possible. This effect can be explained by the great influence of the molecular surroundings on the stability of the molecules in the layer, as the hydrogen bonds between the molecules prevent them from being removed from the layer. Molecules in ordered islands were found to be equally difficult to remove, and to fall back to their initial position during tip retraction. Taking this observation into account, the stable non-isolated molecules were chosen for detailed quantitative analysis of the switching process.

At bias voltages above 50 mV the oxygen can be transferred multiple times between the STM tip and the surface, and the molecule remains on the surface after tip retraction. The oxygen

atom can change bonding many times without damaging the molecule; this was confirmed by taking topographical images of the investigated area before and after the switching process.

The repeated switches of PTCDA molecule appear in the current spectra as telegraph noise. Typically such behaviour was observed when the tip was stabilized above the carboxylic oxygen (~7Å) and a bias voltage above 50 mV was applied to the system. The frequency of the two level fluctuations of the current associated with the two bonding sites of the molecule was found to increase with bias. An additional data acquisition module with temporal resolution of 8 μs was introduced to the system because of that, in order to record fast switches.

As a result of increased resolution of the measurements, very large STM data files were generated, and special effort was required to process them. A section of this thesis is dedicated to the techniques and software developed to process the data. The raw files were split into smaller chunks and processed with the Mathematica package using a specially developed algorithm, without loss of relevant information. As a result, the raw files of 2GB size were reduced to processed files ranging from 500KB to 500MB in size, depending on the number of switches recorded. The accuracy of the data processing was validated by comparing a part of a raw file with the matching processed data, which were found to be in perfect agreement.

Qualitative analysis of the switching process shows that bias voltage and tip height are the influential parameters, which define the state of the junction. Parameter windows with high probability for the junction to be in one specific state were found. This provides the information required to control the two regimes of the junction: tunnelling and transport.

The *I(t)* spectra revealing the two level fluctuations were used to perform quantitative analysis of the switching process. The residence time distribution and fractional occupation were calculated on the basis of the current spectra. The transfer rate analysis revealed that the bias dependence of the transfer rate from the high to the low conductance state was similar to a power law.

Among the many possible mechanisms, a vibrational heating model suggested by Gao et. al. [152] was found to be the most appropriate to describe behaviour of the system. However, a closer look showed that it should be extended to explain the experimentally observed non-linear (on a double log scale) behaviour of the transfer rate out of the tip potential. On the basis of the existing model, a modified one was developed by collaborators from Dresden Technical University [64]. The main difference between the models is the shape of the density of states in the vicinity of the Fermi-level. The original model considered it to be constant,

whereas the new model uses a Lorentzian-form DOS. Moreover, according to the DFT and NEGF calculations, the position of this molecular level shifts depending on the tip height and applied voltage [141]. This effect was also taken into account in the new model, which produced a good agreement between theoretical calculations and experimental measurements. This was a big step towards understanding of the underlying mechanism of the molecular switch, which was made within a collaboration between experimental and theoretical groups.
The summary of the findings:
Part I.
• Electronic and structural properties of the point defects of the PTCDA/Ag(111) interface were investigated;
• Splitting of the LUMO state was observed in the spectroscopic measurements;
• Two models of the defects formation were suggested.
Part II:
• It was shown that PTCDA molecules can be used to build nanocorrals of different shapes on the Ag(111) surface;
• PTCDA was shown to be an ideal system for implementing a molecular switch;
• It was shown that the switching of the molecule corresponds to breaking the bond between an oxygen atom of the molecule and the surface (or the tip) and establishing a new one with the tip (the surface) respectively;
• Two regimes of the switching were found: spontaneous single switch ($V<50$ mV) and repeated current-induced switches ($V>50$ mV);
• Two level fluctuations of the current corresponding to constant switching of the system between tunneling and transport regimes were observed at certain bias voltages;
• It was shown that the preferred state of the system is defined by the bias voltage and tip height, and can be controlled;
• A theoretical model describing the observed behaviour was suggested.

PROSPECTS

All of the experiments described in this paper were done in UHV conditions and at very low temperatures. In order to apply the results in real devices, one has still to repeat the same experiments in ambient conditions. Although it is going to be quite complicated, it should be very exciting, too; if this turns out to be practical, one can think of molecular schemes based

on PTCDA molecules. However, the STM tip still remains a macroscopic object which limits the appliance of the described system in the nanoscopic devices. But the author hopes that the understanding of the underlying physical mechanisms of the switching process, which has been achieved in this work, will make a contribution in the field of molecular electronics.

As for the practical outcome of this work, it shows that molecular switches can show predictable and repeated behaviour, and the approach can be easily replicated with similar kinds of molecular switches. The selection of similar molecules and substrates is already very rich: NTCDA, TTCDA, QTCDA, …and Ag(110), Au(111), Cu(111). Changing the substrate will, of course, lead to a change in the bond strength between the molecules and the surface; for example, on Au(111) PTCDA is known to physisorb [91]. In contrast, Cu(111) surface attracts PTCDA very strongly [178].

Even with PTCDA on Ag(111) there are still many things that can be studied in more detail. For instance, the spontaneous single switch as a function of bias voltage is of particular interest. According to the surface potential map, an oxygen atom should stick with the tip site as soon as the bond between them is established (Fig.1.21). However, this was not the case, and the reason for this remains unclear. Another open question is the observed hysteresis in the capture and release distances (Fig.1.29). Inelastic electron tunneling spectroscopy (IETS) could show the differences or similarity in the vibrational modes in tunneling and transport regimes.

The applicability of the suggested theoretical model should be further checked in the full range of low bias voltages. The only difficulty with this investigation is that one has to wait for a long time to record sufficient amount of switching.

As for the switches at high biases, one can think of increasing the temporal resolution of the measurements that there are fewer or no “missing” switches in the spectra. Also, it would be informative to pass higher voltages through the molecule in order to reach the bias range where the theory predicts deviations from the monotonic increase of the transfer rates out of the tip potential. There are many other directions that can and shall be investigated further, and the author hopes that her work would help in building a foundation for further research in the fascinating emerging area of molecular electronics.

APPENDIX

APPENDIX I. MACHEMATICA PROGRAM. MAIN VERSION

```
$HistoryLength=1;
(*Saving only one previous file in the history in order to reduce memory in use*)
InputFileName="55";
(*Name of a file to work with*)
FilesDirectory="D:\\Users\\Olya\\"<>InputFileName<>"\\";
(*Pathway to the file*)
CreateDirectory["Output"];
(*Creating a folder to save results*)
OutputFileName="Output";
(*Creating a file to save modified spectrum*)
OutputUpTime="TimeUp";
(*Creating a file to save time spent in the upper state*)
OutputDownTime="TimeDown";
(*Creating a file to save time spent in the lower state*)
β=50;
α=20;
NAverNoise=10000;
(*Number of point to average current in the case of no switches*)
SetDirectory[FilesDirectory];
(*Identification a directroy to work with*)
Files=FileNames["*.*"];
(*Opening the files*)
Files=Delete[Files,Position[Files,InputFileName<>".dat"]];
(*Deleting files of a wrong format*)
Files=Delete[Files,Position[Files,InputFileName<>".CRC"]];
(*Deleting files of a wrong format*)
Files=Delete[Files,Position[Files,OutputFileName<>".dat"]];
(*Deleting files of a wrong format*)
Files=Delete[Files,Position[Files,OutputUpTime<>".dat"]];
(*Deleting files of a wrong format*)
```

```
Files=Delete[Files,Position[Files,OutputDownTime<>".dat"]]
(*Deleting files of a wrong format*)
(*List of the files*)
FullCharacteristic=Table[{},{i,Length[Files]}];
LengthFile=Table[0,{i,Length[Files]}];
FileFunction[i_]:=(
 tFullCharacteristic={};
 SummUpCurrent=0;
 SummDownCurrent=0;
 MeanCur=0;
 MeanDist=0;
 NUpPoints=0;
 NDownPoints=0;
 (* Nulling of the variables*)
 DownPoints=True;
 (* Spectrum starts with a junction with low conductrance*)
 Current=ReadList[Files[[i]],Real,RecordLists->True];
 (* Reading data from the file i *)
 Current=Delete[Current,1]; Current=Delete[Current,-1];
 (* Deleting of the first and the last elements *)
 CurrentTrans=Transpose[Current][[2]];
 (* Current *)
 VoltageDistance=Transpose[Current][[1]];
 (* Distance *)
 MaximumValue=Max[CurrentTrans];
 (* Maximum current *)
 MinimumValue=Min[CurrentTrans];
 (* Minimum current *)
 AverageValue=(MaximumValue+MinimumValue)/2;
 (* Average current *)
 LengthFile[[i]]=Length[CurrentTrans];
 (* Saving a  number of points in the file to recalculate the absolute time *)
 If[CurrentTrans[[1]]>AverageValue,DownPoints=False,DownPoints=True];
 (* Checking the switch event *)
```

```
 If[(MaximumValue-Abs[MinimumValue])/2>β,
  (* If there is a switch, run a cycle *)
  For[j=0,j<Length[CurrentTrans],j++;
   If[CurrentTrans[[j]]>AverageValue&&DownPoints,DownPoints=False;
    (* If current value is larger than average and the previous state is with a low
conductance,then a write down a switch to up-state *)
tFullCharacteristic=Append[tFullCharacteristic,{j/125000,AverDownCurrent,VoltageDistanc
e[[j]]}];tFullCharacteristic=Append[tFullCharacteristic,{j/125000,AverUpCurrent,VoltageDis
tance[[j]]}];
   If[CurrentTrans[[j]]>MaximumValue-α,NUpPoints++;
    (*Average current in the up-state *)
    SummUpCurrent+=CurrentTrans[[j]];
   If[CurrentTrans[[j]]<AverageValue&&DownPoints= =False,DownPoints=True;
    (* If current value is smaller than average and the previous state is with a high
conductance,then a write down a switch to down-state
*)tFullCharacteristic=Append[tFullCharacteristic,{j/125000,AverUpCurrent,VoltageDistance
[[j]]}];
tFullCharacteristic=Append[tFullCharacteristic,{j/125000,AverDownCurrent,VoltageDistanc
e[[j]]}]];If[CurrentTrans[[j]]<MinimumValue+α,NDownPoints++;
    (* Average current in the down-state *)
    SummDownCurrent+=CurrentTrans[[j]];
   ],(* If there are no switches run a cycle*)
  If[DownPoints,
    (* Analysis of the down-state*)
    MeanCur=Mean[Transpose[Partition[CurrentTrans,NAverNoise]]];
    (* File's average current without switches *)

MeanCur=Append[MeanCur,Mean[Drop[CurrentTrans,Length[MeanCur]*NAverNoise]]];
    (* Average current for the last points in the file *)
    MeanDist=Mean[Transpose[Partition[VoltageDistance,NAverNoise]]];
    (* File's average voltage without switches *)
MeanDist=Append[MeanDist,Mean[Drop[VoltageDistance,Length[MeanDist]*NAverNoise]]
];
    (* Average voltage for the last points in the file *)
```

```
tFullCharacteristic=Join[tFullCharacteristic,Transpose[{Join[Table[(NAverNoise*t)/125000-
NAverNoise/(125000*2),{t,1,Length[MeanCur]-1}],{(NAverNoise*(Length[MeanCur]-
1))/125000+(Length[CurrentTrans]-(Length[MeanCur]-
1)*NAverNoise)/(2*125000)}],MeanCur,MeanDist}]],
     (* Upper state analysis*)
    MeanCur=Mean[Transpose[Partition[CurrentTrans,NAverNoise]]];
    (* File's average current without switches *)

MeanCur=Append[MeanCur,Mean[Drop[CurrentTrans,Length[MeanCur]*NAverNoise]]];
    (* Average current for the last points in the file *)
    MeanDist=Mean[Transpose[Partition[VoltageDistance,NAverNoise]]];
    (* File's average voltage without switches *)
MeanDist=Append[MeanDist,Mean[Drop[VoltageDistance,Length[MeanDist]*NAverNoise]]
];
    (* Average voltage for the last points in the file *)

tFullCharacteristic=Join[tFullCharacteristic,Transpose[{Join[Table[(NAverNoise*t)/125000-
NAverNoise/(125000*2),{t,1,Length[MeanCur]-1}],{(NAverNoise*(Length[MeanCur]-
1))/125000+(Length[CurrentTrans]-(Length[MeanCur]-
1)*NAverNoise)/(2*125000)}],MeanCur,MeanDist}]]
    ];
  ];
 If[NDownPoints ≠
0,tFullCharacteristic=tFullCharacteristic/.{AverDownCurrent→SummDownCurrent/NDown
Points}];
If[NUpPoints≠0,tFullCharacteristic=tFullCharacteristic/.{AverUpCurrent→SummUpCurrent/
NUpPoints}];
 FullCharacteristic[[i]]=tFullCharacteristic;
ClearAll[Current,CurrentTrans,VoltageDistance,tFullCharacteristic,SummUpCurrent,SummD
ownCurrent,MeanCur,MeanDist,NUpPoints,NDownPoints,DownPoints];
 (* Cleaning a memory *)
 )
Processes=Table[ParallelSubmit[{i},FileFunction[i]],{i,Length[Files]}]
```

```
(* Processes' initialization *)
WaitAll[Processes];
(* Run the processes *)
For[i=1,i<Length[LengthFile],i++;
 (* File time correction *)
 AbsoluteFileTime=(Plus@@LengthFile[[1;;i-1]]+i-1)/125000;
 (* Absolute time recalculating *)
 tFullCharacteristic=Transpose[FullCharacteristic[[i]]];
 (* Extracting the new data from the file *)
 tFullCharacteristic[[1]]=tFullCharacteristic[[1]]+AbsoluteFileTime;
 (* Adding the absolute time to local *)
 FullCharacteristic[[i]]=Transpose[tFullCharacteristic];
 (* Writing down a modified data *)
 ];
FullCharacteristic=Flatten[FullCharacteristic,1];
(* Joining all the data *)
TimeUp={};
TimeDown={};
tFullCharacteristic=FullCharacteristic;
(* Creating a temprorary file to analyze time up and time down*)
For[i=0,i<Length[tFullCharacteristic],i++;
 If[i>1,
  If[i<Length[tFullCharacteristic],
   If[tFullCharacteristic[[i,1]]!=tFullCharacteristic[[i-
1,1]]&&tFullCharacteristic[[i,1]]!=tFullCharacteristic[[i+1,1]],tFullCharacteristic=Delete[tFu
llCharacteristic,i];i--],
   If[tFullCharacteristic[[i,1]]!=tFullCharacteristic[[i-
1,1]],tFullCharacteristic=Delete[tFullCharacteristic,i]]],
If[tFullCharacteristic[[i,1]]!=tFullCharacteristic[[i+1,1]],tFullCharacteristic=Delete[tFullChar
acteristic,i];i--]
  ];
 ]
Export[FilesDirectory<>"Output\\"<>OutputFileName<>"SwOnly.dat",N[tFullCharacteristic,
{Infinity,8}],"TSV"];
```

```
SwitchedFullCharacteristic=tFullCharacteristic;
TimeDown={}
TimeUp={};
For[i=1,i<Length[SwitchedFullCharacteristic],i++;
 If[SwitchedFullCharacteristic[[i,1]]□SwitchedFullCharacteristic[[i-
1,1]]&&i<Length[SwitchedFullCharacteristic],
(* Search of a switch *)
If[SwitchedFullCharacteristic[[i,2]]>SwitchedFullCharacteristic[[i-1,2]],
(* Definition of a type of switch: up or down *)
   TimeUp=Append[TimeUp,{N[SwitchedFullCharacteristic[[i+1,1]]-
SwitchedFullCharacteristic[[i,1]],{Infinity,7}],N[SwitchedFullCharacteristic[[i,1]],{Infinity,7
}],N[(SwitchedFullCharacteristic[[i,2]]+SwitchedFullCharacteristic[[i+1,2]])/2,{Infinity,7}]}]
,
   TimeDown=Append[TimeDown,{N[SwitchedFullCharacteristic[[i+1,1]]-
SwitchedFullCharacteristic[[i,1]],{Infinity,7}],N[SwitchedFullCharacteristic[[i,1]],{Infinity,7
}],N[(SwitchedFullCharacteristic[[i,2]]+SwitchedFullCharacteristic[[i+1,2]])/2,{Infinity,7}]}]
   ]]
 ];
(* Record the files *)
Export[FilesDirectory<>"Output\\"<>OutputFileName<>".dat",N[FullCharacteristic,{Infinity
,8}],"TSV"];
Export[FilesDirectory<>"Output\\"<>OutputUpTime<>".dat",TimeUp,"TSV"];
Export[FilesDirectory<>"Output\\"<>OutputDownTime<>".dat",TimeDown,"TSV"];
```

APPENDIX II. MATHEMATICA PROGRAM. SECOND VERSION

```
FilesDirectory="D:\\Users\\Olya\\100\\";
InputFileName="100";
OutputFileName="Output";
OutputUpTime="TimeUp";
OutputDownTime="TimeDown";
β=50;
α=20;
NAverNoise=10000;
SetDirectory[FilesDirectory];
Files=FileNames["*.*"];
Files=Delete[Files,Position[Files,InputFileName<>".dat"]];
Files=Delete[Files,Position[Files,InputFileName<>".CRC"]];
Files=Delete[Files,Position[Files,OutputFileName<>".dat"]];
Files=Delete[Files,Position[Files,OutputUpTime<>".dat"]];
Files=Delete[Files,Position[Files,OutputDownTime<>".dat"]]
FullCharacteristic={};
NoiseBefore={};
NoiseAfter={};
DownPoints=True;
LastTime=0;
For[i=16,i<Length[Files]-1,i++;
 NUpPoints=0;
 SummUpCurrent=0;
 NDownPoints=0;
 SummDownCurrent=0;
 Current=Import[Files[[i]]];
 Current1=Delete[Current,1];
 Current1=Delete[Current1,-1];
 CurrentTrans=Transpose[Current1][[2]];
 VoltageDistance=Transpose[Current1][[1]];
 MaximumValue=Max[CurrentTrans];
```

```
 MinimumValue=Min[CurrentTrans];
 AverageValue=(MaximumValue+MinimumValue)/2;
 Print["File name = ",Files[[i]],"\n"," Average value = ",Mean[CurrentTrans],"\n"," Maximum
value = ",MaximumValue,"\n"," Minimum value = ",MinimumValue,"\n"," (Max+Min)/2 =
",AverageValue,"\n",MemoryInUse[]];
 If[(MaximumValue-Abs[MinimumValue])/2>β,
  For[j=0,j<Length[CurrentTrans],j++;
If[CurrentTrans[[j]]>AverageValue&&DownPoints,DownPoints=False;FullCharacteristic=A
ppend[FullCharacteristic,{LastTime+j/125000,AverDownCurrent,VoltageDistance[[j]]}];Full
Characteristic=Append[FullCharacteristic,{LastTime+j/125000,AverUpCurrent,VoltageDista
nce[[j]]}]];
   If[CurrentTrans[[j]]>MaximumValue-
α,NUpPoints++;SummUpCurrent+=CurrentTrans[[j]]];
If[CurrentTrans[[j]]<AverageValue&&DownPoints=
=False,DownPoints=True;FullCharacteristic=Append[FullCharacteristic,{LastTime+j/125000
,AverUpCurrent,VoltageDistance[[j]]}];
FullCharacteristic=Append[FullCharacteristic,{LastTime+j/125000,AverDownCurrent,Volta
geDistance[[j]]}]];
If[CurrentTrans[[j]]<MinimumValue+α,NDownPoints++;SummDownCurrent+=CurrentTran
s[[j]]];
   ],
If[DownPoints,MeanCur=Mean[Transpose[Partition[CurrentTrans,NAverNoise]]];MeanCur=
Append[MeanCur,Mean[Drop[CurrentTrans,Length[MeanCur]*NAverNoise]]];
MeanDist=Mean[Transpose[Partition[VoltageDistance,NAverNoise]]];MeanDist=Append[M
eanDist,Mean[Drop[VoltageDistance,Length[MeanDist]*NAverNoise]]];

NoiseBefore=Join[NoiseBefore,Transpose[{Join[Table[LastTime+(NAverNoise*t)/125000-
NAverNoise/(125000*2),{t,1,Length[MeanCur]-
1}],{LastTime+(NAverNoise*Length[MeanCur])/125000+(Length[CurrentTrans]-
Length[MeanCur]*NAverNoise)/(2*125000)}],MeanCur,MeanDist}]],MeanCur=Mean[Trans
pose[Partition[CurrentTrans,NAverNoise]]];MeanCur=Append[MeanCur,Mean[Drop[Current
Trans,Length[MeanCur]*NAverNoise]]];
```

```
MeanDist=Mean[Transpose[Partition[VoltageDistance,NAverNoise]]];MeanDist=Append[M
eanDist,Mean[Drop[VoltageDistance,Length[MeanDist]*NAverNoise]]];
   NoiseAfter=Join[NoiseAfter,Transpose[{Join[Table[LastTime+(NAverNoise*t)/125000-
NAverNoise/(125000*2),{t,1,Length[MeanCur]-
1}],{LastTime+(NAverNoise*Length[MeanCur])/125000+(Length[CurrentTrans]-
Length[MeanCur]*NAverNoise)/(2*125000)}],MeanCur,MeanDist}]]
   ];
 ];
 If[NDownPoints≠
0,FullCharacteristic=FullCharacteristic/.{AverDownCurrent→SummDownCurrent/NDownPo
ints}];

If[NUpPoints≠0,FullCharacteristic=FullCharacteristic/.{AverUpCurrent→SummUpCurrent/
NUpPoints}];
 LastTime=LastTime+Length[CurrentTrans]/125000;

Export[FilesDirectory<>"Output\\"<>OutputFileName<>".dat",N[Join[NoiseBefore,FullChar
acteristic,NoiseAfter],{Infinity,8}],"TSV"];
 TimeUp={};
 TimeDown={};
 For[j=-1,j<(Length[FullCharacteristic]-1)/4-1,j++;
  TimeUp=Append[TimeUp,{N[FullCharacteristic[[2+4j,1]]],N[FullCharacteristic[[3+4j,1]]-
FullCharacteristic[[2+4j,1]]],FullCharacteristic[[2+4j,2]]}];

TimeDown=Append[TimeDown,{N[FullCharacteristic[[4+4j,1]]],N[FullCharacteristic[[5+4j,
1]]-FullCharacteristic[[4+4j,1]]],FullCharacteristic[[4+4j,2]]}];
  ];

Export[FilesDirectory<>"Output\\"<>OutputUpTime<>".dat",Transpose[{TimeUp}],"TSV"];


Export[FilesDirectory<>"Output\\"<>OutputDownTime<>".dat",Transpose[{TimeDown}],"
TSV"];
```

]

APPENDIX III. PLOTS OF THE TRANSFER RATES

III.I. FIRST SERIES

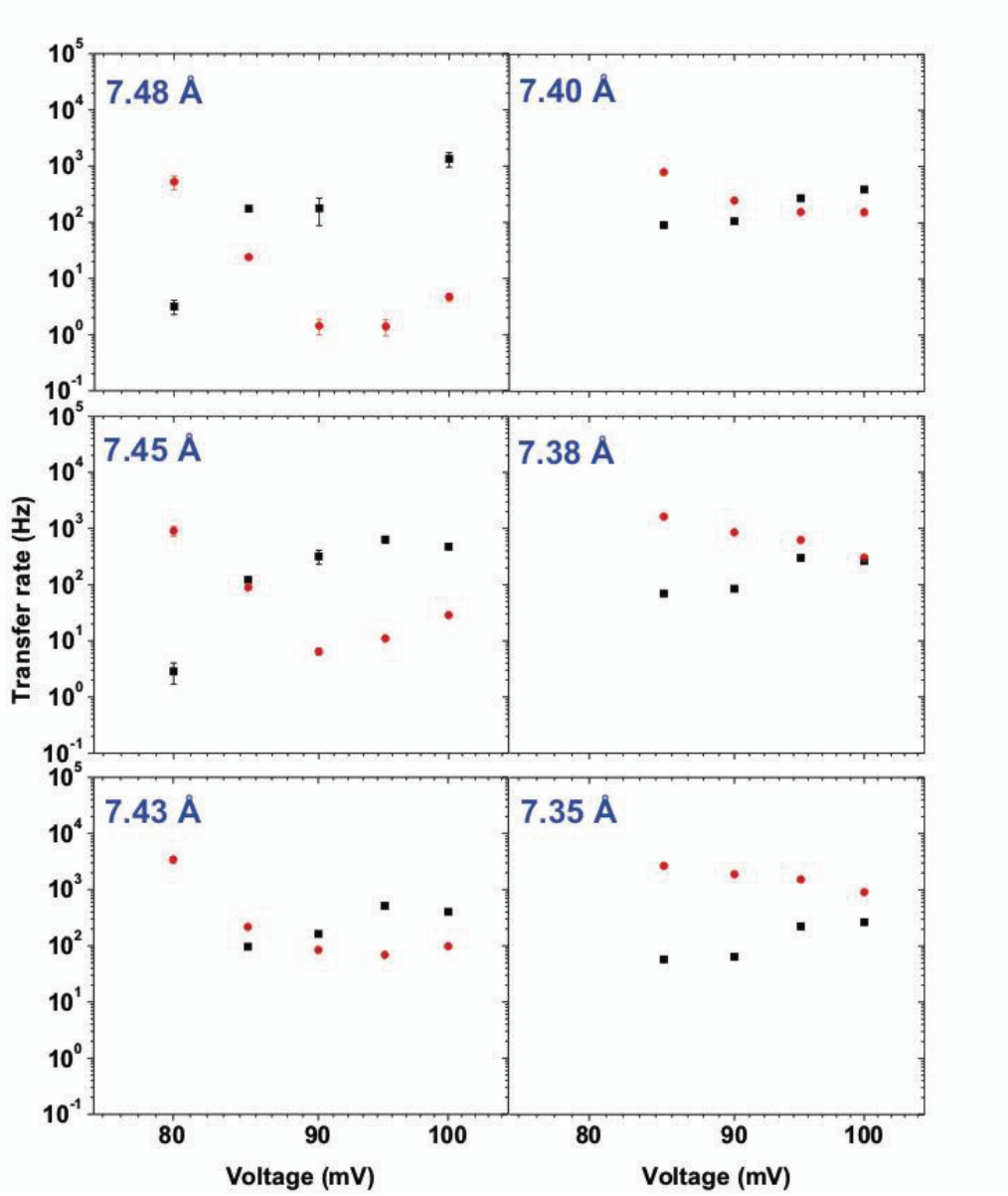

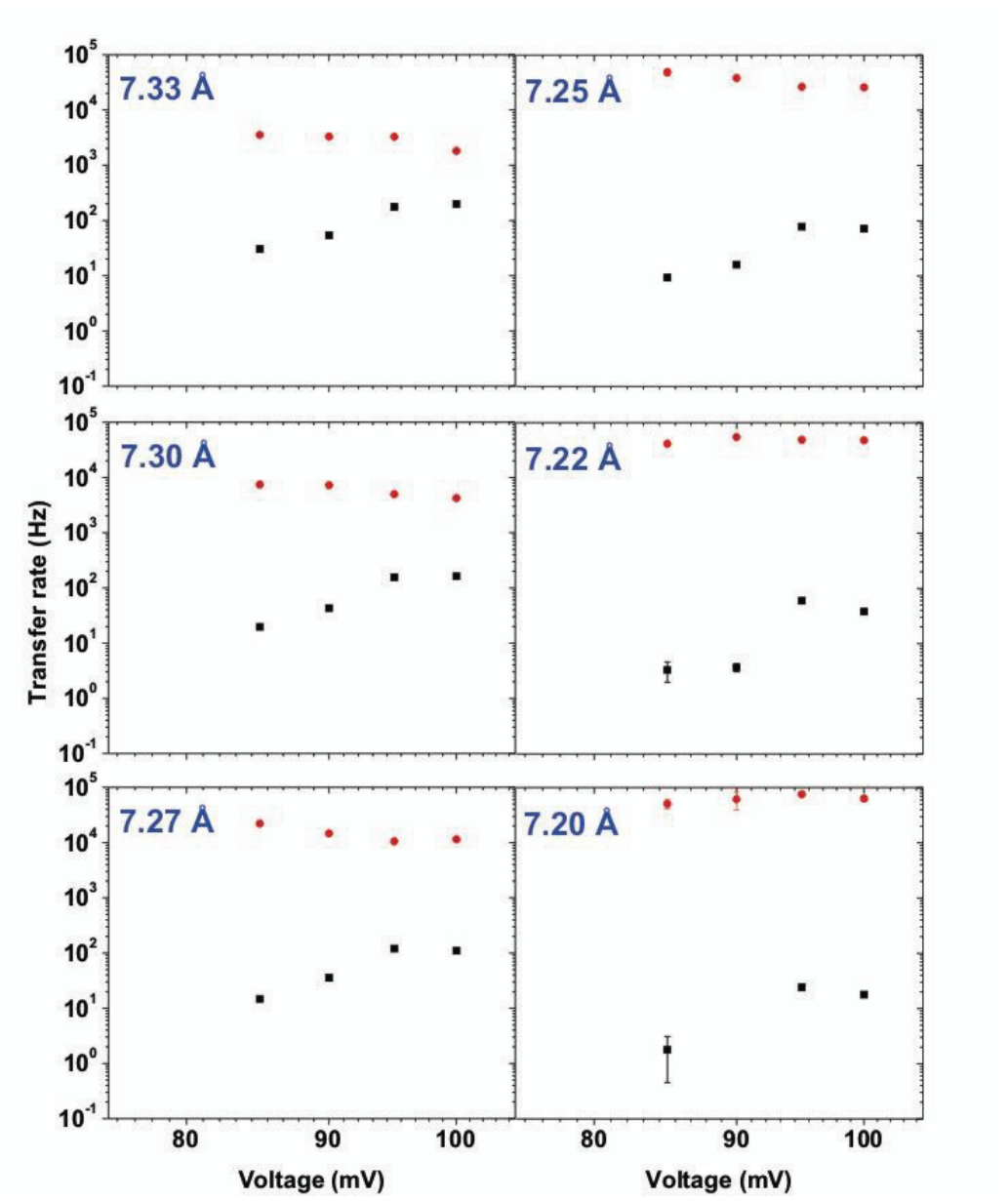
7.33 Å
7.25 Å
7.30 Å
7.22 Å
7.27 Å
7.20 Å
Transfer rate (Hz)
Voltage (mV)
Voltage (mV)
80
90
100

III.II. SECOND SERIES

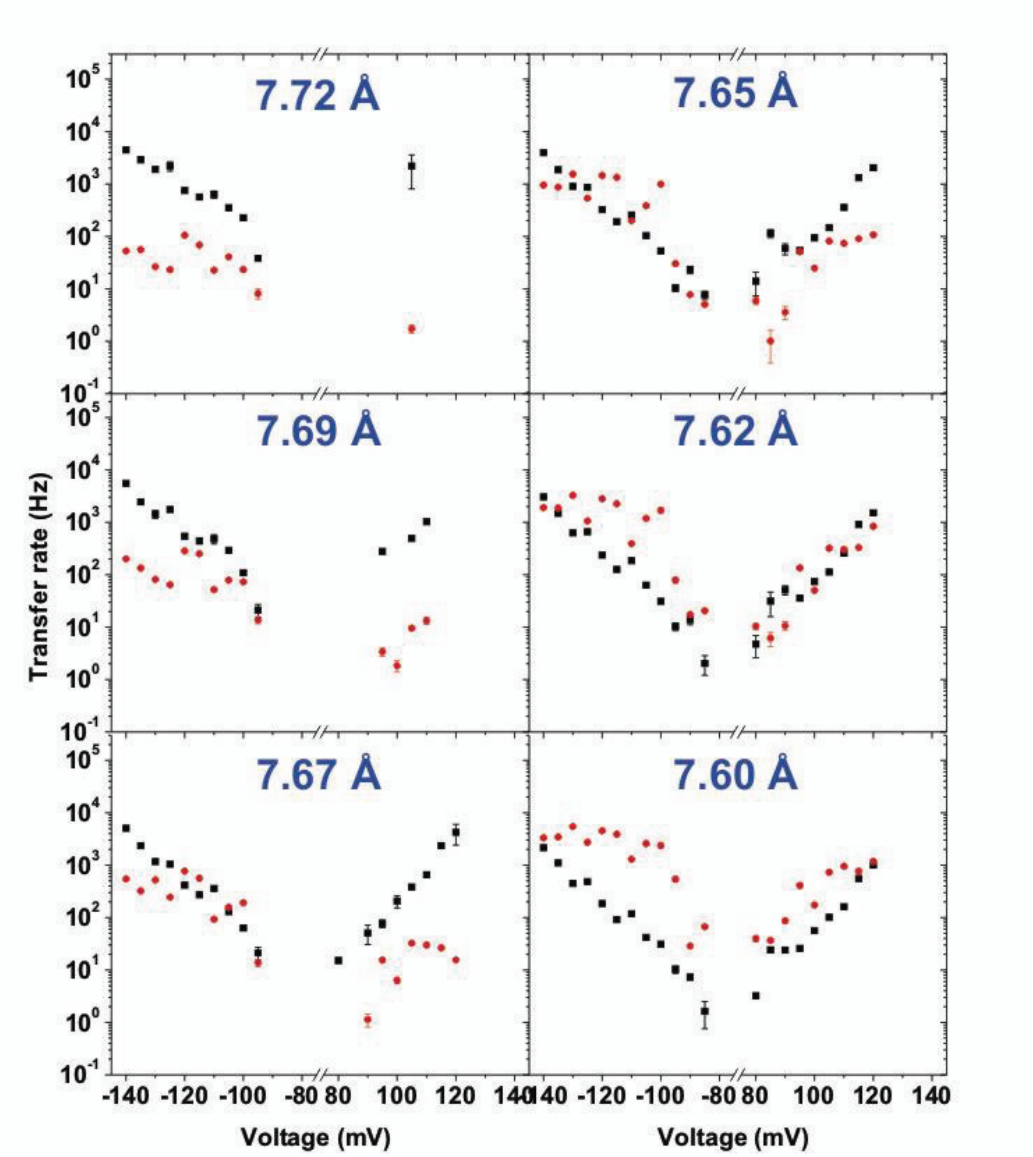

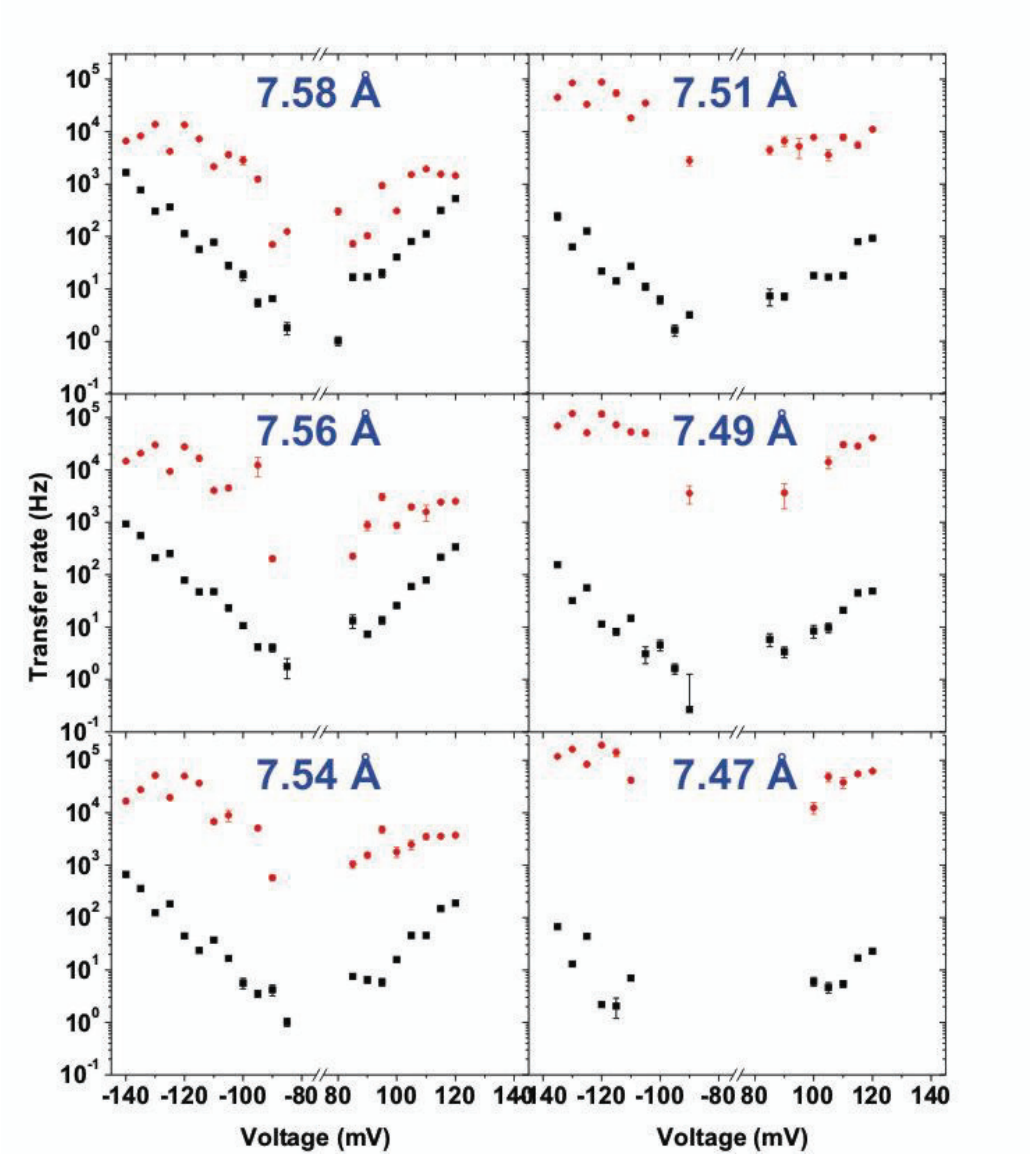
7.58 Å
7.51 Å
7.56 Å
7.49 Å
7.54 Å
7.47 Å
Transfer rate (Hz)
Voltage (mV)
Voltage (mV)

III.II. THIRD SERIES

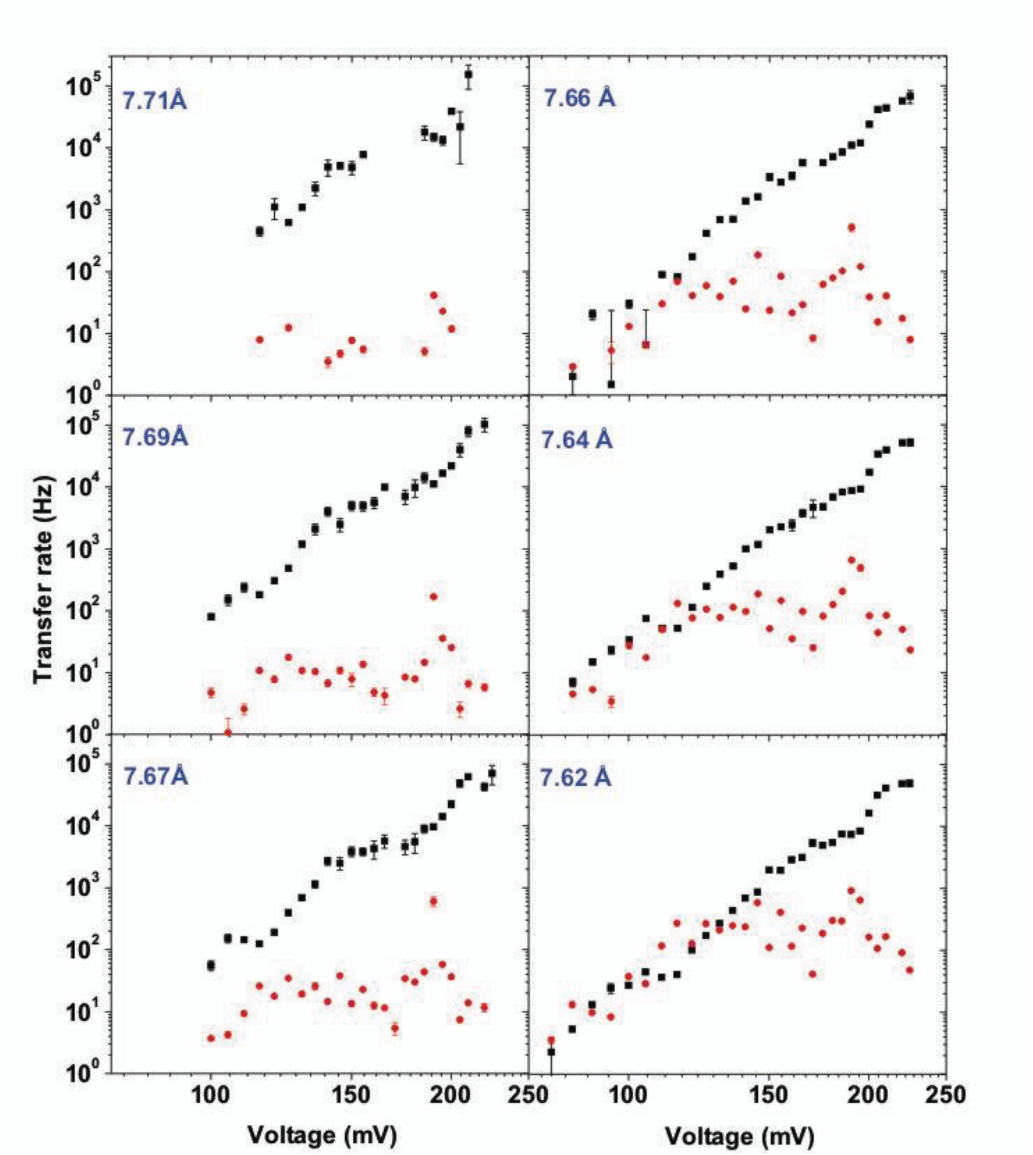

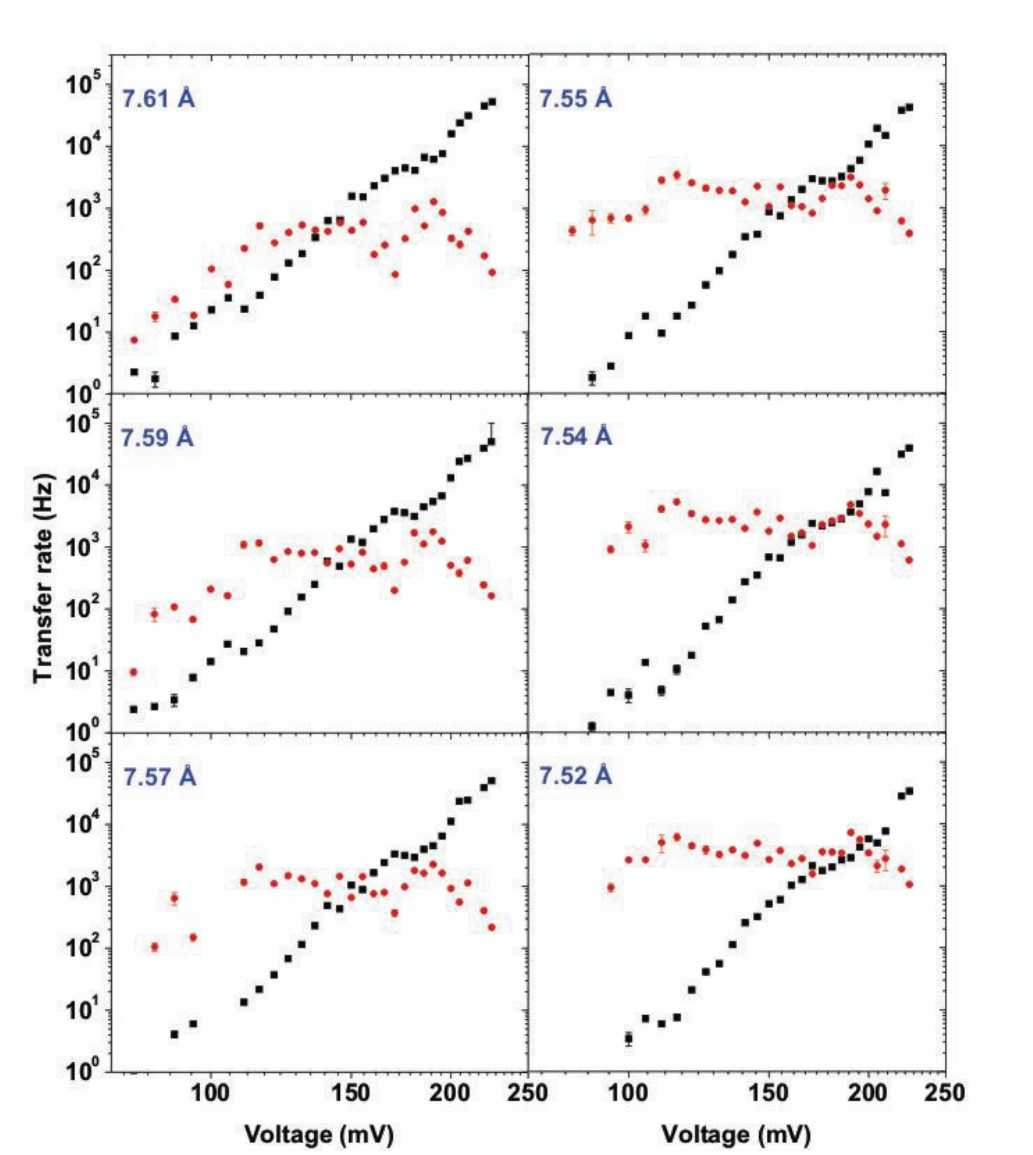
7.61 Å
7.55 Å
7.59 Å
7.54 Å
7.57 Å
7.52 Å
Transfer rate (Hz)
Voltage (mV)
Voltage (mV)

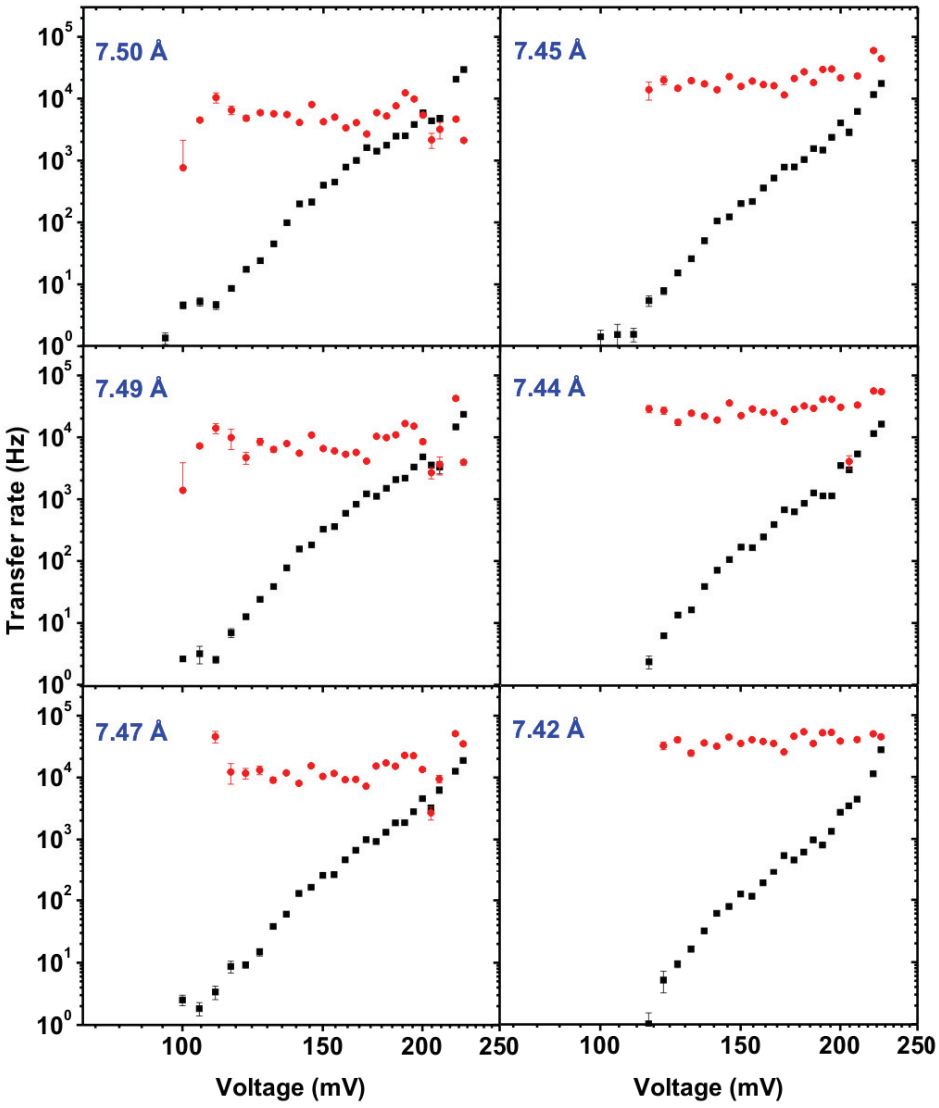
7.50 Å
7.45 Å
7.49 Å
7.44 Å
7.47 Å
7.42 Å
Transfer rate (Hz)
Voltage (mV)
Voltage (mV)

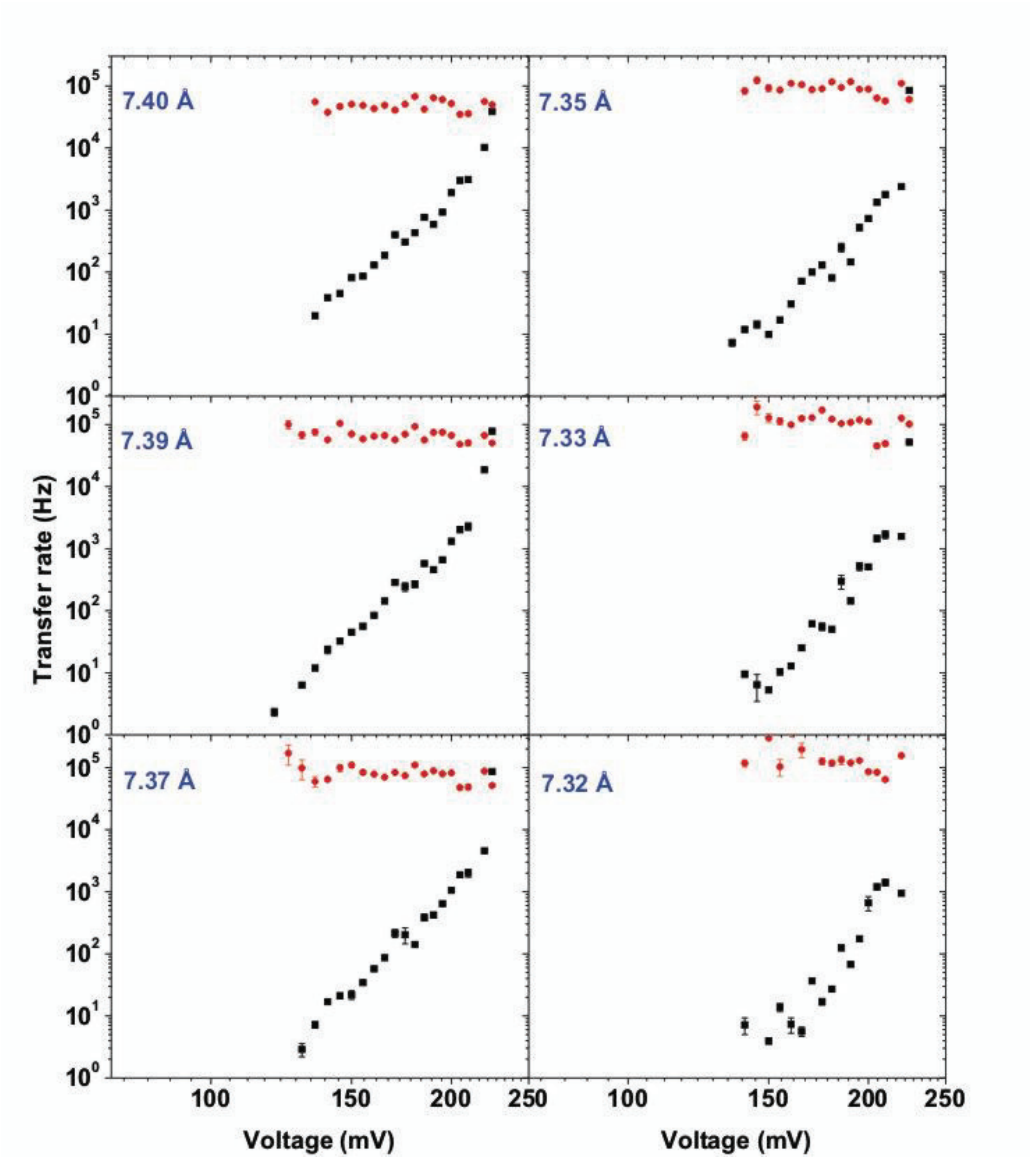
7.40 Å
7.35 Å
7.39 Å
7.33 Å
7.37 Å
7.32 Å
Transfer rate (Hz)
Voltage (mV)
Voltage (mV)

III.IV. FOURTH SERIES

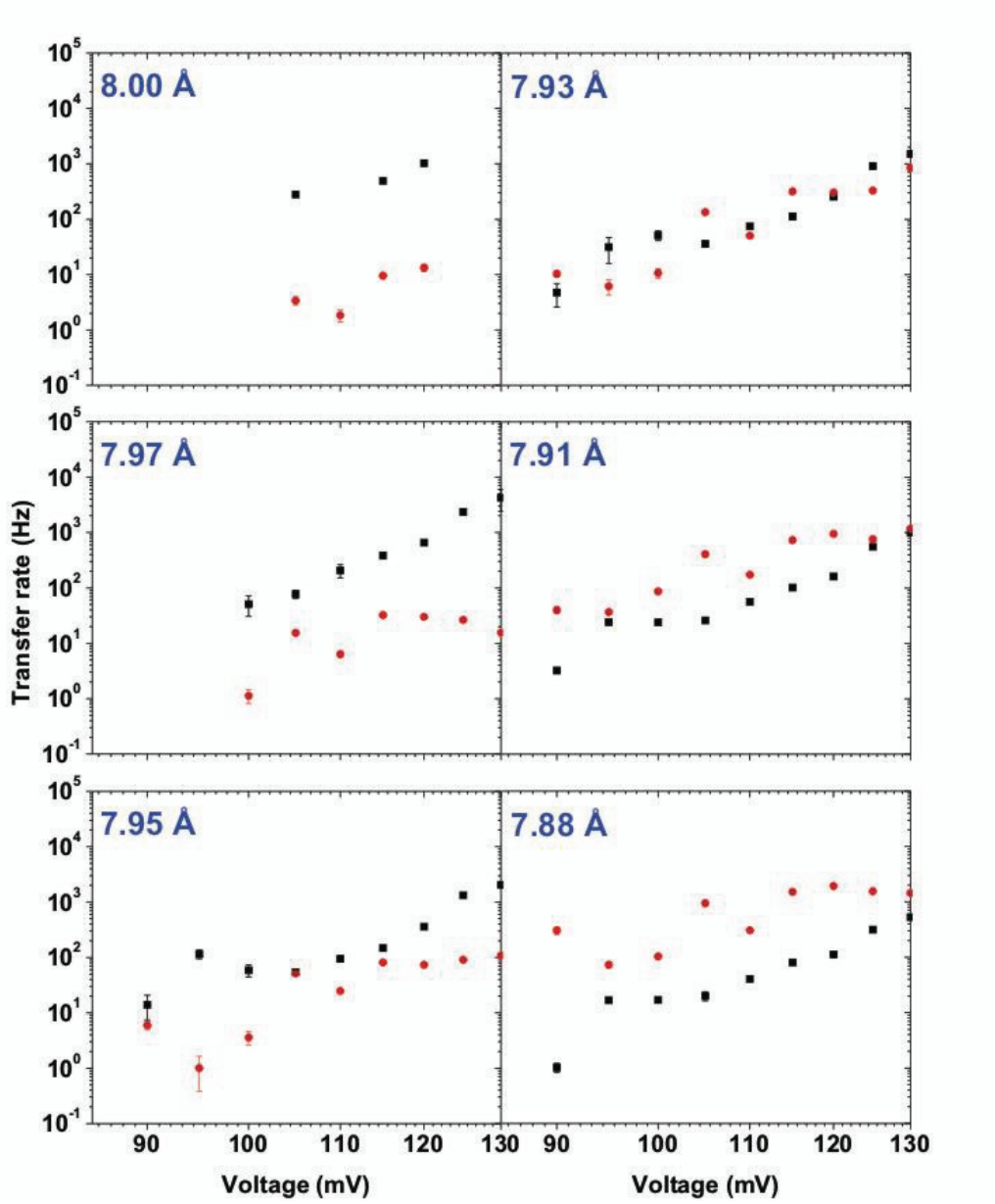

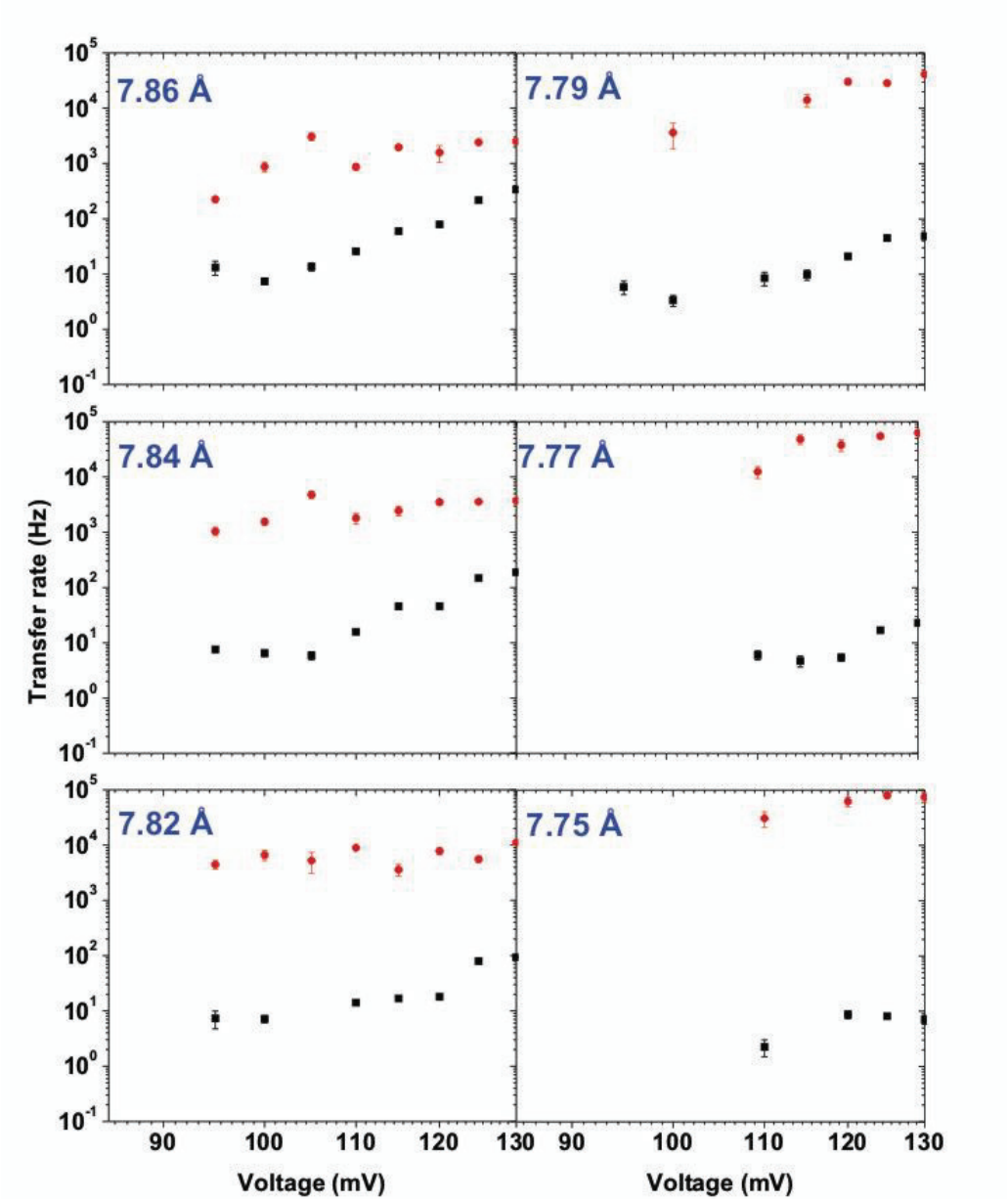

Black points – transfer rate from the high to the low conductance state (tip to surface)

Red points – transfer rate from the low to the high conductance state (surface to tip)

REFERENCES

1. *New Report Analyzes and Forecasts the Prospects for Organic Electronics Materials in the Coming Eight Years.* M2 PRESSWIRE, 2008.
2. Tang, C.W. and S.A. van Slyke, *Organic electroluminescent diodes.* Applied Physics Letters, 1987. **51**(12).
3. Gu, G., et al., *Transparent organic light emitting devices.* Applied Physics Letters, 1996. **68**(19): p. 2606-2608.
4. Dodabalapur, A., *Organic light emitting diodes.* Solid State Communications, 1997. **102**(2-3): p. 259-267.
5. Blochwitz, J., et al., *Low voltage organic light emitting diodes featuring doped phthalocyanine as hole transport material.* Applied Physics Letters, 1998. **73**(6): p. 729-731.
6. Tang, H., F. Li, and J. Shinar, *Bright high efficiency blue organic light-emitting diodes with Al[sub 2]O[sub 3]/Al cathodes.* Applied Physics Letters, 1997. **71**(18): p. 2560-2562.
7. Hoppe, H. and N.S. Sariciftci, *Organic solar cells: An overview.* Journal of Materials Research, 2004. **19**(7): p. 1924-1945.
8. Wöhrle, D. and D. Meissner, *Organic solar cells.* Advanced Materials, 1991. **3**(3): p. 129-139.
9. Horowitz, G., *Organic Field-Effect Transistors.* Advanced Materials, 1998. **10**(5): p. 365-378.
10. Horowitz, G., *Organic thin film transistors: From theory to real devices.* Journal of Materials Research, 2004. **19**(7): p. 1946-1962.
11. Yeh, H.-C., et al., *Non-doped red organic light-emitting diodes.* Journal of Materials Chemistry, 2004. **14**: p. 1293-1298.
12. Tao, S.L., et al., *Highly Efficient Non-Doped Blue Organic Light-Emitting Diodes Based on Fluorene Derivatives with High Thermal Stability.* Advanced Functional Materials, 2005. **15**(10): p. 1716-1721.
13. Walzer, K., et al., *Highly Efficient Organic Devices Based on Electrically Doped Transport Layers.* Chemical Reviews, 2007. **107**(4): p. 1233-1271.
14. Stipe, B.C., M.A. Rezaei, and W. Ho, *Inducing and viewing the rotational motion of a single molecule.* Science, 1998. **279**(5358): p. 1907-9.
15. Yu, L.H. and D. Natelson, *The Kondo Effect in C60 Single-Molecule Transistors.* Nano Letters, 2003. **4**(1): p. 79-83.
16. Park, H., et al., *Nanomechanical oscillations in a single-C60 transistor.* Nature, 2000. **407**(6800): p. 57-60.
17. Reed, M.A., et al., *Conductance of a molecular junction.* Science, 1997. **278**(5336): p. 252-254.
18. Reed, M.A., *Molecular-scale electronics.* Proceedings of the IEEE, 1999. **87**(4): p. 652-8.
19. Nitzan, A. and M.A. Ratner, *Electron transport in molecular wire junctions.* Science, 2003. **300**(5624): p. 1384-1389.
20. Cuniberti, G., G. Fagas, and K. Richter, *Introducing Molecular Electronics.* Springer, Berlin and Heidelberg, 2005.
21. van Ruitenbeek, J., E. Scheer, and H.B. Weber, *Contacting individual molecules using mechanically controllable break junctions.* Introducing Molecular Electronics. Springer-Verlag. 2005, 2005: p. 253-74.
22. Smit, R.H.M., et al., *Measurement of the conductance of a hydrogen molecule.* Nature, 2002. **419**(6910): p. 906-909.
23. Scheer, E., et al., *The signature of chemical valence in the electrical conduction through a single-atom contact.* Nature, 1998. **394**(6689): p. 154-157.
24. Scheer, E., et al., *Conduction Channel Transmissions of Atomic-Size Aluminum Contacts.* Physical Review Letters, 1997. **78**(18): p. 3535.

25. Reichert, J., et al., *Driving Current through Single Organic Molecules.* Physical Review Letters, 2002. **88**(17): p. 176804.
26. Xie, F.Q., et al., *Gate-Controlled Atomic Quantum Switch.* Physical Review Letters, 2004. **93**(12): p. 128303.
27. Champagne, A.R., A.N. Pasupathy, and D.C. Ralph, *Mechanically Adjustable and Electrically Gated Single-Molecule Transistors.* Nano Letters, 2005. **5**(2): p. 305-308.
28. Heersche, H.B., et al., *Kondo Effect in the Presence of Magnetic Impurities.* Physical Review Letters, 2006. **96**(1): p. 017205.
29. Güntherodt, H.J., *Scanning tunneling microscopy I: general principles and applications to clean and adsorbate-covered surfaces*. 1994.
30. Repp, J., et al., *Scanning Tunneling Spectroscopy of Cl Vacancies in NaCl Films: Strong Electron-Phonon Coupling in Double-Barrier Tunneling Junctions.* Physical Review Letters, 2005. **95**(22): p. 225503.
31. Stipe, B.C., M.A. Rezaei, and W. Ho, *Coupling of vibrational excitation to the rotational motion of a single adsorbed molecule.* Physical Review Letters, 1998. **81**(6): p. 1263-6.
32. Stipe, B.C., M.A. Rezaei, and W. Ho, *Localization of Inelastic Tunneling and the Determination of Atomic-Scale Structure with Chemical Specificity.* Physical Review Letters, 1999. **82**(8): p. 1724.
33. Dujardin, G., A.J. Mayne, and F. Rose, *Temperature Control of Electronic Channels through a Single Atom.* Physical Review Letters, 2002. **89**(3): p. 036802.
34. Knorr, N., et al., *Kondo Effect of Single Co Adatoms on Cu Surfaces.* Physical Review Letters, 2002. **88**(9): p. 096804.
35. Wahl, P., et al., *Kondo Effect of Molecular Complexes at Surfaces: Ligand Control of the Local Spin Coupling.* Physical Review Letters, 2005. **95**(16): p. 166601.
36. Martin, M., et al., *Mastering the Molecular Dynamics of a Bistable Molecule by Single Atom Manipulation.* Physical Review Letters, 2006. **97**(21): p. 216103.
37. Hla, S.-W., et al., *Controlled Low-Temperature Molecular Manipulation of Sexiphenyl Molecules on Ag(111) Using Scanning Tunneling Microscopy.* Physical Review Letters, 2004. **93**(20): p. 208302.
38. Iancu, V., A. Deshpande, and S.-W. Hla, *Manipulation of the Kondo Effect via Two-Dimensional Molecular Assembly.* Physical Review Letters, 2006. **97**(26): p. 266603-4.
39. Simic-Milosevic, V., et al., *Electron Induced Ortho-Meta Isomerization of Single Molecules.* Physical Review Letters, 2007. **98**(11): p. 116102.
40. Temirov, R., et al., *Kondo effect by controlled cleavage of a single molecule contact.* Nanotechnology, 2008. **6**(065401).
41. Stroscio, J.A. and D.M. Eigler, *Atomic and Molecular Manipulation with the Scanning Tunneling Microscope.* Science, 1991. **254**(5036): p. 1319-1326.
42. Gauthier, S., *Atomic and molecular manipulations of individual adsorbates by STM.* Applied Surface Science, 2000. **164**(1-4): p. 84-90.
43. Moresco, F., et al., *Conformational Changes of Single Molecules Induced by Scanning Tunneling Microscopy Manipulation: A Route to Molecular Switching.* Physical Review Letters, 2001. **86**(4): p. 672.
44. Moresco, F., *Manipulation of large molecules by low-temperature STM: model systems for molecular electronics.* Physics Reports, 2004. **399**(4): p. 175-225.
45. Gimzewski, J.K. and C. Joachim, *Nanoscale Science of Single Molecules Using Local Probes.* Science, 1999. **283**(5408): p. 1683-1688.
46. Stipe, B.C., et al., *Single-Molecule Dissociation by Tunneling Electrons.* Physical Review Letters, 1997. **78**(23): p. 4410.
47. Albrecht, T., et al., *Transistor-like Behavior of Transition Metal Complexes.* Nanoletters., 2005. **5**(7): p. 1451-1455.

48. Hahn, J.R., H.J. Lee, and W. Ho, *Electronic Resonance and Symmetry in Single-Molecule Inelastic Electron Tunneling.* Physical Review Letters, 2000. **85**(9): p. 1914.
49. Nazin, G.V., X.H. Qiu, and W. Ho, *Atomic Engineering of Photon Emission with a Scanning Tunneling Microscope.* Physical Review Letters, 2003. **90**(21): p. 216110.
50. Qiu, X.H., G.V. Nazin, and W. Ho, *Mechanisms of Reversible Conformational Transitions in a Single Molecule.* Physical Review Letters, 2004. **93**(19): p. 196806.
51. Choi, B.-Y., et al., *Conformational Molecular Switch of the Azobenzene Molecule: A Scanning Tunneling Microscopy Study.* Physical Review Letters, 2006. **96**(15): p. 156106.
52. Aviram, A. and M.A. Ratner, *Molecular rectifiers.* Chemical Physics Letters 1974. **29**(2): p. 7.
53. Joachim, C., J.K. Gimzewski, and H. Tang, *Physical principles of the single-C_{60} transistor effect.* Physical Review B, 1998. **58**(24): p. 16407.
54. Aviram, A., C. Joachim, and M. Pomerantz, *Evidence of switching and rectification by a single molecule effected with a scanning tunneling microscope.* Chemical Physics Letters, 1988. **146**(6): p. 490-495.
55. Moresco, F., et al., *Low temperature manipulation of big molecules in constant height mode.* Applied Physics Letters, 2001. **78**(3): p. 306-308.
56. Tang, H., et al., *Fundamental considerations in the manipulation of a single C60 molecule on a surface with an STM.* Surface Science, 1997.
57. Stroscio, J.A. and R.J. Celotta, *Controlling the Dynamics of a Single Atom in Lateral Atom Manipulation.* Science, 2004. **306**(5694): p. 242-247.
58. Alemani, M., et al., *Electric Field-Induced Isomerization of Azobenzene by STM.* Journal of the American Chemical Society, 2006. **128**(45): p. 14446-14447.
59. Hagen, S., et al., *Reversible switching of tetra-tert-butyl-azobenzene on a Au(1 1 1) surface induced by light and thermal activation.* Chemical Physics Letters, 2007. **444**(1-3): p. 85-90.
60. Katsonis, N., et al., *Synthetic light-activated molecular switches and motors on surfaces.* Progress in Surface Science, 2007. **82**(7-8): p. 407-434.
61. Hla, S.-W. and K.-H. Rieder, *STM CONTROL OF CHEMICAL REACTIONS: Single-Molecule Synthesis.* Annual Review of Physical Chemistry, 2003. **54**(1): p. 307-330.
62. Liljeroth, P., J. Repp, and G. Meyer, *Current-Induced Hydrogen Tautomerization and Conductance Switching of Naphthalocyanine Molecules.* Science, 2007. **317**(5842): p. 1203-1206.
63. Krause, S., et al., *Current-Induced Magnetization Switching with a Spin-Polarized Scanning Tunneling Microscope.* Science, 2007. **317**(5844): p. 1537-1540.
64. Brumme, T., et al., *Dynamical bi-stability of single-molecule junctions: A combined experimental/theoretical study of PTCDA on Ag(111).*
65. Nacci, C., et al., *Conformational switching of single 1,5-cyclooctadiene molecules on Si(001) induced by inelastic electron tunneling.* Physical Review B, 2008. **77**(12): p. 121405.
66. Wang, Y., et al., *Pushing and Pulling a Sn Ion through an Adsorbed Phthalocyanine Molecule.* Journal of the American Chemical Society, 2009. **131**(10): p. 3639-3643.
67. Yongfeng, W., et al., *Structural and Electronic Properties of Ultrathin Tin-Phthalocyanine Films on Ag(111) at the Single-Molecule Level13.* Angewandte Chemie, 2009. **121**(7): p. 1287-1291.
68. Lovinger, A.J., et al., *Structural and morphological investigation of the development of electrical conductivity in ion-irradiated thin films of an organic material.* Journal of Applied Physics, 1984. **55**(2): p. 476-82.
69. Umbach, E., *Characterization of organic overlayers on well-defined substrates.* Progress in Surface Science, 1990. **35**(1-4): p. 113-27.
70. Mobus, M., N. Karl, and T. Kobayashi, *Structure of perylene-tetracarboxylic-dianhydride thin films on alkali halide crystal substrates.* Journal of Crystal Growth, 1992. **116**(3-4): p. 495-504.

71. Jung, M., et al., *The Electronic-Structure of Adsorbed Aromatic-Molecules - Perylene and Ptcda on Si(111) and Ag(111).* Journal of Molecular Structure, 1993. **293**: p. 239-244.
72. Umbach, E., et al., *Highly-ordered organic adsorbates: commensurate superstructures, OMBE, and 1D nanostructures.* Akademie Verlag. Physica Status Solidi B, 1995. **192**(2): p. 389-406.
73. Umbach, E., M. Sokolowski, and R. Fink, *Substrate-interaction, long-range order, and epitaxy of large organic adsorbates.* Applied Physics A (Materials Science Processing), 1996. **A63**(6): p. 565-76.
74. Schmitz-Hubsch, T., et al., *Epitaxial growth of 3,4,9,10-perylene-tetracarboxylic-dianhydride on Au(111): a STM and RHEED study.* Physical Review B, 1997. **55**(12): p. 7972-6.
75. Ogawa, T., et al., *3,4 : 9,10-perylenetetracarboxylic dianhydride (PTCDA) by electron crystallography.* Acta Crystallographica Section B-Structural Science, 1999. **55**: p. 123-130.
76. Shklover, V., et al., *Differences in vibronic and electronic excitations of PTCDA on Ag(111) and Ag(110).* Elsevier. Surface Science, 2000. **454-456**: p. 60-6.
77. Tautz, F.S., et al., *Strong electron-phonon coupling at a metal/organic interface: PTCDA/Ag(111).* Physical Review B, 2002. **65**(12): p. 125405/1-10.
78. Tautz, F.S., et al., *Vibrational properties of ultrathin PTCDA films on Ag(110).* Physical Review B, 2000. **61**(24): p. 16933-16947.
79. Wagner, V., et al., *Raman analysis of first monolayers of PTCDA on Ag(111).* Applied Surface Science, 2003. **212-213**: p. 520-4.
80. Kraft, A., et al., *Lateral adsorption geometry and site-specific electronic structure of a large organic chemisorbate on a metal surface.* Physical Review B, 2006. **74**(4): p. 041402(R).
81. Temirov, R., et al., *Free-electron-like dispersion in an organic monolayer film on a metal substrate.* Nature, 2006. **444**(7117): p. 350-353.
82. Schneider, M., E. Umbach, and M. Sokolowski, *Growth-dependent optical properties of 3,4,9,10-perylenetetracarboxylicacid-dianhydride (PTCDA) films on Ag(1 1 1).* Chemical Physics, 2006. **325**(1): p. 185-192.
83. Rohlfing, M., R. Temirov, and F.S. Tautz, *Adsorption structure and scanning tunneling data of a prototype organic-inorganic interface: PTCDA on Ag(111).* Physical Review B, 2007. **76**(11): p. 115421-16.
84. Tautz, F.S., *Structure and bonding of large aromatic molecules on noble metal surfaces: The example of PTCDA.* Progress in Surface Science, 2007. **82**(12): p. 479-520.
85. Pump, F., et al., *Quantum transport through STM-lifted single PTCDA molecules.* Applied Physics A: Materials Science & Processing, 2008. **93**(2): p. 335-343.
86. Forrest, S.R., *Ultrathin organic films grown by organic molecular beam deposition and related techniques.* Chemical Reviews, 1997. **97**(6): p. 1793-1896.
87. Umbach, E., K. Glockler, and M. Sokolowski, *Surface "architecture" with large organic molecules: interface order and epitaxy.* Elsevier. Surface Science, 1998. **404**: p. 20-31.
88. Wurthner, F., *Perylene bisimide dyes as versatile building blocks for functional supramolecular architectures.* Chemical Communications, 2004(14): p. 1564-1579.
89. Glockler, K., et al., *Highly ordered structures and submolecular scanning tunnelling microscopy contrast of PTCDA and DM-PBDCI monolayers on Ag(111) and Ag(110).* Surface Science, 1998. **405**(1): p. 1-20.
90. Kilian, L., E. Umbach, and M. Sokolowski, *Molecular beam epitaxy of organic films investigated by high resolution low energy electron diffraction (SPA-LEED): 3,4,9,10-perylenetetracarboxylicacid-dianhydride (PTCDA) on Ag(111).* Surface Science, 2004. **573**(3): p. 359-78.
91. Kilian, L., et al., *Role of Intermolecular Interactions on the Electronic and Geometric Structure of a Large pi-Conjugated Molecule Adsorbed on a Metal Surface.* Physical Review Letters, 2008. **100**(13): p. 136103-4.

92. Henze, S.K.M., et al., *Vertical bonding distances of PTCDA on Au(111) and Ag(111): Relation to the bonding type.* Surface Science, 2007. **601**(6): p. 1566-1573.
93. Hauschild, A., et al., *Molecular distortions and chemical bonding of a large pi-conjugated molecule on a metal surface.* Physical Review Letters, 2005. **94**(3): p. 036106-036109.
94. Hla, S.-W., *Scanning Tunneling Microscope Atom and Molecule Manipulations: Realizing Molecular Switches and Devices.* Japanese Journal of Applied Physics, 2008. **47**(7): p. 7.
95. Joachim, C. and M.A. Ratner, *Molecular Electronics Special Feature: Molecular electronics: Some views on transport junctions and beyond.* Proceedings of the National Academy of Sciences, 2005. **102**(25): p. 8801-8808.
96. Kroger, J., et al., *Surface state electron dynamics of clean and adsorbate-covered metal surfaces studied with the scanning tunnelling microscope.* Progress in Surface Science, 2005. **80**(1-2): p. 26-48.
97. Gauyacq, J.P., A.G. Borisov, and A.K. Kazansky, *Impurity-induced localisation of the 2D surface-state continuum on a metal surface* Applied Physics A (Materials Science Processing), 2004. **78**(2): p. 141-147.
98. Crommie, M.F., C.P. Lutz, and D.M. Eigler, *Imaging standing waves in a two-dimensional electron gas.* Nature, 1993. **363**(6429): p. 524-527.
99. Lu, X., et al., *Spatially Mapping the Spectral Density of a Single C60 Molecule.* Physical Review Letters, 2003. **90**(9): p. 096802.
100. Silien, C., et al., *Influence of adsorbate-substrate interaction on the local electronic structure of C60 studied by low-temperature STM.* Physical Review B, 2004. **69**(11): p. 115434.
101. Bendounan, A., et al., *Electronic structure of 1 ML NTCDA/Ag(1 1 1) studied by photoemission spectroscopy.* Surface Science, 2007. **601**(18): p. 4013-4017.
102. Li, J.T., et al., *Kondo scattering observed at a single magnetic impurity.* Physical Review Letters, 1998. **80**(13): p. 2893-2896.
103. Repp, J., et al., *Controlling the Charge State of Individual Gold Adatoms.* Science, 2004. **305**(5683): p. 493-495.
104. Repp, J., et al., *Imaging Bond Formation Between a Gold Atom and Pentacene on an Insulating Surface.* Science, 2006. **312**(5777): p. 1196-1199.
105. Wu, S.Y., T. Ogawa, and W. Ho, *Atomic-Scale Coupling of Photons to Single-Molecule Junctions* Science, 2006. **312**(5778): p. 1362-1365.
106. Romaner, L. and et al., *Theoretical study of PTCDA adsorbed on the coinage metal surfaces, Ag(111), Au(111) and Cu(111).* New Journal of Physics, 2009. **11**(5): p. 053010.
107. Grobis, M., X. Lu, and M.F. Crommie, *Local electronic properties of a molecular monolayer: C60 on Ag(001).* Physical Review B, 2002. **66**(16): p. 161408.
108. Binnig, G., et al., *Tunneling Spectroscopy and Inverse Photoemission: Image and Field States.* Physical Review Letters, 1985. **55**(9): p. 991.
109. Limot, L., et al., *Surface-State Stark Shift in a Scanning Tunneling Microscope.* Physical Review Letters, 2003. **91**(19): p. 196801.
110. Kröger, J., et al., *Stark effect in Au(111) and Cu(111) surface states.* Physical Review B, 2004. **70**(3): p. 033401.
111. Temirov, R., et al., *A novel method achieving ultra-high geometrical resolution in scanning tunnelling microscopy.* New Journal of Physics. **10**(053012): p. 11.
112. Bulovic, V., et al., *Study of localized and extended excitons in 3,4,9,10-perylenetetracarboxylic dianhydride (PTCDA) I. Spectroscopic properties of thin films and solutions.* Chemical Physics, 1996. **210**(1-2): p. 1-12.
113. Wüsten, J., et al., *Post deposition purification of PTCDA thin films.* Applied Surface Science, 2005. **252**(1): p. 104-107.
114. Eigler, D.M. and E.K. Schweizer, *Positioning single atoms with a scanning tunnelling microscope.* Nature, 1990. **344**(6266): p. 524-526.

115. Yildirim, H., A. Kara, and T.S. Rahman, *Tip-induced adatom extraction and cluster manipulation.* Physical Review B (Condensed Matter and Materials Physics), 2007. **75**(20): p. 205409-7.
116. Bouju, X., C. Joachim, and C. Girard, *Single-atom motion during a lateral STM manipulation.* Physical Review B, 1999. **59**(12): p. R7845.
117. Zeppenfeld, P., C.P. Lutz, and D.M. Eigler, *Manipulating atoms and molecules with a scanning tunneling microscope.* Ultramicroscopy (The Netherlands), 1991. **42-44**: p. 128.
118. Cuberes, M.T., R.R. Schlittler, and J.K. Gimzewski, *Room-temperature repositioning of individual C60 molecules at Cu steps: Operation of a molecular counting device.* Applied Physics Letters, 1996. **69**(20): p. 3016-3018.
119. Jung, T.A., et al., *Controlled Room-Temperature Positioning of Individual Molecules: Molecular Flexure and Motion.* Science, 1996. **271**(5246): p. 181-184.
120. Bartels, L., G. Meyer, and K.H. Rieder, *Basic Steps of Lateral Manipulation of Single Atoms and Diatomic Clusters with a Scanning Tunneling Microscope Tip.* Physical Review Letters, 1997. **79**(4): p. 697.
121. Meyer, G., et al., *Controlled Atom by Atom Restructuring of a Metal Surface with the Scanning Tunneling Microscope.* Physical Review Letters, 1997. **78**(8): p. 1512.
122. Bouju, X., et al., *Mechanics of (Xe)N atomic chains under STM manipulation.* Physical Review B, 2001. **63**(8): p. 085415.
123. Hla, S.W., et al., *Controlled lateral manipulation of single diiodobenzene molecules on the Cu(111) surface with the tip of a scanning tunnelling microscope.* Surface Science, 2000. **454-456**: p. 1079-1084.
124. Gerhard, M., et al., *Controlled Manipulation of Atoms and Small Molecules with a Low Temperature Scanning Tunneling Microscope.* Single Molecules, 2000. **1**(1): p. 79-86.
125. Hla, S.-W., et al., *Inducing All Steps of a Chemical Reaction with the Scanning Tunneling Microscope Tip: Towards Single Molecule Engineering.* Physical Review Letters, 2000. **85**(13): p. 2777.
126. Kühnle, A., et al., *Understanding atom movement during lateral manipulation with the STM tip using a simple simulation method.* Surface Science, 2002. **499**(1): p. 15-23.
127. Hla, S.-W., K.-F. Braun, and K.-H. Rieder, *Single-atom manipulation mechanisms during a quantum corral construction.* Physical Review B, 2003. **67**(20): p. 201402.
128. Grill, L., et al., *Controlled manipulation of a single molecular wire along a copper atomic nanostructure.* Physical Review B, 2004. **69**(3): p. 035416.
129. Braun, K.F. and S.W. Hla, *Probing the Conformation of Physisorbed Molecules at the Atomic Scale Using STM Manipulation.* Nanoletters., 2005. **5**(1): p. 73-76.
130. Gross, L., et al., *Trapping and moving metal atoms with a six-leg molecule.* Nat Mater, 2005. **4**(12): p. 892-895.
131. Braun, K.F. and S.W. Hla, *Force measurement with a scanning tunneling microscope.* Physical Review B (Condensed Matter and Materials Physics), 2007. **75**(3): p. 033406-4.
132. Deshpande, A., et al., *Atom-By-Atom Extraction Using the Scanning Tunneling Microscope Tip-Cluster Interaction.* Physical Review Letters, 2007. **98**(2): p. 028304-4.
133. GrillL, et al., *Rolling a single molecular wheel at the atomic scale.* Nat Nano, 2007. **2**(2): p. 95-98.
134. Eigler, D.M., C.P. Lutz, and W.E. Rudge, *An atomic switch realized with the scanning tunnelling microscope.* Nature, 1991. **352**(6336): p. 600-603.
135. Tilinin, I.S., M.A. Van Hove, and M. Salmeron, *Quantum coherence in surface-tip transfer of adatoms in AFM/STM.* Physical Review B, 1998. **57**(8): p. 4720.
136. Bartels, L., et al., *Dynamics of Electron-Induced Manipulation of Individual CO Molecules on Cu(111).* Physical Review Letters, 1998. **80**(9): p. 2004.

137. Dujardin, G., et al., *Vertical Manipulation of Individual Atoms by a Direct STM Tip-Surface Contact on Ge(111).* Physical Review Letters, 1998. **80**(14): p. 3085.
138. Lee, H.J. and W. Ho, *Single-bond formation and characterization with a scanning tunneling microscope.* Science, 1999. **286**(5445): p. 1719-22.
139. Hahn, J.R. and W. Ho, *Oxidation of a Single Carbon Monoxide Molecule Manipulated and Induced with a Scanning Tunneling Microscope.* Physical Review Letters, 2001. **87**(16): p. 166102.
140. Saw-Wai, H., M. Gerhard, and R. Karl-Heinz, *Inducing Single-Molecule Chemical Reactions with a UHV-STM: A New Dimension for Nano-Science and Technology.* ChemPhysChem, 2001. **2**(6): p. 361-366.
141. Toher, C., et al., *Unravelling electron correlation effects in molecular wires.* 2009.
142. Harmon, K.M., et al., *Hydrogen bonding: part 78. Ab initio molecular orbital study of intra- and intermolecular hydrogen bonding in choline and betaine and their compounds with HF and H2O.* Journal of Molecular Structure, 2001. **597**(1-3): p. 177-190.
143. Hauschild, A., et al., *Molecular Distortions and Chemical Bonding of a Large pi -Conjugated Molecule on a Metal Surface.* Physical Review Letters, 2005. **94**(3): p. 036106.
144. Lide, D.R., *CRC Handbook of Chemistry and Physics*. 89 ed, ed. D.R. Lide. 2008.
145. Duhm, S., et al., *PTCDA on Au(1 1 1), Ag(1 1 1) and Cu(1 1 1): Correlation of interface charge transfer to bonding distance.* Organic Electronics, 2008. **9**(1): p. 111-118.
146. Rocha, A.R., et al., *Spin and molecular electronics in atomically generated orbital landscapes.* Physical Review B (Condensed Matter and Materials Physics), 2006. **73**(8): p. 085414-22.
147. Gadzuk, J.W., *Inelastic resonance scattering, tunneling, and desorption.* Physical Review B, 1991. **44**(24): p. 13466.
148. Tikhodeev, S.G. and H. Ueba, *Relation between inelastic electron tunneling and vibrational excitation of single adsorbateson metal surfaces.* Physical Review B, 2004. **70**(12): p. 125414.
149. Ueba, H., et al., *Adsorbate motions induced by inelastic-tunneling current: Theoretical scenarios of two-electron processes.* The Journal of Chemical Physics, 2005. **123**(8): p. 084707-8.
150. Tikhodeev, S.G. and H. Ueba, *How Vibrationally Assisted Tunneling with STM Affects the Motions and Reactions of Single Adsorbates.* Physical Review Letters, 2009. **102**(24): p. 246101-4.
151. Čížek, M., M. Thoss, and W. Domcke, *Theory of vibrationally inelastic electron transport through molecular bridges.* Physical Review B, 2004. **70**(12): p. 125406.
152. Gao, S., M. Persson, and B.I. Lundqvist, *Theory of atom transfer with a scanning tunneling microscope.* Physical Review B, 1997. **55**(7): p. 4825.
153. Elste, F., et al., *Current-induced conformational switching in single-molecule junctions.* Applied Physics A: Materials Science & Processing, 2008. **93**(2): p. 345-354.
154. Collier, C.P., et al., *A [2]Catenane-Based Solid State Electronically Reconfigurable Switch.* Science, 2000. **289**(5482): p. 1172-1175.
155. Ohara, M., Y. Kim, and M. Kawai, *Electric field response of a vibrationally excited molecule in an STM junction.* Physical Review B (Condensed Matter and Materials Physics), 2008. **78**(20): p. 201405-4.
156. Hla, S.-W., G. Meyer, and K.-H. Rieder, *Selective bond breaking of single iodobenzene molecules with a scanning tunneling microscope tip.* Chemical Physics Letters, 2003. **370**(3-4): p. 431-436.
157. Iancu, V. and S.-W. Hla, *Realization of a four-step molecular switch in scanning tunneling microscope manipulation of single chlorophyll-a molecules.* Proceedings of the National Academy of Sciences, 2006. **103**(37): p. 13718-13721.
158. Kogan, S., *Electronic noise and fluctuations in solids*. 1996, New York: Cambrige University Press.

159. Pizzagalli, L., J.C. Okon, and C. Joachim, *Moving a silver atom on a Si(001) surface with a tip?* Surface Science, 1997. **384**(1-3): p. L852-L857.
160. Lyo, I.-W. and P. Avouris, *Field-Induced Nanometer- to Atomic-Scale Manipulation of Silicon Surfaces with the STM.* Science, 1991. **253**(5016): p. 173-176.
161. Louis, A.A. and J.P. Sethna, *Atomic Tunneling from a Scanning-Tunneling or Atomic-Force Microscope Tip: Dissipative Quantum Effects from Phonons.* Physical Review Letters, 1995. **74**(8): p. 1363.
162. Lauhon, L.J. and W. Ho, *Direct Observation of the Quantum Tunneling of Single Hydrogen Atoms with a Scanning Tunneling Microscope.* Physical Review Letters, 2000. **85**(21): p. 4566.
163. Lauhon, L.J. and W. Ho, *Single molecule thermal rotation and diffusion: Acetylene on Cu(001).* The Journal of Chemical Physics, 1999. **111**(13): p. 5633-5636.
164. Lastapis, M., et al., *Picometer-Scale Electronic Control of Molecular Dynamics Inside a Single Molecule.* Science, 2005. **308**(5724): p. 1000-1003.
165. Rice, S.A., *Molecular dynamics: Optical control of reactions.* Nature, 2000. **403**(6769): p. 496-497.
166. Stokbro, K., et al., *STM-Induced Hydrogen Desorption via a Hole Resonance.* Physical Review Letters, 1998. **80**(12): p. 2618.
167. Lorente, N. and M. Persson, *Theory of Single Molecule Vibrational Spectroscopy and Microscopy.* Physical Review Letters, 2000. **85**(14): p. 2997.
168. Stipe, B.C., M.A. Rezaei, and W. Ho, *Single-Molecule Vibrational Spectroscopy and Microscopy.* Science, 1998. **280**(5370): p. 1732-1735.
169. Yazdani, A., D.M. Eigler, and N.D. Lang, *Off-Resonance Conduction Through Atomic Wires.* Science, 1996. **272**(5270): p. 1921-1924.
170. Walkup, R.E., D.M. Newns, and P. Avouris, *Role of multiple inelastic transitions in atom transfer with the scanning tunneling microscope.* Physical Review B, 1993. **48**(3): p. 1858.
171. Montroll, E.W. and K.E. Shuler, *The application of the theory of stochastic processes to chemical reactions.* Advances in Chemical Physics, 1958. **1**(361).
172. Lang, N.D., Comments on Condensed Matter Physics, 1989. **14**(253).
173. Hewson, A.C. and D.M. Newns, *On the local polaron model and its applications to intermediate valence systems.* Journal of Physics C: Solid State Physics, 1980. **13**(24): p. 4477-4494.
174. Kobitski, A.Y., R. Scholz, and D.R.T. Zahn, *Theoretical studies of the vibrational properties of the 3,4,9,10,-perylene tetracarboxylic dianhydride (PTCDA) molecule.* Journal of Molecular Structure: THEOCHEM, 2003. **625**(1-3): p. 39-46.
175. Temirov, R., et al., *Bonding and vibrational dynamics of a large π-conjugated molecule on a metal surface.* Journal of Physics: Condensed Matter, 2008. **20**(22): p. 224010.
176. Bardeen, J., *Tunnelling from a Many-Particle Point of View.* Physical Review Letters, 1961. **6**(2): p. 57.
177. Tersoff, J. and D.R. Hamann, *Theory of the scanning tunneling microscope.* Physical Review B, 1985. **31**(2): p. 805.
178. Besocke, K., *An easily operable scanning tunneling microscope.* Surface Science, 1987. **181**(1-2): p. 145-153.
179. Madhavan, V., et al., *Tunneling into a single magnetic atom: Spectroscopic evidence of the Kondo resonance.* Science, 1998. **280**(5363): p. 567-569.

LIST OF PUBLICATIONS

JOURNAL PUBLICATIONS:

1. C. Toher, R. Temirov, A. Greuling, F. Pump, O. Neucheva, M. Kaczmarski, G. Cuniberti, M. Rohlfing, S. Tautz "Unravelling electron correlation effects in molecular wires", PNAS, 2010, submitted
2. Ch.H. Schmitz, C.Rang, Y. Bai, I. Kossev, J. Ikonomov, Y. Su, K. Kotsis, S. Soubatch, O. Neucheva, F.S. Tautz, F. Neese, H.-P. Steinrück, J. M. Gottfried, K. H. Dötz and M. Sokolowski "A Comparative Study of a Triphenylene Tricarbonyl Chromium Complex and Its Uncoordinated Arene Ligand on the Ag(111) Surface: Influence of the Complexation on the Adsorption", J. Phys. Chem. C, 2009, 113 (15), pp 6014–6021
3. F. Pump, R. Temirov, O. Neucheva, S. Soubatch, F.S. Tautz, M. Rohlfing, G. Cuniberti "Quantum transport through STM-lifted single PTCDA molecules", Appl. Phys A (2008) 93: 335–343
4. R. Temirov, S. Soubatch, O. Neucheva, A.C. Lassise and F.S. Tautz "A novel method achieving ultra-high geometrical resolution in scanning tunnelling microscopy", New J. Phys. 10 (May 2008) 053012 (11pp)
5. O.A. Neucheva, A.A. Evstrapov, Yu.B. Samsonenko and G.E. Cirlin "Interaction of optical radiation with GaAs nanowhisker arrays", Technical Physics Letters 33 (11) / November, 2007, pp 923-925

ORAL PRESENTATIONS:

1. O. Neucheva, Ch. Weiss, R. Temirov and F.S. Tautz "Molecular switch: PTCDA on Ag(111)", 26th European Conference on Surface Science, Parma, August 31 – September 4, 2009
2. O. Neucheva, Ch. Weiss, R. Temirov and F.S. Tautz "Current-induced switching of PTCDA on Ag(111)", DPG Spring Meeting 2009, Dresden, March 22-27, 2009

POSTER PRESENTATIONS:

1. O. Neucheva, R. Temirov, and S. Tautz “Mechanics at the molecular scale: Insight into the physical mechanisms” DPG Spring Meeting 2010, Regensburg, March, 22-26, 2010
2. O. Neucheva, Ch. Weiss, R. Temirov and F.S. Tautz “Molecular switch: PTCDA on Ag(111)”, International CECAM-Workshop “Quantum Transport on the Molecular Scale”, Bremen, September 14 – 18, 2009.
3. O. Neucheva, R. Temirov, A. Lassise and F.S. Tautz “Structural point defects at the PTCDA/Ag(111) interface”, 25th European Conference on Surface Science, Liverpool, July 27 – August 1, 2008
4. O. Neucheva, R.Temirov, S. Soubatch, A.C. Lassise and F.S. Tautz “Applications of LT-Scanning Tunnelling Microscopy: Spectroscopy, Charge Transport and Imaging of Single Molecules”Summer School Modern Concepts for Creating and Analyzing Surfaces and Nanoscale Materials, Sant Feliu de Guixols, Girona, Spain May 12-16, 2008
5. O. Neucheva, R.Temirov, S. Soubatch, A.C. Lassise and F.S. Tautz “Applications of LT-Scanning Tunnelling Microscopy: Spectroscopy, Charge Transport and Imaging of Single Molecules”, International WE Heraeus Physics School: Functional Hybrid Material Design, Bremen, June 16 – 27, 2008
6. O. Neucheva, R. Temirov, A. Lassise, S. Soubatch and S.Tautz “Single molecule manipulations: PTCDA on Ag(111)”, DPG Spring Meeting 2008, Berlin, February, 25-29, 2008

1. **Soft Matter**
   From Synthetic to Biological Materials
   Lecture manuscripts of the 39th IFF Spring School March 3 – 14, 2008
   Jülich, Germany
   edited by J.K.G. Dhont, G. Gompper, G. Nägele, D. Richter, R.G. Winkler (2008),
   c. 1000 pages
   ISBN: 978-3-89336-517-3

2. **Structural analysis of diblock copolymer nanotemplates using grazing incidence scattering**
   by D. Korolkov (2008), III, 167 pages
   ISBN: 978-3-89336-522-7

3. **Thermal Nonequilibrium**
   Thermal forces in fluid mixtures
   Lecture Notes of the 8th International Meeting on Thermodiffusion,
   9 – 13 June 2008, Bonn, Germany
   edited by S. Wiegand, W. Köhler (2008), 300 pages
   ISBN: 978-3-89336-523-4

4. **Synthesis of CMR manganites and ordering phenomena in complex transition metal oxides**
   by H. Li (2008), IV, 176 pages
   ISBN: 978-3-89336-527-2

5. **Neutron Scattering**
   Lectures of the JCNS Laboratory Course held at the Forschungszentrum Jülich and the research reactor FRM II of TU Munich
   edited by R. Zorn, Th. Brückel, D. Richter (2008), ca. 500 pages
   ISBN: 978-3-89336-532-6

6. **Ultrafast Magnetization Dynamics**
   by S. Woodford (2008), 130 pages
   ISBN: 978-3-89336-536-4

7. **Role of Surface Roughness inTribology: from Atomic to Macroscopic Scale**
   by C. Yang (2008), VII, 166 pages
   ISBN: 978-3-89336-537-1

8. **Strahl- und Spindynamik von Hadronenstrahlen in Mittelenergie-Ringbeschleunigern**
   von A. Lehrach (2008), II, 171 Seiten
   ISBN: 978-3-89336-548-7

9. **Phase Behaviour of Proteins and Colloid-Polymer Mixtures**
   by C. Gögelein (2008), II, 147 pages
   ISBN: 978-3-89336-555-5

10. **Spintronics – From GMR to Quantum Information**
    Lecture Notes of the 40th IFF Spring School March 9 – 20, 2009
    Jülich, Germany
    edited by St. Blügel, D. Bürgler, M. Morgenstern, C. M. Schneider,
    R. Waser (2009), c. 1000 pages
    ISBN: 978-3-89336-559-3

11. **ANKE / PAX Workshop on SPIN Physics**
    JINR, Dubna, Russia / June 22. – 26, 2009
    Org. Committee: A. Kacharava, V. Komarov, A. Kulikov, P. Lenisa, R. Rathmann,
    H. Ströher (2009), CD-ROM
    ISBN: 978-3-89336-586-9

12. **Entwicklung einer Nanotechnologie-Plattform für die Herstellung Crossbar-basierter Speicherarchitekturen**
    von M. Meier (2009), 135 Seiten
    ISBN: 978-3-89336-598-2

13. **Electronic Oxides –**
    Correlation Phenomena, Exotic Phases and Novel Functionalities
    Lecture Notes of the 41st IFF Spring School March 8 – 19, 2010
    Jülich, Germany
    edited by St. Blügel, T. Brückel, R. Waser, C.M. Schneider (2010), ca. 1000 pages
    ISBN: 978-3-89336-609-5

14. **4th Georgian-German School and Workshop in Basic Science**
    Tbilisi, Georgia / May 3 – 7, 2010
    Org. Committee: E. Abrosimova, R. Botchorishvili, A. Kacharava, M. Nioradze,
    A. Prangishvili, H. Ströher (2010); CD-ROM
    ISBN: 978-3-89336-629-3

15. **Neutron Scattering**
    Lectures of the JCNS Laboratory Course held at Forschungszentrum Jülich and the research reactor FRM II of TU Munich
    edited by Th. Brückel, G. Heger, D. Richter, G. Roth and R. Zorn (2010),
    ca 350 pages
    ISBN: 978-3-89336-635-4

16. **Ab *initio* investigations of magnetic properties of ultrathin transition-metal films on *4d* substrates**
    by A. Al-Zubi (2010), II, 143 pages
    ISBN: 978-3-89336-641-5

17. **Investigation of a metal-organic interface realization and understanding of a molecular switch**
    by O. Neucheva (2010), 134 pages
    ISBN: 978-3-89336-650-7

Schlüsseltechnologien / Key Technologies
Band / Volume 17
ISBN 978-3-89336-650-7

JÜLICH
FORSCHUNGSZENTRUM